POLYESTER MORTAR: PROPERTIES, ENERGY ABSORPTION AND DUCTILITY

*Dr. Moetaz. M. El-Hawary, Dr. Saud Al-Otaibi and Ali Abdul-Jaleel
Building and Energy Technologies Department, Kuwait Institute for Scientific Research
P.O.Box 24885, Kuwait. Email: mhawary@safat.kisr.edu.kw

ABSTRACT

Due to its superiority and advantages, a type of polymer mortar based on polyester is proposed as a construction material. A mix consists of polyester to sand of ratio 1:5 was found to be the optimum. Samples were tested in compression at different ages to determine the compressive strength and the optimum hardening period. Other essential mechanical and physical properties of the material were evaluated. The stress-strain diagram of the material in compression was also established. The diagram was used to evaluate the modulus of elasticity, toughness, resilience and ductility of the proposed material. Along with the observed very high energy absorption capabilities of the material, ultimate strains, reaching 40%, were noticed. The observed high resilience along with high tensile and flexural strengths of the material will reduce the cracking in the tension zone and hence, increase the material durability. It was concluded that the proposed material is much superior to conventional concrete. The presented paper contains the properties of the proposed material.

Keywords: Polyester, mortar, ductility, polymer, durability.

INTRODUCTION

Although the concrete- polymer materials are relatively new in the construction industry, they received wide attention and extensive research works were conducted on these materials.
Polymers are generally inert, environmental- friendly, non-toxic materials. They are also chemical resistance, durable, strong and flexible materials along with their adhesive, rapid hardening and moisture resistance properties. As for conventional concrete, polymer concrete can be easily moulded in the fluid state and becomes hard after polymerization. The advancement in polymer technology made it possible to produce a tailored type of polymer that suits the required specifications and applications.
Epoxy and polyester are the most widely used types of polymers in the structural industry. Extensive research was conducted on polymer concrete and polymer modified concrete. This includes flexural behavior of polymer concrete [1], its use in repair [2], properties of polyester concrete [3], use of recycled polyester in concrete [4], behavior of epoxy modified concrete [5], and structural design of polymer modified beams [6] .
Due to the harsh environment in Kuwait, conventional concrete structures often experience some kind of premature deterioration that causes lack of serviceability. This deterioration affects the cost of the structure as it requires some type of rehabilitation and repair, the aesthetic appearance of the structure and might affect the safety of the structure. This deterioration is in general the result of the interaction between the constitutive materials and the environment. As the environment cannot be altered, the deterioration may be controlled by the introduction of a new durable constitutive material. Some work was conducted on the durability of an epoxy mortar system [7],on the mechanical behavior of polymer concrete [8] and on the durability of

conventional concrete repaired using different types of polymers in the Kuwaiti marine environment [9].

Concrete consists of a matrix or a binding material and filler. The interaction between the cementitious binder in conventional concrete and the environment is the main reason for the concrete deterioration. The introduction of polymer binder will eliminate leaching, carbonation, alkali- aggregate reaction and sulphate attack. It will also reduce permeability, which in turn will reduce corrosion and chloride penetration. Polymer binders are also chemical resistant and posses higher strength, which means that smaller sections may be used, and that tensile cracking may be eliminated or reduced. Polymers are faster in hardening and require no curing, which is one of the tedious tasks in the hot weather of Kuwait.

The reason for the limited structural use of polymer concrete is the cost. This cost, however, is decreasing internationally due to the modern manufacturing techniques and the mass production. The cost of polyester has dropped significantly in the past years and this trend is expected to continue. Cost of polymers, being a petrochemical product, should be less in Kuwait especially if a special type of polymer is tailored to suit the structural industry. In calculating costs, the savings due to the elimination of repair and curing, the use of smaller sections, the increased life span and the fast erection of the structure should be kept in mind.

The quarrying for coarse aggregates in Kuwait has been banned for environmental reasons. Fine aggregates, however, are available in abandon and may be utilized in the production of polymer mortar which may be used as a structural building material instead of conventional concrete. The proposed material is expected to render the same advantages as polymer concrete, mentioned before, with a little increase in cost , that is diminishing with time. This building material may be produced using only local available resources. The investigation of the behavior of polymer mortar as a building material in the Kuwaiti environment is proposed. Polyester polymer is utilized at this stage.

CONSTITUENT MATERIALS AND MIX DESIGN

The type of polymer utilized for this work is Nitomortar EP™ , which is based on polyester resin, specially formulated to minimize shrinkage to 0.8%. The material is recommended by the manufacturer as multipurpose high strength repair compound. The polyester was delivered as two components, liquid and powder. The liquid contains the resin while the powder contains solid hardener and fillers, which were tested for size distribution using sieve analysis, Table 1, and used as part of the fine aggregates. Natural sand of the sizes shown in Table 2, was used as the remaining part of the fine aggregates required for the mortar mix.

To determine the optimum mortar mix design, samples of different polymer to sand ratios were cast and tested. Ratios of 1:4, 1:5, 1:6 and 1:7 and 1:8 were tried. Filler delivered with polyester was considered as part of the sand. Resin was added to the hardener and filler at the ratio recommended by the manufacturer. The mix was thoroughly mixed by hand for two minutes before the extra sand was added. The mix was then mixed thoroughly and was poured into moulds. Cube samples of two different sizes, 150 and 50mm were used for comparison. Release agent was applied in all moulds to allow easy release of specimens. Samples were vibrated on the vibrating table, covered for two days for curing before being demoulded. Three samples were prepared for each mix. Samples made using polymer to sand ratios of 1:8 and 1:7 were found to be very weak and some of them were broken during handling. Those ratios were hence discarded. Remaining samples were tested in compression after 28 days. Results are shown in Table 3.

The results indicated that both the 1:4 and 1:5 ratios of polyester to sand may be utilized. Although the ratio 1:4 gives higher strength, the ratio 1:5, however, was selected as optimum, as the increase in strength is of the same order as the increase in the amount of polyester and hence the increase in cost. The increase in strength was found to be 24.6% compared to 20% increase in the amount of polyester. The increase in the amount of sand will also improve the volume stability and reduce shrinkage. The ratio 1:5 also gives strength in excess of 40 MPa which is usually the maximum specified for normal structures. This ratio was utilized in all remaining tasks of this project. Analogous results were obtained using either 150mm or 50mm cubes.

MECHANICAL PROPERTIES

The selected mix and the procedure described above were used to investigate the mechanical properties of the polyester mortar.

Compressive Strength
Using the optimum selected ratio of polymer to sand, cubes were cast and compressive strengths were evaluated at 1, 2, 3, 5, 7 and 10 days. Averages of three results at each age are shown in Fig. 1. Almost same results were obtained at all ages which indicates that the materials gains full strength in 24 hours and may be tested at any time after the first day. Average compressive strength of the material was found to be 60.2 MPa.

Tensile Strength
To evaluate the tensile strength of the proposed material, standard cylinders were cast and tested in split. Average tensile strength was found to be 4.6 MPa, which represent 7.7% of the average compressive strength.

Flexural Strength
Flexural strength was evaluated using beams of size 700x150x150 mm, tested under four points loading as shown in Fig. 2. Loads, deflections and flexural strengths were recorded. Average flexural strength was found to be 11.58 MPa, which is 19.2% of compressive strength. While the average mid-span deflection was found to be 6.887 mm.
To evaluate the effect of casting members at different times, beams were cast at two and three intervals at different ages. The beams were tested in flexure using the four points loading as before. Beams failed along the construction joints. Flexural strength was found to be less for the three intervals beams as the failure was due to combined flexure and shear, while failure for the two intervals case was inside the pure bending zone.

Bond Strength
Bond strength was also evaluated. Standard cylinders were cast with a 10mm steel bar inserted centrically and longitudinally before being subjected to pull out test. Due to the high bond strength, however, yielding of steel was observed before the pull out of the bars which were inserted full length. The test was repeated with the bars partially embedded in the cylinders, Fig. 3. Average bond strength of ten samples was calculated and found to be 8.58 MPa , representing 14.3 % of the average compressive strength.

Effect of High Temperature
To capture the effect of high temperatures, cubes were heated for 8 hours to $90C^o$ and $180C^o$, before being tested in compression. Samples at $180C^o$ were allowed to cool to room temperature before being tested, while at $90C^o$ three samples were tested hot and three were cooled before being tested.   Compressive strengths for the mentioned three cases are shown in Table 4. It was found that, while hot, samples at 90 C^o C lost 47% of their strength. However after cooling, the residual strength was found to be 7.9% higher than the original due to material hardening. Residual strength at 150C was found to be 3.2% higher than original.

Ductility and Other Mechanical Properties
Polymer mortar cubes were cast using the mix and procedure described before. Samples were used to produce and evaluate the stress-strain curves in compression. Stress-strain of one of the samples is shown in Fig. 4. A very high ductility was observed which demonstrate the potential of utilizing the proposed material in applications where high energy absorption is required. This includes earthquake resistant structures, road barriers, impact resistant structures and blast resistant buildings. Ductility was defined as either D_1 or D_2 where:

D_1 = Strain at break / strain at peak   (1)

And

D_2 = Toughness / resilience   (2)

Toughness represents the total energy that may be absorbed by the material or the total area under the stress-strain curve and resilience represents the elastic energy or the area under the linear part of the stress-strain curve.

Average resilience was found to be 37.31 N.m and average toughness 134.42 N.m, making the energy ductility, D_2, equals 3.6. While the average strain at peak was found to 5% and the ultimate strain is 37.75% making the strain ductility reaches the very high value of 7.5. The modulus of elasticity, slope of the linear part of the curve, was also evaluated and found to be 1.837 GPa.

PHYSICAL PROPERTIES

Some important physical characteristics of the utilized polymer mortar were evaluated, including density, water absorption, thermal conductivity and thermal expansion. The average specific gravity was found to be 2.01 and the average absorption is o.25%. The coefficient of thermal expansion was found to be 1.8648×10^{-5} and the thermal conductivity coefficient is 0.70004 w/m k°.
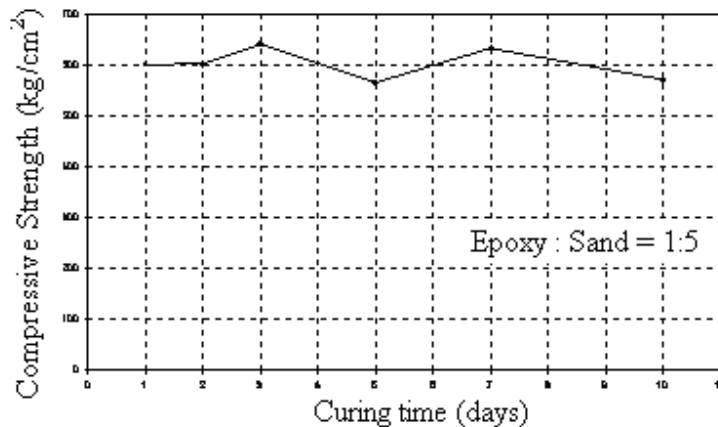
Fig. 1: Average compressive strength against time

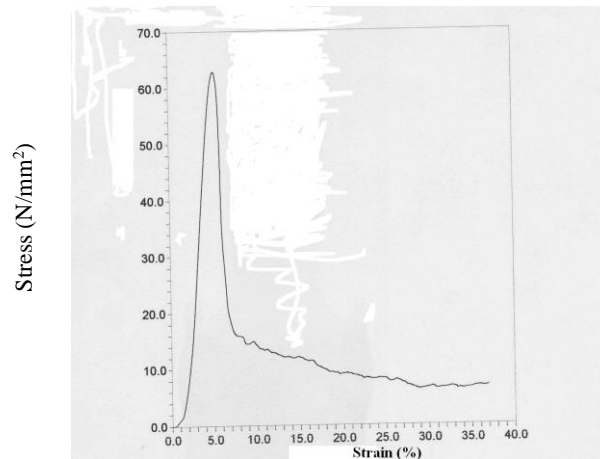**Fig. 2: Flexural testing of beams**

Fig. 3: Testing bond strength

Fig. 4: Stress-strain curve

Table 1: Sieve Analysis of the Filler

SIEVE #	DIAM. (mm)	% FINER
3/8"	9.5	100.00
4	4.75	100.00
8	2.36	100.00
16	1.18	99.90
30	0.6	94.00
50	0.3	29.70
100	0.15	25.00
200	0.075	22.40

Table 2: Sieve Analysis of Sand

SIEVE #	DIAM. (mm)	% FINER
3/8"	9.5	100.00
4	4.75	99.48
8	2.36	96.82
16	1.18	90.20
30	0.6	74.14
50	0.3	27.64
100	0.15	7.88
200	0.075	4.98

Table 3: Compressive strength of mortar cubes

Ratio of Polyester to sand	Compressive strength (MPa)
1:4	52.28
1:5	41.96
1:6	20.31

Table 4: Compressive strength for cubes subjected to heat

Specimen No.	Compressive strength at 90C° (MPa)	Residual strength for samples heated to 90C° (MPa)	Residual strength for samples heated to 180C° (MPa)
1	30.4	63.5	61.9
2	33.2	66.1	62.1
3	31.5	65.2	62.4
Average	31.7	64.9	62.1

CONCLUSIONS

The mechanical and physical characteristics of a proposed polymer mortar based on polyester resin have been investigated. The following were concluded:

1. The ratio of polymer to fine aggregates of 1:5 was found to be optimum.
2. The material was found to reach its full strength in one day, which is expected to eliminate the cost of curing, speed construction and reduce cost of formworks. Elimination of curing along with the elimination of the use of coarse aggregates will improve quality control and assure consistency.
3. The material was found to reach a high compressive strength that exceeds 60 MPa. High corresponding tensile, flexure and bond strengths were also encountered.
4. The construction joints are reduced compared to conventional concrete, but was not eliminated.
5. Although the material was found to lose almost half of its strength when heated to 90o, it gains and exceeds its original strength when cooled to room temperature.
6. The material was found to sustain very high ultimate strains that reach almost 40% compared to that of 4% of normal concrete and was also found to possess outstanding ductilities and high ability to absorb energy.   The material is hence recommended for structures where high deflections, impacts or dynamic loading are expected or where high energy absorption, in general, is required.

ACKNOWLEDGMENTS

REFERENCES

1. Abdel-Fattah, H. & El-Hawary, M.M. (1999), "Flexural Behavior of Polymer Concrete", Construction and Building Materials,13.
2. Fowler, D.W. (1989), "Future Trends in Polymer Concrete", Special Publication 116-118, ACI, pp.129-143.
3. Vipulandan, C.& Paul, E. (1993), "Characterization of Polyester Polymer and Polymer Concrete", Journal of Materials in Civil Engineering, 15(1), pp 62-82.
4. Rebeiz, K.S. (1995), "Time-Temperature Properties of Polymer Concrete Using Recycled PET", Cement and Concrete Composites, 17, pp 119-124.
5. Abdel-Fattah, H., El-Hawary, M.M. & Falah, A, (2000), "Effect of Elevated Temperature on the Residual Fracture Toughness of Epoxy Modified Concrete", Kuwait Journal of Science and Engineering, 27(1).
6. El-Hawary, M.M. & Rahal, K, (2000), "Experimental Investigation of Shear Strength of Resin-Modified Concrete", Proceedings of the Turkish Cement Manufacturers Association, II. International Symposium, Cement and Concrete Technology in the 2000's, Istanbul, Turkey.
7. El-Hawary, M.M.(1998), "Testing for Engineering and Durability Properties of an Epoxy Mortar System" , Kuwait Journal of Science and Engineering, 25(1).
8. El-Hawary, M.M. & Abdel-Fattah, H.(1998), "Effect of Temperature on the Mechanical Behavior of Resin Concrete", Proceedings of the Arab Conference on Repair and Rehabilitation of Structures, Cairo, Egypt.
9. El-Hawary, M.M,, Al-Khaiat, H. & Fereig, S. (2000), "Performance of Epoxy- Repaired Concrete in Marine Environment", Cement and Concrete Research,30(2).

EFFECT OF DIFFERENT WASTES ADDITIVES ON COMPRESSION STRENGTH OF CONCRETE

*Dr. AQEEL SHAKIR Al-ADILI

Building and Construction Engineering Department, University of Technology, P.O.Box: 46027 , Baghdad, Iraq. Tel. +9647901766126 e-mail : aqeeladili@hotmail.com

ABSTRACT

This paper studies the influence of different additives to the concrete mixtures with different percentages, to determine the compressive strength, and concrete density (As light weight concrete). Different types of additives were used in this research, including rubber cuttings, iron splinters, wood sawdust, rice husk, and silica gel, with 5% , 10% ,15% ,and 20% percent of each one. Compressive strength, flexural tensile strength, and variation of density have been examined for each specimen at all percents of additives, and comparing with the reference concrete (without additions) specimens. From the obtained test results, the study concluded that the use of these additives in concrete significantly affects both the compression strength, flexural tensile strength (rise or fallout), especially at 5% of adding materials, as well as utilization of additives in concrete to produce low density mixtures with rice husk mixtures or as high density concrete when using iron splinter in the concrete mixtures.

Keywords : Additives – agro wastes - urban wastes – Compressive strength - Light weight concrete.

INTRODUCTION

Concrete is one of the most widely used construction materials, due to its good durability comparing to cost. However, when the concrete member is subjected to severe environments, its durability can significantly decline due to corrosion of concrete and embedded reinforcements. Nowadays, the use of additives as a cement replacement is on the rise.

Scientists are continuously on the look out for materials which can be used as substitutes for conventional materials or which possess such properties as would enable their use for new designs and innovations. Concrete using additives and alternative materials fall under this subject. The successful utilization of waste materials depends on its use being economically competitive with the alternative natural material, these costs are primarily made up of handling, processing and transportations. For these mentioned reasons, many research works were endeavored to make use of the enormous quantity of waste like: rubber tires (chopped worn-out tires), iron splinters (scrap), wood saw dust, ash rice husk and silica gel, to investigate the basic properties of concrete mixes with different additives, produce light weight concrete, to increase compression strength and flexural tensile strength, and reduce costs of constructions, as well as, reduce environmental pollution and preventing the accumulation of the raw materials.

Additives of concrete, generally have two main categories; organic wastes (agro-wastes), like, wood sawdust, cork granular, coconut pith, and rice husks; and inorganic wastes (urban wastes) like broken brick aggregate, silica gel, flexicrete, iron splinters, silica fume, and chopped worn-out tires [1].

Hence, the aim of this study is to investigate some properties of concrete mixes with different additives e.g. compression strength, flexural tensile strength, density (as light weight concrete) and their influences on concrete behavior. The additives included in this work are, rubber

cuttings (Chopped worn-out tires), iron splinters, saw dust, rice husk, and silica gel.

Inorganic Wastes (Urban wastes)

Rubber cuttings (Chopped worn-out tires)
Chopped worn-out tires (Ch.W.T.) concrete consist of cement, aggregate chopped worn-out tiers, and water at various proportions. Since the chopped worn-out tires have low density, the product has the property of light weight. the size of Ch.W.T particles varies, and almost pass through the No. 4 (5mm) sieves. Furthermore, Ch.W.T have favorable characteristics such as, high resistance to weather changing conditions, very low water absorption, light weight with absolute density around 0.92-0.95 gr/cm^3 and density 0.45 gr/cm^3 [2] ,as well as thermal insulation .

Silica gel
Silica gel consist of SiO_2 as mineral formation. This material has been adopted by ASTM-192 as standard expanding aggregate to measure the effectiveness of some inorganic mineral powders in improving the dimensional stability concrete [3].

Iron splinters
The iron splinter concrete consists of cement, coarse aggregate which is partially replaced with steel punching as an iron – scrap, normal fine aggregate which replaced with an iron lathing or splinter wastes, and water in addition to an appropriate admixture. As the steel punching and iron lathing wastes are of high density, the resulting concrete has the property of high density also. Iron- splinter concrete contains boron compound which works as a light element in order to increase the ability of this concrete to capture fast neutrons [7]. The carbon steel (iron) wastes which are locally available as by-product can be also used as a partial replacement of sand in a different proportion by volume of fine aggregate.

Organic Wastes (Agro-wastes)

Saw dust
Natural organic materials such as wood saw dust have been used for making lightweight concrete. Saw dust is abundantly available in most places but it often contains substance which retards the hydration and hardening of cement. The extent of deleterious effect varies with the type of wood, and hardwood like mango and Sal are known to seriously inhibit hydration [5]. High drying shrinkage of sawdust-cement limits its use to design where freedom of movement is possible. The introduction of sand into cement-sawdust mix has been found to reduce the drying shrinkage, while reducing thermal insulation and increasing density.
A common characteristic of lightweight concrete is their comparatively high moisture movement with the consequent changes in dimensions accompanying changes in moisture content. Sawdust cement products show a relatively higher percentage of volume change as reflected in the moisture movement,[5].

Rice husks
Lightweight concrete using rice husk as aggregate has been used for making precast blocks and slabs for walls and slabs for wall partitions [9]. The waste products of rice husk, generated from the accumulation of the outer covering of rice grains during the milling process. This additive is used as a pozzolana by special process to confirm the engineering requirements.

Experimental Work
The experimental work have been carried out according to Iraqi specification code,1989 [6] and B.S.1881,1970 [4] for compressive strength tests, and according to ASTM C192-88[3] for flexural tensile strength tests. The additives were used with different volume percentages of (5%,10%,15%, and 20 %) with water cementitious ratio (w/c) of 0.5, and the mixing ratios of 1:1.5:3 for saw dust, silica jel, rice husk, and rubber cuttings, while 1:2:4, for the rubber cutting, iron splinter and rice husk. Three specimens of each ratios were casted and cured for 28 days.

Table-1 shows the chemical analysis of the cement which used in this study. Moreover the chemical analysis of rice husk and rubber cutting have been made to find out the contents of these additives (table-2 &3).

Table 1: Chemical analysis of cement used in this research*

Oxides	% by weight
CaO	60.79
MgO	3.55
SiO_2	19.53
SO_3	2.17
Fe_2O_3	2.95
Al_2O_3	4.78
K_2O	0.68
Na_2O	0.18
Loss on ignition	1.37
Insoluble residue	0.51
Lime saturation factor	0.87

* The analysis was made by NCCL,Iraq.

Table 2: Chemical analysis of rice husk

Oxide composition	Content %
SiO_2	87.5
CaO	1.5
MgO	1.7
R_2O_3	3.6
SO_3	0.4
Loss on ignition	5.3

Table 3: Chemical composition of Tires (rubber)cuttings *

Composition	Content %
Rubber hydrocarbon	48
Carbon black	31
Acetone extract	15
Ash	2
Residue chemical balance	4

* Analysis was made at Babylon Tires Factory.

Discussion of the Results

The test result shows that there are different behaviors for concrete with each type of additives. This research revealed that the compressive strength increase by 5% for all additives except for

rice husk where it decreases with the increasing addition percentage (in both ratios of mixing), (table-4) .

Rubber cuttings have noticeable increase of compression strength at 5% of additions (Figuer-1). This increase is about 8.4%, from reference concrete (with no additives concrete) and decrease for other percentages (in both ratios of mixing). This could be attributed to the inclusions of cuttings inside existing voids and pores through mixture, which behaves as bond material. While, when increasing the addition ratio (more than 5%), the rubber will act as weakness regions.

As with regard to iron splinter added to concrete, the test shows significant increasing in 5% and 10% addition to the concrete (Figure-2). This percentage (5%) is the preferable content of iron splinter to increase compressive strength (about 16.5%), due to reinforcement behavior in concrete, and bonding mixture. Silica gel has the same behavior as iron splinter with increasing ratio to about 15% (Figure-3). As well as, wood dust increase the compressive strength about 13% at when using 5% addition percentage compared to reference concrete, (Figure-4). This can be attributed to the high content of SiO_2 in sawdust, and the fibers texture of this material, which reflect in concrete mixture.

Table 4: The compressive strength of the concrete samples with different additives types.

	Rubber cuttings (tires) N/mm^2		Iron splinters (scrap) N/mm^2	Wood Sawdust N/mm^2	Rice husk N/mm^2		Silica gel N/mm^2
Mixing ratio / Add. Percent.	1:1.5:3	1:2:4	1:2:4	1:1.5:3	1:1.5:3	1:2:4	1:1.5:3
0 %	25.53	23.6	23.6	25.51	24.08	23.8	25.47
5 %	28.76	25.5	27.5	28.3	15.19	21.7	29.30
10 %	23.36	21.4	26.2	21.4	14.20	21.1	26.58
15 %	16.88	17.3	24.9	17.3	13.64	20.82	26.1
20 %	15.52	14.8	18	24.08	13.12	20.05	25.82

However, rice husk shows descending behavior in all addition percentages in both mixing ratios (Figure-5), which could be a result of elongated shapes of husk and the high content of the loss of ignitions.

The results of light weight concrete density with additives show significant density decreasing (from normal concrete) for rice husk than rubber cuttings, silica gel, wood sawdust,(Figuer-6&7),(table-5). While iron splinter (scrap) concrete showed different behavior, which is increasing the density of concrete with increasing of additive percents (Figuer-6). This may be result of the high density of iron and the imperfection inclusions in the scrap. In contrast, rice husk have low density and elongated shapes which allow more of voids and pores in the concrete mixture to provide light weight concrete.
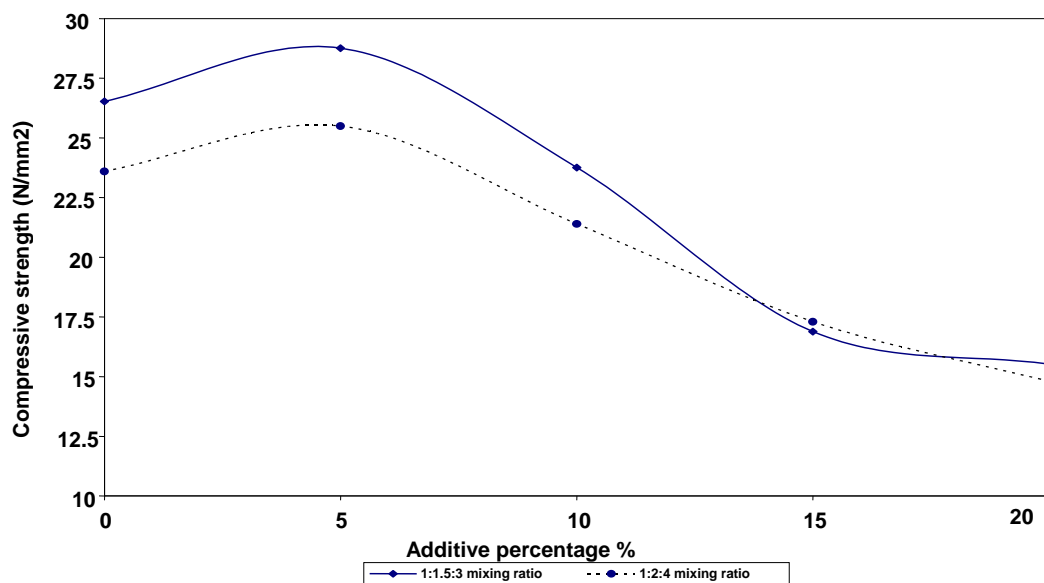
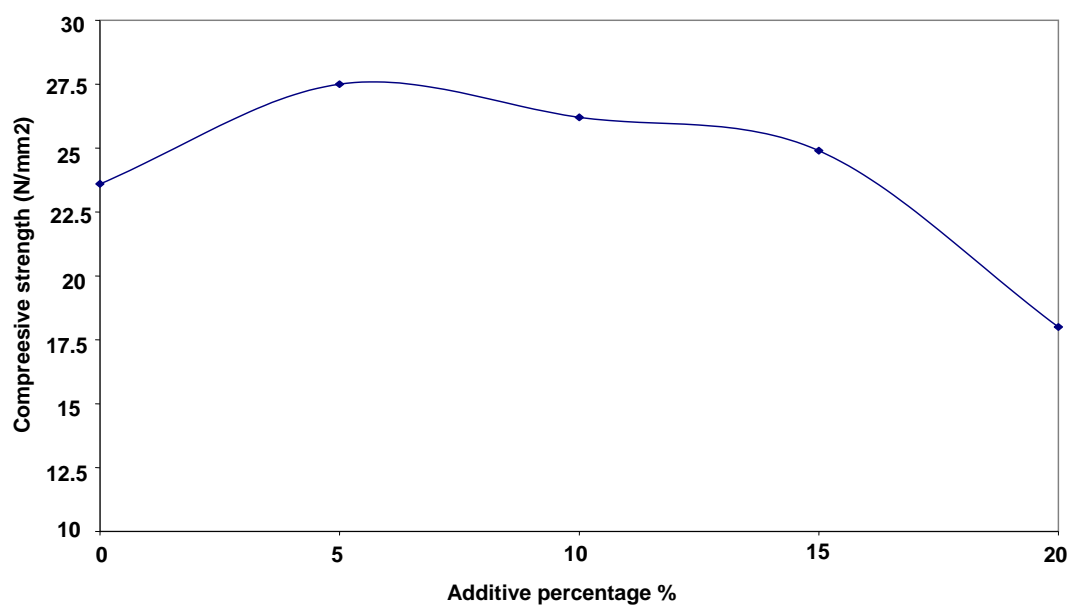**Fig. 1: Compressive strength of concrete with rubber cuttings additives.**

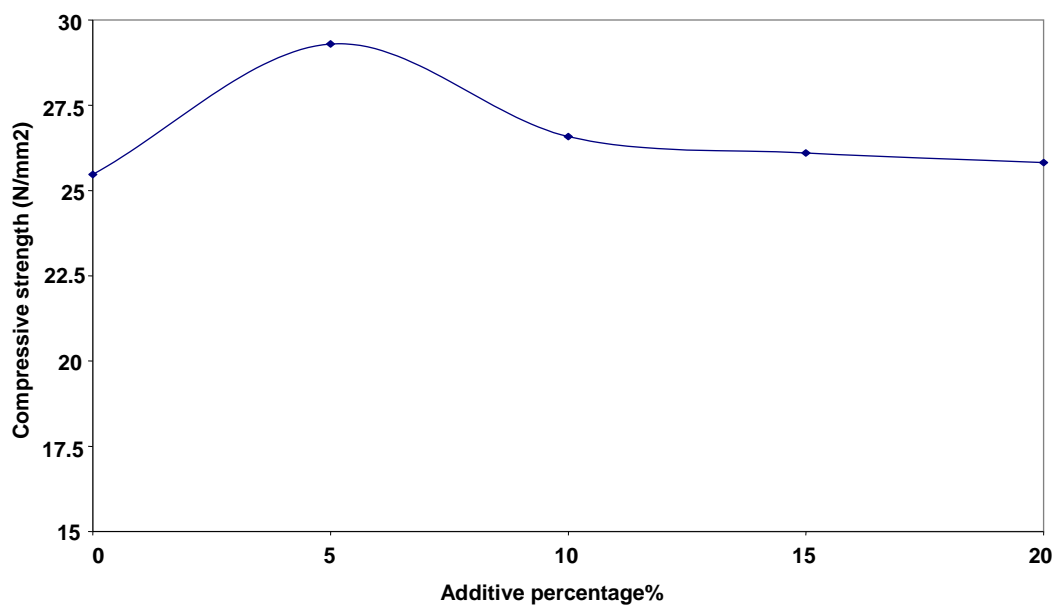**Fig. 2: Compressive strength of concrete with iron splinter additives.**

Fig. 3: Compressive strength of concrete with silica gel additives
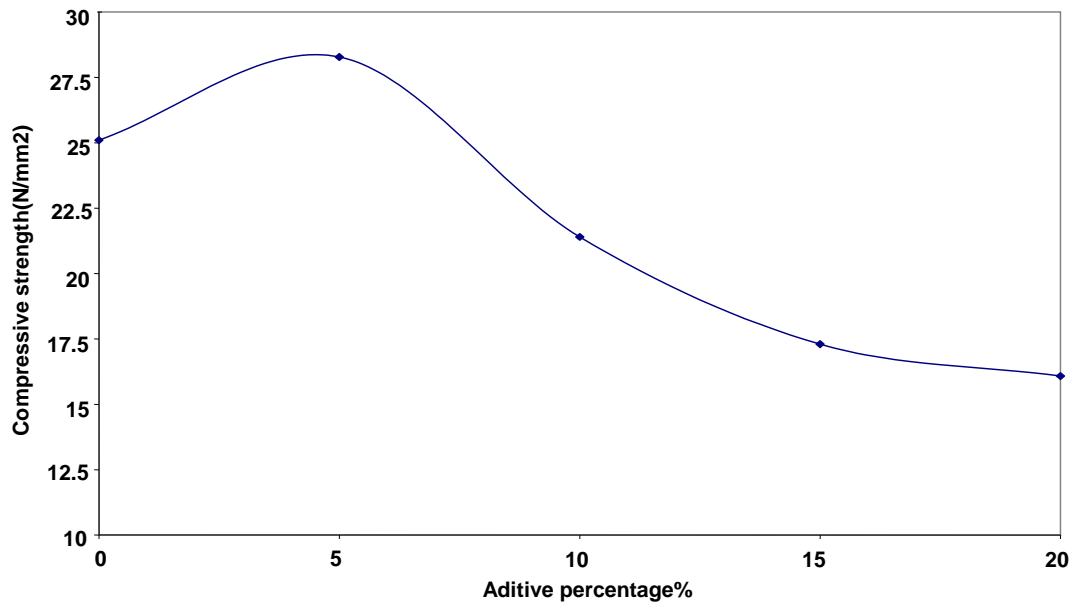

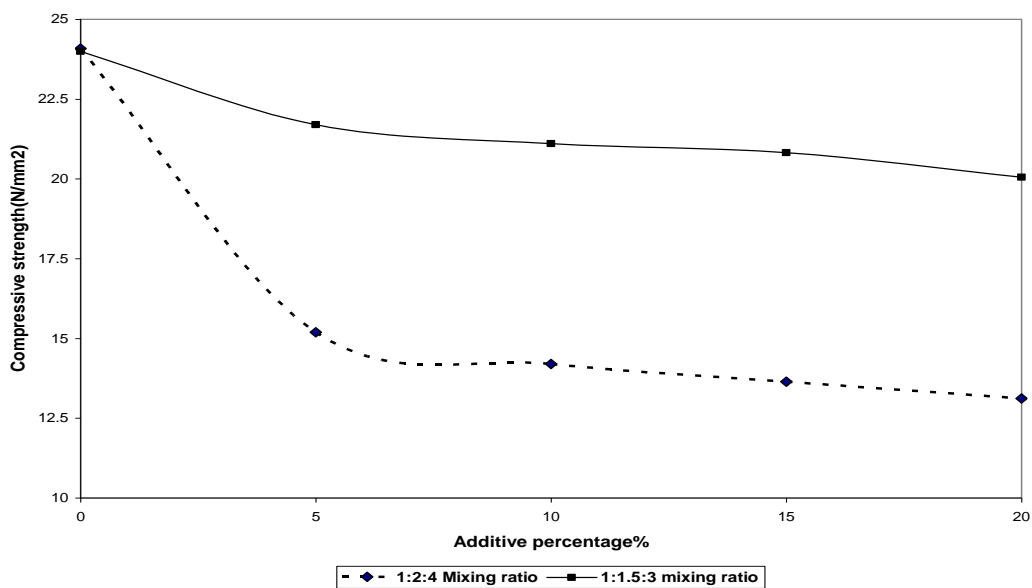**Fig. 4: Compressive strength of concrete with sawdust additives**

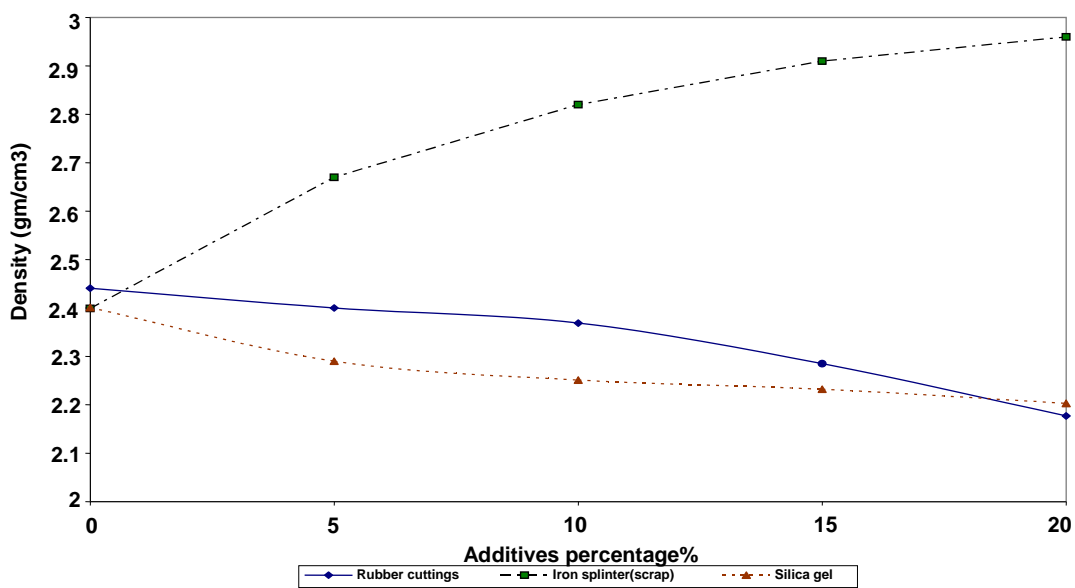**Fig. 5: Compressive strength of concrete with rice husk additives.**

Fig. 6: Density of concrete with inorganic wastes (Urban wastes) additives.
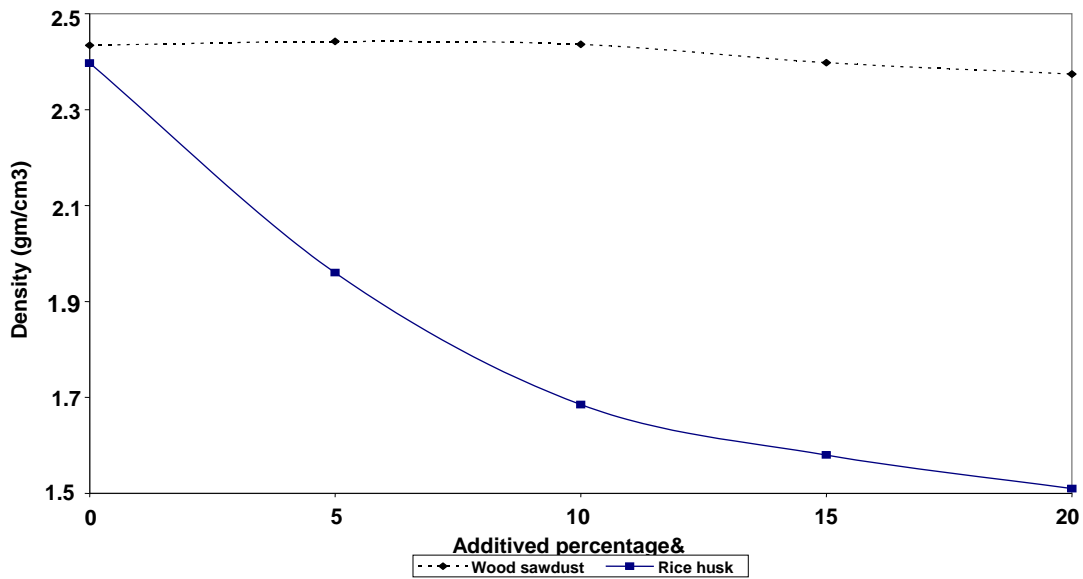
Fig. 7: Density of concrete with organic wastes (Agro-wastes) additives.

Table 5: The density of concrete with different percentages of additives.

Additive%	Rubber cuttings g/cm^3	Iron splinters (scrap) g/cm^3	Wood sawdust g/cm^3	Rice husk g/cm^3	Silica gel g/cm^3
0 %	2.401	2.399	2.400	2.397	2.401
5 %	2.40	2.67	2.442	1.96	2.290
10 %	2.369	2.82	2.436	1.685	2.251
15 %	2.285	2.91	2.398	1.58	2.232
20 %	2.177	2.96	2.374	1.51	2.203

Figure-8, shows the behavior of flexural tensile strength of concrete due to the addition of different percentage of rubber cuttings, iron splinter, wood sawdust, and rice husk. From this figure, the development of flexural strength of concrete with rubber cuttings is decreased applciably with the increase in rubber cuttings contents. This is attributed to the voids ratio and aggregate–cement paste bonding, while in contrast, flexural tensile strength of concrete with iron splinter shows higher flexural strength corresponding to reference concrete (with no additives), the percentage of increase is 29% from the reference concrete in adding percentage of 20% of iron splinter in concrete. This is due to the increasing of bonds inside concrete and producing higher internal integrity. On the other hand, wood sawdust play good role in concrete behavior to increase strength, but the maximum strength was with 10% of sawdust. Moreover, rice husk ash in concrete mixture with adding percentage 5% gives higher flexural strength than reference concrete, while decreased the flexural strength when percentage of rice husk was increased (table-6), (Figure-8).
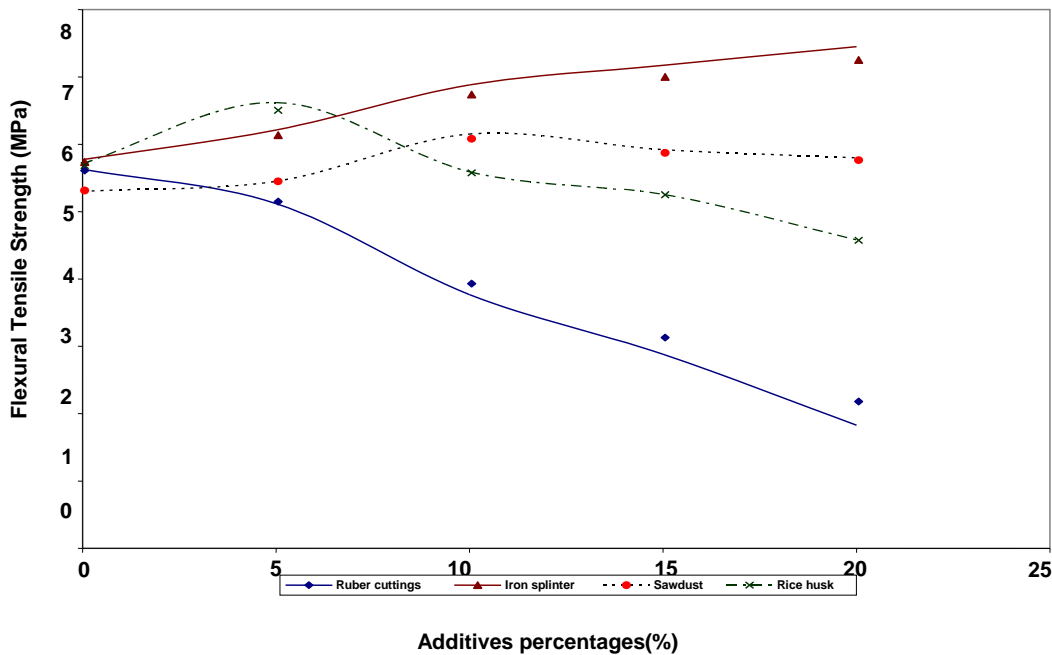
Fig. 8: Flexural Tensile strength of concrete with adding different additives percentages.

Table 6: Flexural tensile strength of concrete with different percentages of additives.

Additive%	Rubber cuttings MPa	Iron splinters (scrap) MPa	Wood sawdust MPa	Rice husk MPa
0 %	5.63	5.77	5.3	5.71
5 %	5.12	6.21	5.45	6.62
10 %	3.77	6.88	6.15	5.59
15 %	2.88	7.17	5.92	5.23
20 %	1.83	7.45	5.80	4.48

CONCLUSIONS

This study has been carried out to investigate the behavior of concrete due to adding organic and non organic wastes mixtures. The study concludes the followings aspects;

1. This research revealed that the compressive strength increased by 5% of all additives percentages except for rice husk which caused a decrease with all addition percentage (in both ratios of concrete mixing).
2. Rubber cuttings have noticeable increase of compression strength at 5% additions. This increase is about 8.4%,
3. As with regards to iron splinter, percentage of 5% is the preferable content of iron splinter to increase compressive strength (about 16.5%). While wood dust increased compressive strength about 13% at 5% of additive materials.
4. Rice husk showed decrease in all addition percentages in both mixing ratios of concrete.
5. Light weight concrete density showed less density decreasing (from normal concrete) for rubber cuttings, silica gel, wood sawdust, than rice husk. While iron splinter (scrap) concrete showed different behavior, where increasing the density of concrete with increasing of additive percentages.

6. Flexural tensile strength of mixed concrete with rubber cutting decreases considerably by increasing additive, in contrast, iron splinter led to increase in flexural strength up to 29% from reference concrete when adding 20% of iron splinter, However, wood sawdust increased flexural strength but the preferable percentage is 10%, and 5% of rice husk in concrete mixture.

7. This study showed the possibility of utilization of different wastes to produce light weight concrete, as well as increasing compression and flexural tensile strength of concrete, and future research can be made to improve the concrete by mixing two or three of those wastes with concrete and reducing costs.

REFERENCES

1. ACI Committee 213, Guide for Structural Lightweight aggregate Concrete, ACI manual of concrete practice, part-1, materials and general properties of concrete, 1990.
2. Al-Sakini,J.S.(1998), Behavior and Characteristics of Chopped Worn-Out Tires Light Weight Concrete, M.Sc. thesis, Univ. of Technology, Iraq. 110 p.
3. ASTM, C192(1988), Standard Practice for Making and Curing Test Specimens in the Laboratory, Annual book of ASTM standard, Philadelphia, Vol.04,02
4. British Standard Institute(1970), Method of Making and Curing Concrete Test Specimens, BS 1881, Part-3, London.
5. CBRI, Central Building Research Institute(1986), Coconut pith cement concrete for Thermal Insulation, Building Materials, No.9, Roorkee, India.
6. Iraqi Specifications Code(1989), Ministry of Planning, Iraq.
7. Nassir,W.A.(2000), Utilization of Iron Scrap for Production High Density Concrete for Gamma Ray and Neutron Generate Shielding, M.Sc. thesis, Univ. of Technology, Iraq. 135 p.
8. NCCL, National Center of Constructions Laboratories, Ministry of housing and Building, Baghdad, Iraq.
9. Singh, S.M. and Aggarwal, L.K.(1977), Portland Cement Bonded Panel Products From Agricultural Wastes, Research and Industry, Vol.22, No.4, pp. 242-245 .

INFLUENCE OF NANO-SILICA ADDITION ON PROPERTIES OF CONVENTIONAL AND ULTRA-HIGH PERFORMANCE CONCRETES

Rafik Abbas

Associate Professor, Institute of Graduate Studies and Research, Alexandria University, Egypt

ABSTRACT

Cementitious and concrete materials are mainly used on a large scale and in huge quantities for roads, dams, bridges and building constructions. The mechanical behavior of these materials depends to a great extend on structural elements and phenomena which are effective on a micro and nanoscale. New efforts and possibilities of material engineering on nanoscale may lead to improve mechanical and physical properties as well as durability of composite construction materials. This paper intends to study the use of nano-silica with 99.5% silica content and average particle size of 15 nm as addition in concretes with different strength levels. Besides, comparison between the influence of SF and NS on concrete performance was also addressed. Therefore, the experimental program was divided into two parts aiming at investigating the effect of NS addition on the properties of conventional and ultra-high performance concretes (UHPC). Results indicated that nano-silica addition reduced the concrete workability. The incorporation of nano-silica resulted in a significant early increase in compressive, splitting tensile and flexural strengths of conventional concrete. Addition of both silica fume and nano-silica by total amount of 10 %, may lead to an increase in the 28-day compressive strength of low cement content and high cement content concretes up to 40 % and 50 %, respectively, over the strength of comparable concretes. It was observed that the pozzolanic contribution of nano-silica becomes significant from the very early age, compared to silica fume, which begins its pozzolanic reactivity at the age of 7 days or later. This mechanism explained the outstanding mechanical performance of nano-silica concrete. Test results also showed that nano-silica may be applied successfully in ultra-high performance concrete, where strength level over 230 MPa was achieved.

INTRODUCTION

Recently, the technology of nano-structured material is developing at high speed and will be applied extensively with many materials and applications. Although cement is a common building material, its main hydrate calcium-silicate-hydrate gel is considered as natural nano-structured material [1, 2]. Lately introduced concretes are mainly dependent on the structure refining and the improvement of paste-aggregate interface through incorporating additions and admixtures. Slag, fly ash and silica fume (SF) were used to improve cement-based composites, and have achieved great successes, such as High-Performance Concrete, Ultra-High Performance concrete (UHPC) also known as Reactive Powder Concrete, etc. Silica fume (SF) belongs to the category of highly pozzolanic materials because it consists essentially of silica in non-crystalline form with a high specific surface, and thus exhibits great pozzolanic activity. The SF may be regarded as the main material that led the revolutionary production of high performance cement-based composites.

Nano-particles have been gaining increasing attention and been applied in many fields to fabricate new materials due to their unique physical and chemical properties. If nano-particles

---

are integrated with cement-based building materials, the new materials might possess some outstanding properties. Nano-silica (NS) is introduced as alternative to silica fume due to its exceptional pozzolanic activity, which is more obvious than that of silica fume. Nano-silica can react with calcium hydroxide crystals, and produce calcium-silicate-hydrate gel. Thus, the size and amount of calcium hydroxide crystals are significantly decreased, consequently, increasing the strength of the cement composite [3, 4].

Many research works have introduced the nano-silica as highly active pozzolanic material. Attempts have been made to benefit from its characteristics. Ji [5] studied the water permeability of concrete incorporating nano-silica. He stated that the microstructure of nano-silica concrete is more uniform and compact, leading to reduction in water permeability. Qing et al. [6] studied the effect of nano-silica addition on properties of hardened cement paste as compared to silica fume. The results suggested that with a small amount of added NS, the CH crystals at the interface between hardened cement paste and aggregate at early ages may be effectively absorbed in high performance concrete (HPC). Li et al. [7] experimentally studied the abrasion resistance of concrete containing nano-particles for pavement. Both nano-titanium and nano-silica were employed, respectively, to be as the additives. The relationship between the indices of abrasion resistance and compressive strength of concrete is obtained, which indicates that the abrasion resistance of concrete increases with increasing compressive strength.

In this study, the use of nano-silica with 99.5% silica content and average particle size of 15 nm as addition in concretes with different strength levels was considered. Besides, comparison between the influence of SF and NS on concrete performance was also addressed.

EXPERIMENTAL PROGRAM

The experimental program described herein is divided into two parts aiming at investigating the effect of NS addition on the properties of conventional and ultra-high performance concretes (UHPC).

Part 1: Effect of NS Addition on the Properties of Conventional Concrete

Materials
The cement used in this part was CEM I 32.5N produced by Amreyah Company. The cement had a Blaine fineness of 3300 cm^2/gm, a specific gravity of 3.15 and a 28-days compressive strength of 36 N/mm^2. Silica fume (SF) having a silica content of 96.5%, a specific gravity of 2.10 and a specific surface area of 20000 cm^2/gm was used. Nano-silica (NS) produced by M K Impex Co., Mississauga, Canada was used in the current study. The NS had silica content of 99.5%, specific gravity of 2.56 and average particle size of 15 nm. The fine aggregate used was natural sand with a fineness modulus of 2.66 and specific gravity of 2.63. The coarse aggregate used was crushed limestone with a maximum size of 20 mm and specific gravity of 2.58.

Mix proportions
Two sets of concrete mixes were prepared with different cement content (350 and 450 kg/m3) and water/cementitious materials ratios (w/cm) of 0.57 and 0.42. Each set is composed of seven mixes. The first mix is the control mix. The second and the third mixes contain 5.0 and 10.0 % SF. The fourth and the fifth mixes contain 2.5 and 5.0 % NS. The last two mixes contains both SF and NS (7.5% SF + 2.5 %NS and 5.0% SF + 5.0% NS). Both SF and NS are expressed as percent of cement weight and they are added as cement replacement. Details of mix proportions are given in Tables 1 and 2. The concrete mixes were prepared using a tilting drum mixer.

Mixing procedure
Trial mixes were carried out to determine the best method to disperse the NS uniformly in the concrete mix. Based on trial mixes results, the NS particles were stirred with half of mixing water at high speed (120 rpm) for 1 min. The coarse and fine aggregate were first charged in the mixer and pre-mixed with one-quarter of the water content (without NS) for about one minute, after which cement was added and mixed for additional one minute. Half of the mixing water (containing NS) was then added while mixing for one minute followed by the addition of SF in slurry form (if applicable). After mixing for 1.5 min, the rest of the water was added and the

concrete was mixed for two min. The total time required for mixing was about 8 min. After mixing, slump, air content measurements and slump loss up to 60 min were carried out.

Specimen preparation

Four types of specimens were made: 100x100x100 mm cubes, 150x300 mm and 75x150 mm cylinders, 100x100x500 mm prismatic beams and 75x75x285 mm prisms. Specimens were cast immediately after mixing in two layers, with each layer compacted on vibrating table. All specimens were exposed to identical curing conditions. After casting, specimens were covered with wet hessian and plastic sheets in the laboratory for 24 hrs, then demolded and cured in water at room temperature until testing age. The drying shrinkage specimens were water cured for 28 days and then allowed to air-dry during testing. Free calcium hydroxide was measured on paste specimens prepared by screening fresh concrete on No. 100 sieve.

Test Details

Compressive strength was measured using 100x100x100 mm cubes. Splitting tensile strength test followed the ASTM C 330 procedure. Flexural strength was measured in accordance with ASTM C 78 using 100x100x500mm beams. Static modulus of elasticity was measured according to ASTM C 469. Drying shrinkage measurements was carried out on75x75x285 mm prisms according to ASTM C 157.

Table 1: Mix proportions and fresh properties of concrete mixes having cement content of 350 kg/m^3.

Mix No.	Cement	Silica Fume	Nano Silica	Water	Sand	Coarse Aggregate	w/cm	Slump (mm)	Air Content (%)
CC-350	350	--	--	200	640	1100	0.57	130	1.40
SF1-350	332.5	17.5	--	200	630	1100	0.57	115	1.50
SF2-350	315	35	--	200	620	1100	0.57	110	1.65
NS1-350	341.25	--	8.75	200	635	1100	0.57	105	1.60
NS2-350	332.5	--	17.5	200	635	1100	0.57	80	1.75
C1-350	315	26.25	8.75	200	625	1100	0.57	70	1.80
C2-350	315	17.5	17.5	200	625	1100	0.57	65	1.85

Table 2: Mix proportions and fresh properties of concrete mixes having cement content of 450 kg/m^3.

Mix No.	Cement	Silica Fume	Nano Silica	Water	Sand	Coarse Aggregate	w/cm	Slump (mm)
CC-450	450	--	--	200	580	1100	0.42	125
SF1-450	427.5	22.5	--	200	570	1100	0.42	110
SF2-450	405	45	--	200	560	1100	0.42	90
NS1-450	438.75	--	11.25	200	580	1100	0.42	100
NS2-450	427.5	--	22.5	200	575	1100	0.42	70
C1-450	405	33.75	11.25	200	565	1100	0.42	60
C2-450	405	22.5	22.5	200	580	1100	0.42	55

Part 2: Effect of NS Addition on the Properties of Ultra-High Performance Concrete

Materials

Sulfate Resisting Cement produced by Alexandria Portland Cement Company was used in all mixes. The chemical compound compositions of cement were; 52.2% C_3S; 23.4% C_2S; 0.4% C_3A; and 14.9% C_4AF, with Blaine fineness of cement was 3250 cm^2/gm. Natural siliceous sand with grain size ranging from 0.15 to 0.6 mm and specific gravity of 2.65 was used in all mixes. This fine sand was obtained by screening the natural sand. Crushed quartz in a powder form with Blain fineness of 3100 cm^2/gm, and a specific gravity of 2.85 was incorporated. Locally produced quartz powder with a SiO_2 content of 98%, Blaine fineness of 3100 cm^2/gm, and a specific gravity of 2.85 was used. A superplasticizer namely Viscocrete 5400 complying with ASTM

C494 Type F was used. Viscocrete 5400 is an aqueous solution of modified polycarboxylate. The SF and NS are the same as the used in the first part.

Mix proportions
Two mixes were investigated in this part; their composition was based on previous work done by the author [8, 9]. Details of mix proportions are given in Table 3. The w/c ratios were 0.19 and 0.21. Nano-silica was added as cement replacement in percentages of 2.0, 4.0, 6.0 and 8.0% of cement weight.

Mixing, casting, and curing regimes
The NS particles were stirred with half of mixing water at high speed (120 rpm) for 1 min. Mixing was performed in a high speed-mixer to facilitate the dispersion of water and superplasticizer. Cement, sand, SF and quartz were pre-mixed for one minute, after which mixing water containing NS and half of the total amount of superplasticizer was added and mixing continued for two minutes, followed by one-minute rest. Second half of superplasticizer, diluted in an equal volume of water, was added followed by two minutes mixing, and one-minute rest. Final mixing was applied for two minutes. The total mixing time was nine minutes.

Small size specimens were used to meet the requirement of the compression-testing machine. The prepared specimens were 51x51x51 mm cubes for compression tests and 40x40x160 mm prisms for flexure tests. Specimens were compacted in successive layers using vibrating table. Specimens were maintained at ambient temperature during the setting process. All Specimens were demolded 24 hrs after mixing. Specimens were then subjected to different curing regimes. Two curing regimes were chosen based on previous work done by the author [8]. The first regime consists of water curing period of 3 days at ambient temperature, followed by heat treatment at 100°C for duration of 1 day. The second regime is similar to the first one, except that the heat treatment duration was extended to 3 days. Specimens were then tested 24 hrs after the completion of the curing regime.

Table 3: Composition of Ultra-high Performance Concrete mixtures.

Materials	Mix proportions (ratios by weight)		Mix proportions (kg/m^3)	
	A	**B**	**A**	**B**
Cement (C)	1.00	1.00	815	800
Silica fume (SF)	0.25	0.25	205	200
Water (W)	0.19	0.21	155	168
Sand(150-600μm) (S)	1.10	1.10	900	880
Milled quartz (Q)	0.40	0.40	325	320
Superplasticizer (Sp)	0.04	0.04	32.6	32
Water/Binder ratio	0.15	0.17	0.15	0.17

RESULTS AND DISCUSSION

Influence of NS on Properties of Conventional Concrete
The effect of addition of nano-silica (NS) on the fresh and hardened properties of conventional concrete is presented in the following section. Results are compared to concrete mixes containing silica fume (SF).

Effect on Fresh Properties
The slump and slump loss of different concrete mixes are given in Tables 1 and 2. No significant change was found in the density of fresh concrete due to the incorporation of NS. Reduced bleeding and increased cohesiveness of concrete was noticed during casting for concrete mixes containing high content of NS (i.e., 5.0 %). Similar to SF, the concrete slump was reduced considerably as the percentage of cement replaced by NS increased. Slump of mixes NS2-350 that contained 5.0% NS was about 60% of that for mix CC-350. High cement content concrete mixes (450 kg/m^3) showed similar trend to that of low cement content concrete mixes. Slump value of mix NS2-450, incorporating 5.0% NS, was 55% of the slump value of mix CC-450. This agrees well with Li et al. [7]. The effect of NS on slump reduction was higher than SF. The

addition of 5.0% NS decreased the slump value by 70% compared to mixes containing 10% SF. Preliminary mixes containing NS replacement percent of 10% were very sticky and could not be mixed. This indicates the need for increasing the water content to overcome the effect of NS in reducing the workability. In fact, each kilogram of NS added to the concrete increased the water demand by approximately 0.4 kilogram. This is due primarily to the extreme high surface area of NS particles.

The incorporation of SF and NS did not mitigate the slump reduction; on the contrary higher slump reduction was obtained, as seen from mixes C1-350 and C2-350. The air content of fresh mixes is given in Table 1. It is clear that the addition of NS increase the entrapped air in concrete mixes in amounts higher than that observed with SF. The air content of mix NS2-350 was higher than mix CC-350 by 25%. Besides, the incorporation of both SF and NS increased the air content, compared to mixes containing either SF or NS. The slump loss versus elapsed time of concrete mixes having cement content of 450 kg/m^3 is illustrated in Figure 1. It is clear that the slump loss followed the same order as the initial slump. However, the rate of slump loss was higher for mixes having higher initial slump value. The slump loss of mix CC-450 after 60 min was 70 % of its initial slump value. Mix NS2-450 incorporating 5.0% NS lost 60% of its initial slump. Mixes incorporating both SF and NS (e.g., C2-450) lost 55% of its initial slump value. The presented results revealed that the effect of NS is detrimental on the slump of concrete and its effect is more pronounced than SF.
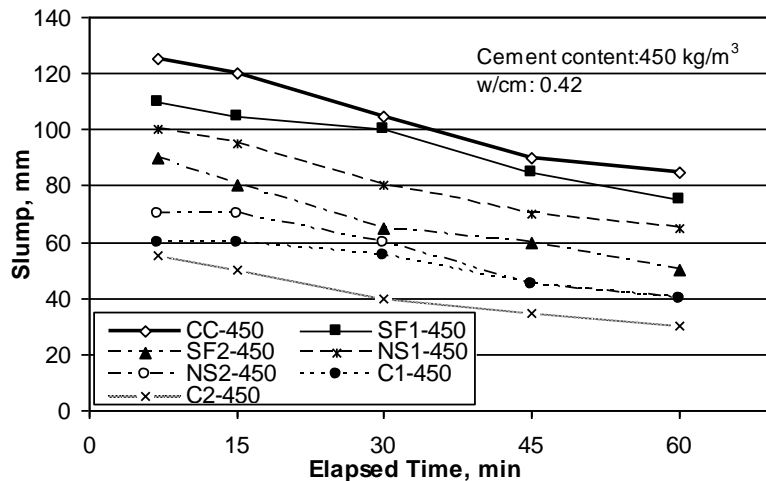

Fig. 1: Slump loss versus elapsed time for mixes having cement content of 450 kg/m^3.

Effect on Hardened Properties

The compressive strength for all concrete mixes at the ages of 1, 3, 7, 14, 21, 28, 56 and 90 days of water curing are listed in Tables 4 and 5. The splitting tensile strength of all concrete mixes at the ages of 1, 3, 7, 28, 56 and 90 days are also included in Tables 4 and 5. All results are illustrated in Figures 2 - 7. Results of flexural strengths at the ages of 3, 7, and 28 days and modulus of elasticity at 7 and 28 days are given in Table 6.

Table 4: Compressive and splitting tensile strengths of mixes having cement content of 350 kg/m^3.

Mix No.	Compressive Strength, MPa								Splitting tensile strength, MPa					
	1day	3days	7days	14days	21days	28days	56days	90days	1day	3days	7days	28days	56days	90days
CC-350	6.8	12.8	20.2	24.2	25.5	27.0	28.2	30.2	0.61	1.15	1.82	2.43	2.54	2.72
SF1-350	7.2	12.9	22.0	28.9	30.4	33.3	34.5	35.1	0.64	1.16	1.96	2.70	2.80	2.85
SF2-350	7.8	13.6	24.4	31.3	32.3	34.6	36.6	38.6	0.71	1.22	2.22	2.79	2.72	3.13
NS1-350	8.5	15.8	27.4	29.8	31.4	33.3	35.4	36.8	0.77	1.31	2.22	2.69	2.87	2.98
NS2-350	9.2	17.6	29.0	33.5	33.5	35.3	37.2	38.5	0.83	1.59	2.44	2.86	3.16	3.20
C1-350	9.8	17.6	31.3	34.3	34.7	36.9	38.8	40.1	0.92	1.66	2.66	3.14	3.30	3.41
C2-350	10.5	18.8	32.9	36.7	37.1	38.5	40.6	42.7	1.04	1.87	2.93	3.43	3.62	3.74

Table 5: Compressive and splitting tensile strengths of mixes having cement content of 450 kg/m³.

Mix No.	Compressive Strength, MPa								Splitting tensile strength, MPa					
	1day	3days	7days	14days	21days	28days	56days	90days	1day	3days	7days	28days	56days	90days
CC-450	9.7	18.2	28.8	34.5	36.4	38.5	41.0	43.1	0.98	1.85	2.92	3.90	4.15	4.37
SF1-450	10.2	18.4	31.3	38.5	40.9	45.0	47.8	50.3	1.04	1.86	3.15	4.34	4.36	4.58
SF2-450	11.2	19.4	36.2	44.8	46.2	49.2	50.8	55.1	1.09	1.89	3.42	4.30	4.20	4.82
NS1-450	13.5	23.1	41.7	42.5	44.9	47.5	50.6	52.6	1.19	2.02	3.42	4.16	4.51	4.60
NS2-450	14.5	26.0	45.2	47.8	47.9	50.4	51.8	53.9	1.28	2.45	3.77	4.41	4.60	4.94
C1-450	15.3	26.9	47.5	51.2	53.1	54.6	57.4	60.1	1.36	2.44	3.92	4.61	4.85	5.01
C2-450	16.7	29.3	49.7	52.0	57.7	58.6	60.2	62.0	1.45	2.62	4.11	4.67	5.07	5.19

Figure 2 (a) shows the effect of NS on the compressive strength of concrete containing 350 kg/m³ up to the age of 7 days. Results are compared to conventional mixes and mixes incorporating SF. As seen from the Figure, strengths of NS concretes are higher than the control mix. This is noticeable in Figure 2 (b) which represents mixes with high cement content and low w/c ratio. Concrete strength increased with increased NS content. At the age of one day, mix NS2-350 that contains the highest amount of NS (5.0%) exhibited a strength improvement that was about 35 % over the strength of the control mix (CC-350). At the same age, mix NS2-450 containing 5.0% NS showed strength improvement of 50% over the control mix (CC-450). Mixes containing 2.5 % NS also showed a strength gain over the control mix. This gain was more pronounced for mix with high cement content (NS1-450), where percentage gains of about 40 % was achieved. The gain for low cement content mix (NS1-350) was 25%. On the other, hand, SF concretes showed strength enhancement over the conventional concrete, but with lower percent gain than the NS concretes. Mixes incorporating 10% SF exhibited a strength improvement of 15% over conventional concretes. Physical mechanism of SF plays the major role at that age. By the age of 3 days, the same trend is observed, where mixes containing NS manifested higher strength. At the age of 7 days, NS mixes continued their higher strength gain over conventional concrete and SF concretes. Mix NS2-450 showed the highest strength improvement of 60%, compared to the control mix (CC-450). Silica Fume mixes also showed a strength improvement of 25 % over conventional concrete. It is clear that the strength enhancement due to the incorporation of SF achieved higher gain at the age of 7 days compared to that of 1 and 3 days. Mixes containing both SF and NS exhibited the most strength improvement over the strength of either SF or NS concretes; with higher efficiency for mixes incorporating 5.0 % SF and 5.0 % NS (see Tables 3 and 4). This is noticeable from the age of one day. At 7 days, mix C2-350 exhibited a strength improvement that was about 60 % over the strength of the control mix (CC-350). Similarly, mix C2-450 manifested a strength improvement that was about 70 % over the strength of the control mix (CC-450). It is clear that the effect of NS in improving concrete strength begins at early ages.
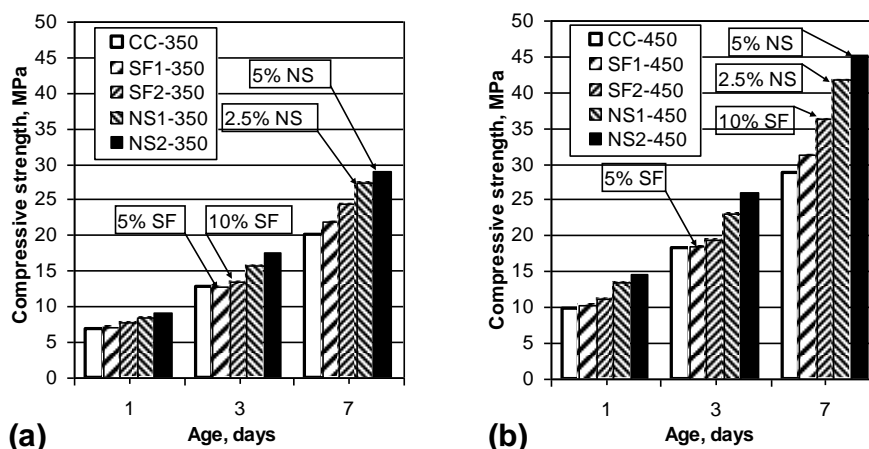
Fig. 2: Effect of NS on compressive strength development; (a) mixes with cement content 350kg/m³, and (b) mixes with cement content 450kg/m³

Figures 3 and 4 shows the compressive strength of all mixes up to the age of 90 days. Up to the age of 7 days, the highest compressive strength was shown by mixes incorporating both SF and NS, followed by mixes containing NS and the mixes containing SF in that order. At the age of 14 days, the order begins to change, where mixes SF2-350 and SF2-450 containing 10% SF exhibited higher compressive strength of 5.0% than mixes NS1-350 and NS1-450, respectively.
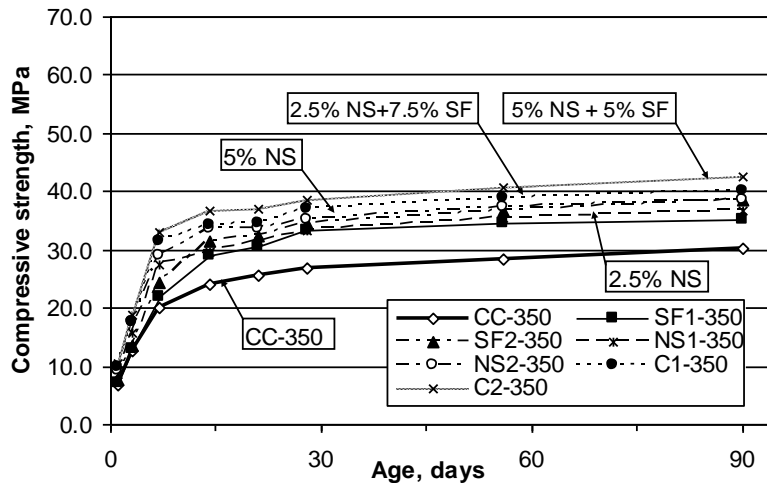

Fig. 3: Effect of NS on compressive strength development for different mixes having cement content of 350kg/m³.

By the age of 28 days, the percentages of strength enhancement were 42%, 36%, 30%, 23%, 28% and 23% for C2-350, C1-350, NS2-350, NS1-350, SF2-350 and SF1-350, respectively over the strength of control mix (CC-350). Mixes having cement content of 450 kg/m³ exhibited similar behavior. The effect of SF in improving concrete strength seems to be at maximum beginning from the age of 14 days. This will discussed later based on the residual quantity of calcium hydroxide. By the age of 90 days, the rate of strength development in NS mixes seems to be minimal, as may be seen from Figures 2 and 3. Meanwhile, mixes containing both SF and NS (e.g., C2-350 and C2-450) achieved the highest strength level among other mixes, profiting from the early strength gain of NS and late strength gain of SF. Thus, it may be stated that the maximum benefit of using NS in concrete regarding strength enhancement may be achieved at early ages.
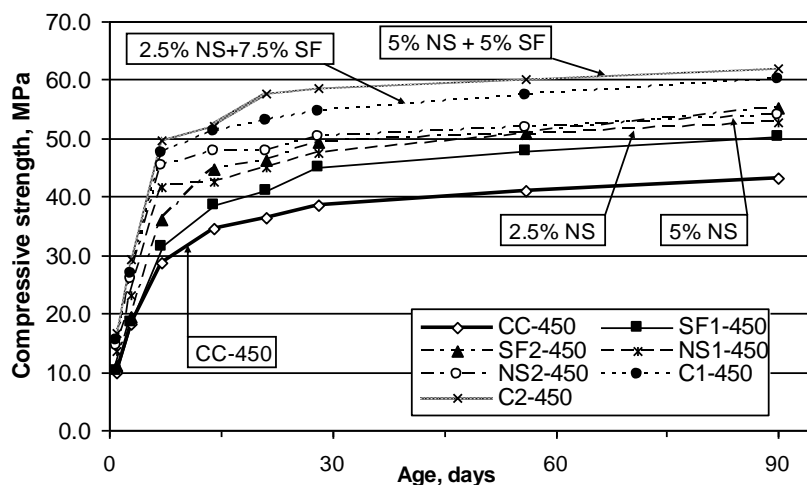

Fig. 4: Effect of NS on compressive strength development for different mixes having cement content of 450kg/m³.

Results of splitting tensile strength tests varied in the same manner as compressive strength but with less degrees of enhancement (see Tables 4 and 5). In concrete NS2-350 improvements up to 34% in splitting tensile strength at 7 days over the control mix (CC-350) was achieved as compared to 43% in case of compressive strength. Mix NS2-450 enhancement up to 29% in splitting tensile strength at 7 days was shown as compared to 55% in case of compressive strength. At the age of 28 days, the effect of NS on the splitting tensile strength was reduced. For instance, mix NS2-450 only showed a percent enhancement of 13% in splitting tensile strength over control mix. Silica fume mixes exhibited similar behavior. Accordingly, mixes incorporating both SF and NS manifested also the same trend. Results indicated that splitting tensile strength to compressive strength ratio at 28 days was about 11% for conventional concrete and was reduced to 8.0 % for mixes containing 5.0% NS.

The flexural strengths for all mixes at the ages of 3, 7 and 28 days are given in Table 6. As expected, results of the flexural strength tests varied in the same manner as splitting tensile strength, as seen from Table 6. Mix NS2-350 incorporating 5.0% NS showed strength enhancement of 35% and 15% over the control mix (CC-350) at ages of 7 and 28 days, respectively. Mix C2-350 containing 5.0% SF and 5.0% NS exhibited strength improvement of 40% and 28% over the control mix at ages of 7 and 28 days, respectively. Mix NS2-450 showed strength improvement of 20% and 11% over control mix CC-450 at ages of 7 and 28 days, respectively. Similarly, mix C2-450 showed strength enhancement of 38% and 30% over control mix CC-450 at ages of 7 and 28 days, respectively. It is clear that the maximum benefit of using NS is through its incorporation with SF. Results indicated that the flexural strength to compressive strength ratio at 28 days was 15% and 12% for CC-350 and CC-450 (control mixes), respectively. These ratios were 12% and 10% for mixes NS2-350 and NS2-450, respectively.

Thus, it can be stated on a quantitative basis that for NS mixes the increase in splitting tensile strength and flexural strength are less pronounced than that in compressive strength. The reduction in strength ratio observed for splitting tensile strength and flexural strength is expected. This may be related to the content of nano-particles. When NS is incorporated, the workability of concrete is reduced, leading to increase the number of micro-cracks in concrete and weak zones, which results in the decrease of tensile strength of concrete.

The modulus of elasticity for all mixes at the ages of 7 and 28 days are shown in Table 6.at the age of 7 days, the modulus of elasticity for mix NS2-350 was higher than that for mix CC-350 by about 1.5 GPa (7%). However, this difference increased slightly with age. At the age of 28 days, the static modulus of mix NS2-350 became higher than that for CC-350 by 1.7 GPa. Comparing the static modulus of the high cement content concretes CC-450 and NS2-450 gives similar conclusion. Besides, the static modulus of mix C2-350 became higher than that for CC-350 by 1.8 GPa and 2.5 GPa at the ages of 7 and 28 days, respectively. This confirms the conclusion made above regarding the higher performance for mixes incorporating both SF and NS.

Table 6: Flexural strength and Modulus of Elasticity of mixes having cement content of 350 and 450 kg/m³.

Mix No.	Flexural Strength, MPa			Modulus of Elasticity, GPa		Mix No.	Flexural Strength, MPa			Modulus of Elasticity, GPa	
	3days	7days	28days	7days	28days		3days	7days	28days	7days	28days
CC-350	2.3	3.03	4.14	21.6	24.2	CC-450	2.81	3.74	4.71	22.6	27.6
SF1-350	2.32	3.27	4.25	21.1	25.3	SF1-450	2.83	3.63	4.58	23.2	27.8
SF2-350	2.44	3.7	4.65	21.6	25.6	SF2-450	2.89	4.21	5.15	25.3	29.8
NS1-350	2.62	3.7	4.49	22.5	24.9	NS1-450	3.2	4.11	4.88	23.2	27.1
NS2-350	3.18	4.07	4.76	23.1	25.9	NS2-450	3.88	4.52	5.27	24.0	29.4
C1-350	3.17	4.23	4.88	22.4	26.1	C1-450	3.87	4.79	5.71	25.3	30.3
C2-350	3.39	4.24	5.30	23.4	26.7	C2-450	4.14	5.18	6.13	25.9	31.3

Results of drying shrinkage tests of control mix CC-450, SF mix SF2-450, NS mix NS2-450 and SF-NS mix C2-450 after 28 days of water curing are illustrated in Figure 5. The drying shrinkage in SF and NS concretes were similar to that of control concrete up to 90 days. This was expected for SF concrete, where SF content up to 10 percent by mass of cement has no

influence on shrinkage of concrete. Tests results showed that the incorporation of NS in concrete did not have any significant effect on the drying shrinkage over control mix.
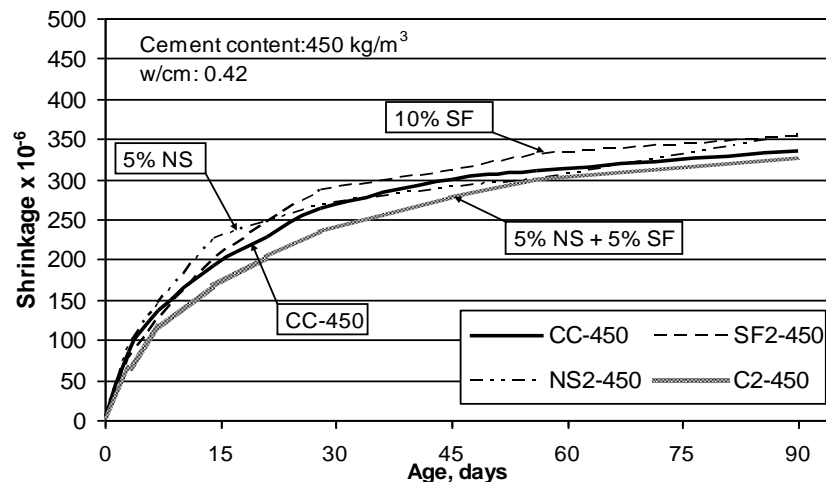

Fig. 5: Effect of NS on drying shrinkage of different mixes having cement content of 450kg/m^3.

The extent of a pozzolanic reaction can be followed by monitoring the decrease in calcium hydroxide. The amorphous or glassy silica reacts with calcium hydroxide formed from calcium silicate hydration. From quantitative analysis, a distinct reduction in the content of calcium hydroxide was monitored at the age of one day for mixes incorporating NS. This was also the case for SF mixes but with slower reduction rate. At the age of 14 days, the contents of calcium hydroxide for SF and NS concretes were quite similar. Mixes incorporating both SF and NS gathered both behaviors and expressed the lowest calcium hydroxide among other mixes since the age of one day up to 28 days. The contents of calcium hydroxide remaining in the paste specimens at the age of 28 days were in the order: C2-450 (1.29%), C1-450 (1.54%), NS2-450 (1.97%), SF2-450 (2.10), NS1-450 (2.22%) and SF1-450 (2.59%). The content of calcium hydroxide in the control mix (CC-450) at the age of 28 days was about 7.0%. The main effects of pozzolanic reaction are strength development and smaller pore-size distribution. Jo et al. [10,11] reported similar behavior for NS pastes.

It can be stated that the compressive strength was developed in concretes containing NS particles in every case higher than that of control concrete. The highest strength development was observed in concretes with low w/c ratio and high cement content. Results of splitting tensile strength, flexural strength and static modulus of elasticity listed above confirm the positive effect of NS. The difference in the strength development of the investigated concretes can be attributed to the pozzolanic reaction. As mentioned above, NS are thought to be more effective in pozzolanic reaction than SF. This was confirmed through the free lime content measurements. In addition, the NS would fill the pores to increase the concrete strength, as silica fume does. Therefore, it may be stated that the addition of NS to concretes improves their strength characteristics. The strength of the concretes was found to increase as the NS content increased from 2.5% to 5.0%. However, it should be noted that using higher content of NS must be accompanied by adjustments to the water and superplasticizer dosage in the mix. Otherwise, using this much quantity of NS could actually lower the strength of composites instead of improving it [10], although this finding was not observed in this study. The alternative solution proposed by the current study of incorporating both SF and NS confirmed its effectiveness in improving the performance of concrete.

Influence of NS on Properties of Ultra-High Performance Concrete

The effectiveness of NS in rich concretes (mixes with high cement content and low w/c ratio) supports its use in ultra-high strength cement composites. One of the most suitable applications is the Ultra-high Performance Concrete also known as 'Reactive Powder Concrete' (RPC) and under trade name "DUCTAL". In the following, the effect of adding NS as cement replacement

on the compressive and flexural strengths of UHPC will be evaluated. Nano-silica was added in percentages of 2.0, 4.0, 6.0 and 8.0% of cement weight.

The effect of NS on the strength of UHPC are given in Table 7 and illustrated in Figures 6 and 7. The strength ratio, which is the ratio between the flexural strength and the compressive strength, is also given in Table 7. Different parameters were introduced in investigating the influence of NS addition on the strength of UHPC. Based on the compressive strength of control mixes without NS, it is clear that the compressive strength of mix A, characterized by lower w/c ratio, is higher than mix B. For instance, mix A was higher than mix B by 8.0% (14 MPa) under curing regime (I). The difference was 11% (18.1MPa) under curing regime (II). As expected, the curing regime (II) was more effective on the strength than curing regime (I). This is due to the prolonged duration of heat treatment adopted in the second curing regime (3 days). These parameters also showed an effective influence on the flexural strength and the strength ratio. However, it is clear that the mix composition is more significant than the curing regime. For mix A the strength ratio ranged between 0.163 and 0.165. This ratio was reduced and ranged between 0.140 and 0.143 for mix B. Besides, it is obvious that the curing regime (II) enhances the flexural strength of UHPC, consequently the strength ratio; however, it is of secondary effect.

Figure 6 illustrates the effect of NS as cement replacement (expressed as percent of cement weight) on the compressive strength of UHPC. It is clear that the addition of NS enhanced the strength of UHPC. The strength enhancement was related to the mix proportions and the applied curing regime. Mix A undergoing curing regime (I) showed strength enhancement and attained a max value at 6.0% NS. At higher percent replacement, the strength decreased to a level lower than the control mix. Similar trend was exhibited when subjected to curing regime (II), but with the highest strength at 4.0% replacement. Mix B subjected to curing regime (I) exhibited maximum strength improvement at 4.0% NS; however, mix containing 6.0% NS showed comparable strength value. Besides, mix B containing 8.0% NS exhibited the lowest strength value among all mixes. The curing regime (II) also enhanced the strength of mix B over the curing regime (I). The highest improvement in strength was exhibited by mix incorporating 6.0% NS; however, comparable results was shown by mix containing 4.0% NS. Based on the overall trend illustrated in Figure 6, it is clear that the highest strength enhancement is achieved at 4.0% NS. The highest compressive strength value was 234.7 MPa, this was attained by mix A undergoing the second curing regime. This value is higher than that recorded by the control mix by 20% (40.2MPa).

Table 7: Effect of NS addition on the compressive and flexural strengths of UHPC mixes under different curing regimes.

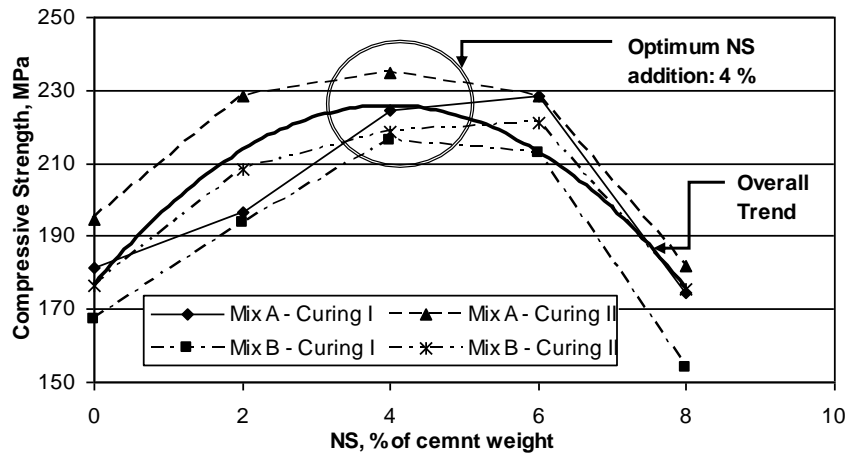| Mix Designation	Curing Regime	NS (% of cement weight)	Compressive Strength, MPa	Flexural Strength, MPa	Strength Ratio	Curing Regime Details
A	I	0.0	181.3	29.6	0.163	Three days water curing and one day heat treatment at 100º C
		2.0	196.7	29.9	0.152	
		4.0	224.6	33.3	0.148	
		6.0	228.5	35.7	0.156	
		8.0	174.4	23.6	0.135	
	II	0.0	194.5	32.1	0.165	Three days water curing and three days heat treatment at 100º C
		2.0	228.3	35.6	0.156	
		4.0	234.7	39.4	0.168	
		6.0	228.4	34.6	0.151	
		8.0	181.7	29.0	0.160	
B	I	0.0	167.2	23.4	0.140	Three days water curing and one day heat treatment at 100º C
		2.0	193.4	31.4	0.162	
		4.0	216.2	32.2	0.149	
		6.0	212.6	31.6	0.149	
		8.0	154.1	18.3	0.119	
	II	0.0	176.4	25.3	0.143	Three days water curing and three days heat treatment at 100º C
		2.0	208.4	33.2	0.159	
		4.0	218.8	35.8	0.164	
		6.0	221.3	33.8	0.153	
		8.0	175.4	21.3	0.121	

Fig. 6: Effect of NS on compressive strengths of UHPC under different curing regimes.

Figure 7 illustrates the effect of NS as cement replacement on the flexural strength of UHPC. It is clear that the addition of NS improved the flexural strength of UHPC. However, the improvement was lower than that observed for the compressive strength. The effect of different parameters on the flexural strength is similar to the compressive strength. The lowest flexural strength was recorded for mix B subjected to curing regime (I) at different NS percentage. The highest flexural strength was achieved by mix B subjected to curing regime (II) and containing 4% NS. The percent enhancement in flexural strength was 22.0% (7.3 MPa) over the highest value expressed by the control mixes. Based on the overall trend illustrated in Figure 6, it is clear that the highest strength enhancement is achieved at 4.0% NS. The strength ratio given in table 7, gives a better understanding on the effect of NS addition on the flexural strength. It is clear that the addition of NS with percentage higher than 6.0% is detrimental to the flexural strength. Strength ratio of 0.135 was manifested by mix A subjected to curing regime (I) and containing 8.0% NS. Lower strength ratios were exhibited by mix B containing 8.0% NS under both curing regimes. In other words, UHPC mixes containing high water content (mix B) showed the lowest strength improvement. This result is in sharp contrast with the general well-known trend in conventional concrete. Besides, it was observed during mixing that the presence of NS improves the workability of UHPC mixtures. Many authors when incorporating SF in UHPC mixes recorded similar observation [9, 12]. This was explained based on the enhancement of rheological characteristics of UHPC by the lubricating effect resulting from the perfect sphericity of the silica fume particles. This explanation may be adopted for NS.
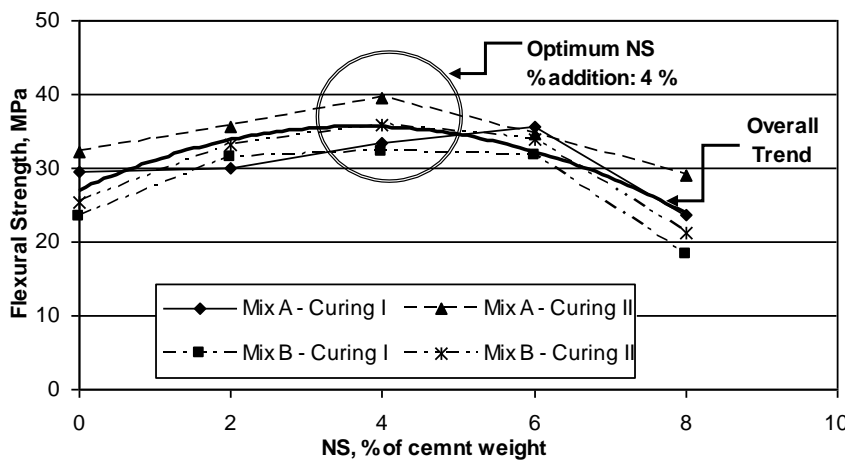

Fig. 7: Effect of NS on flexural strengths of UHPC under different curing regimes.

In the light of the experimental data, the optimum content of NS in UHPC may be in the ranges of 4.0 – 6.0% of the weight of cement. Based on the results reported by Yazici et al. [13], the efficiency of NS over other mineral admixtures is obvious, where autoclave was applied to achieve similar strength level to that attained in this study by NS. The effectiveness of NS in enhancing the strength under prolonged heat treatment (3 days) is without doubt due to the high pozzolanic activity of NS.

CONCLUSIONS

Based on the study reported here, the following conclusions may be drawn:

1. Concrete workability was reduced due to the increase in the percentage of cement replaced by nano-silica. Nano-silica concrete requires additional amount of water to overcome such adverse effect. It was observed throughout the study that each kilogram of NS added to the concrete increased the water demand by approximately 0.4 kilogram.
2. Nano-silica addition results in a significant early increase in compressive, splitting tensile and flexural strengths of concrete. The improvement was more pronounced in case of high cement content low w/c ratio concrete
3. According to the results obtained, the addition of 5.0 percent nano-silica is suggested. This may lead to an increase in the 7-day compressive strength of low cement content and high cement content concretes by up to 45 % and 55 %, respectively, over the strength of comparable concretes without nano-silica.
4. Addition of both silica fume and nano-silica by total amount of 10 %, may lead to an increase in the 28-day compressive strength of low cement content and high cement content concretes by up to 40 % and 50 %, respectively, over the strength of comparable concretes.
5. The pozzolanic contribution of nano-silica becomes significant from the very early age, compared to silica fume, which begins its pozzolanic reactivity at the age of 7 days or later. This mechanism explained the outstanding mechanical performance of nano-silica concrete, which is a significant advantage over silica fume and is especially important in the pre-cast industry.
6. The increase in splitting tensile and flexural strengths of nano-silica concrete is less pronounced than that in compressive strength.
7. The drying shrinkage in nano-silica concretes was comparable to that of control and silica fume concretes up to 90 days.
8. Test results showed that nano-silica may be applied successfully in ultra-high performance concrete, where strength level over 230 MPa was achieved.
9. Prolonged heat treatment (up to 3 days) is beneficial in accelerating the pozzolanic reaction of ultra-high performance concrete incorporating nano-silica.

It is too early to predict the future of nano-silica or nanomaterials at large in concrete. Further work is strongly recommended to achieve better understanding of its performance and durability aspects.

REFERENCES

1. Richardson, I.G. (2000), "The Nature of the Hydration Products in Hardened Cement Paste", Cement and Concrete Composites, 22, pp. 97–113.
2. Zhang, X.Z. (2000), "Nanostructure of Calcium Silicate Hydrate Gels in Cement Paste", Journal of American Ceramic Society, 83 (10), pp. 2600-2604.
3. Ye, Q. (2001), "Research on the Comparison of Pozzolanic Activity between Nano-SiO$_2$ and Silica Fume", Concrete, 3, pp. 19-22.
4. Chen, R.S. and Ye, Q. (2002), "Research on the Comparison of Properties of Hardened Cement Paste between Nano-SiO$_2$ and Silica Fume Added", Concrete, 1, pp. 7-10.
5. Ji, T. (2005), "Preliminary Study on the Water Permeability and Microstructure of Concrete Incorporating Nano-SiO$_2$", Cement and Concrete Research, 35, pp. 1943-1947.
6. Qing, Y., Zenan, Z., Deyu, K. and Rongshen, C. (2007), "Influence of Nano-SiO2 Addition on Properties of Hardened Cement Paste as Compared with Silica Fume", Construction and Building Materials, 21, pp. 539-545.

7.   Li, H., Zhang, M. and Ou, J. (2006), "Abrasion Resistance of Concrete Containing Nano-Particles for Pavement", Wear, 260, pp. 1262-1266.

8.   El-Hefnawy, A. and Abbas, R. (2003),"Effect of Curing Conditions on The Performance Of Reactive Powder Concrete", Proceeding of The International Conference on Performance of Construction Materials in The New Millennium, Cairo, Egypt, February 18-20.

9.   Kurdi, A., Khoury, S. and Abbas, R. (2001), "A new concrete for the 21 century: reactive powder concrete", Alexandria Engineering Journal, 40 (6), pp. 893-909.

10. Jo, B., Kim, C. and Lim, J-H. (2007) "Characteristics of Cement Mortar with Nano-SiO2 Particles", ACI Materials Journal, 104, July-August, pp. 404-407.

11. Jo, B., Kim, C., Tae, G. and Park, J. (2007) "Characteristics of Cement Mortar with Nano-SiO_2 Particles", Construction and Building Materials, 21, pp. 1351-1355.

12. Dugat, J., Roux, N. and Bernier, G. (1996) "Mechanical Properties of Reactive Powder Concretes", Materialsand Structures, 29 (May), pp. 233-240.

13. Yazıcı, H., Yardımcıa, M. Y., Aydına, S., Karabuluta A. (2008), "Mechanical Properties of Reactive Powder Concrete Containing Mineral Admixtures under Different Curing Regimes" Construction and Building Materials Journal, available online since July 2008, doi:10.1016/j.conbuildmat.2008.08.003.

EVALUATION OF VARIOUS PROPERTIES OF CERAMIC FLOOR GLAZED TILES

Dr. Hanan A. El Nouhy
Researcher, Housing and Building National Research Center, Cairo, Egypt
Email: elnouhy66@yahoo.com

ABSTRACT

This study aims at evaluating the various properties of ceramic floor tiles from the Egyptian local market. Fifteen factories are registered at the Egyptian Industrial Union-Construction Material Chambers- Ceramic Department. Test specimens were obtained from the local market for the fourteen factories during three months period (January till March 2008). The specimens were all "of first choice" type. The specimens were tested to determine water absorption, apparent porosity, apparent relative density and bulk density. Evaluation of modulus of rupture, breaking strength, resistance to surface abrasion for glazed tiles as well as coefficient of friction were carried out according to both ESS (Egyptian standards Specifications) and ISO (International Organization for Standardization). Test results indicated that most of the factories satisfy the requirements of both ESS and ISO for modulus of rupture and breaking strength. The resistance to surface abrasion for specimens from the fourteen factories was classified as Class 3. The dynamic coefficient of friction was in the range of 0.26μ to 0.66μ.

Keywords: ceramic floor, glazed tiles, absorption percentage, modulus of rupture, abrasion resistance, dynamic coefficient of friction.

INTRODUCTION

A survey of the different ceramic factories was carried out in order to obtain specimens for evaluation. Concerning water absorption, there are two very common test protocols for measuring the water absorption of ceramic tiles. In the United States, test procedure ASTMC373 "Standard Test Method for Water Absorption, Bulk Density. Apparent Porosity, and Apparent Specific Gravity of Fired Whiteware Products," as designated by the American Society for Testing and Materials (ASTM). The other common test procedure is ISO10545 -3 "Determination of water absorption, apparent porosity, apparent relative density and bulk density," as designated by the International Standards Organization (IS0). [1]

Technologists apply the name whitewares to fine ceramic products and the term simply reflects the fact that most of the products are white (or near white) in color. Ware is technical name for a ceramic object that is solid in commerce. Whitewares are distinguished or classified in commerce according to technical subgroups based on use. The classifications are also correlated with the amount of void space in the fired ceramic, which is called its porosity. In the historical development of traditional ceramics, porosity was measured indirectly as water absorption expressed as a percentage of the dry weight.

The general relationship in whitewares is that low porosity associated with high mechanical strength, high resistance to breakage, and excellent durability.

Whitewares products may be glazed to increase their utility and improve their appearance. A glaze is a glass coating formed by melting or fusing an applied particulate mass over all or part of the ceramic wares surface.

Glazes provide a smooth surface that can easily be cleaned, and they also prevent water from

being absorbed by the product, promoting sanitation and improving performance. [2]

Countless instruments and techniques have been invented to measure the adherence of the resistance to the slippery. Among the existent systems, stands out the English system denominated TORTUS, that measures the dynamic coefficient of friction according to the ISO/DIS 10545-17 standard, method A. This system has been relatively well accepted for different applications of industrial interest. [3]

The Italian law sets 0.4 as the minimum dynamic coefficient of friction for public areas [4]. Carani et al had suggested that COFs (coefficient of friction) of 0.3 and 0.5 should be the minimum acceptable values for antislip tiles respectively. [4]

MATERIALS AND METHODS

The ceramics used in this study were glazed floor tiles obtained from the Egyptian local market. Each sample consisted of twenty tiles and represented a factory.

Three tests were carried on the samples according to both the ESS (Egyptian Standard Specifications) 293 and ISO(International Organization for Standardization) 10545 as the methods of the three tests according to both standards are the same. The three tests are as follows; determination of water absorption, apparent porosity, apparent relative density and bulk density, determination of modulus of rupture and breaking strength, and determination of resistance to surface abrasion for glazed tiles.

The determination of coefficient of friction was carried out according to (ISO/DIS 10545-17).

The test method for determination of water absorption, apparent porosity, apparent relative density and bulk density was carried out according to ISO 10545-3 [5] and ESS 293-1 [6]. The significance of determining the water absorption of the ceramic tiles is that based on the value of water absorption, the limits of breaking strength, and modulus of rupture of the specimens is specified according to ISO 13006 [7] and ESS 3168 [8-12]. The thickness of the specimens is also taken into account when determining the limits of breaking strength and modulus of rupture. In other words, both water absorption and thickness of the specimen are the two criteria that determine the limits of breaking strength and modulus of rupture of the specimens. The sample of each type of tile under test consisted of 10 whole tiles. According to IS0 10545-3 and ESS 293-1, there are two methods to determine the water absorption: Boiling method and the vacuum method. Specimens were tested according to the vacuum method. Apparent porosity, relative density and bulk density were also determined for the samples in order to meet the requirements of both standards (ESS and IS0).

The determination of modulus of rupture and breaking strength was according to ESS 293-10 [13] and ISO10545-4 [14]. Breaking strength is defined as follows: (force obtained by multiplying the breaking load by the ratio (span between support rods)/(width of the test specimen). It should be noted that the breaking strength is expressed in newtons. Seven test specimens were tested for each sample.

The resistance to surface abrasion for glazed tiles used for floor covering was carried out according to ESS 293-3 and ISO 10545-7. The test is carried out by rotation of an abrasive load on the surface and assessment of the wear by means of visual comparison of abraded test specimens and non-abraded tiles. Eleven test specimens were tested for each sample. In addition, eight test specimens were required for the visual assessment. The procedure requires one test specimen for each state of abrasion (and accordingly classifies the tiles according to the corresponding class), and subsequently an additional three test specimens to check the result at the visual-failure point.

The dynamic coefficient of friction is measured by means of a slider moving at constant speed over a horizontal surface. A portable self-powered mobile apparatus traverses tiles across the surface to be tested. A friction foot of 4S rubber under a fixed load is used to measure the dry and wet dynamic coefficient of friction. The slides moved over four different paths, each path was 1m in length. Two paths were for the dry dynamic coefficient of friction and two paths were for the wet dynamic coefficient of friction. For each path, five readings were recorded. Both the wet and dry average coefficient of friction of each individual test path as well as the overall wet and dry average was reported. A sufficient number of test tiles to allow a path of 1 m is required. The tiles are placed as close together as is possible to provide an even flat test path. As mentioned earlier, the test was carried out according to ISO/DIS 10545-17.

TEST RESULTS AND ANALYSIS

Water absorption, apparent porosity, apparent relative density and bulk density.

Test results of water absorption, apparent porosity, apparent relative density and bulk density are shown in table 1. The results show that water absorption of the ceramics samples obtained from the different factories ranged from 1.54% to 9.22%. It should be noted that the vacuum method fills almost all the open pores.

The test was carried out as follows; the tiles were placed vertically, with no contact between them, in the vacuum chamber. Pressure was evacuated to (10±1) kPa and maintained for 30 minutes. Then, while maintaining the vacuum, sufficient water was admitted slowly to cover the tiles by 5cm. The vacuum was released and the tiles were allowed to remain submerged for 15 minutes. Tiles were placed on a flat surface and lightly dried in turn.

Immediately after this procedure, tiles wereweighed and the results were recorded to the same accuracy as for the dry state.

After impregnation under vacuum of the test specimens, the mass of each specimen was determined while suspended in water. Weighing was carried out by placing the specimen in a wire loop halter, or basket that is suspended from one arm of the balance. Before actually weighing, the scale was counterbalanced with the wire loop in place and immersed in water to the same depth as is used when the specimens are in place.

The apparent porosity is the relationship of the volume of the open pores of the test specimen to its exterior volume. The apparent porosity results ranged from 5.81% to 18.84% for the samples from the various factories.

The apparent relative density of the impervious portion of the test specimen ranged from 2.23 to 2.46.

The bulk density of a specimen is the quotient of its dry mass divided by the exterior volume, including pores. The results ranged from 1.75g/cm^3 to 1.99gm/cm^3.

Figure 1 shows the relationship between water absorption and apparent porosity with respect to the fourteen factories. The ratio between water absorption and apparent porosity was 0.33 to 0.49.

Table 1: Test results of water absorption, apparent porosity, apparent relative density and bulk density

Factories	Absorption (%)	Apparent porosity (%)	Apparent density	Bulk density (gm/cm^3)
1	6.90	17.84	3.16	2.59
2	6.18	14.44	2.74	2.35
3	5.59	17.04	3.68	3.04
4	5.85	14.56	2.91	2.48
5	5.70	12.33	2.47	2.16
6	4.10	9.07	2.43	2.21
7	5.42	11.84	2.48	2.19
8	4.08	8.95	2.41	2.20
9	3.69	8.20	2.42	2.22
10	5.31	11.87	2.54	2.23
11	1.54	3.52	2.37	2.29
12	4.25	9.52	2.47	2.24
13	2.49	5.81	2.47	2.33
14	9.22	18.84	2.52	2.04

As mentioned earlier, the limits of breaking strength and modulus of rupture depends on both water absorption and thickness of specimen.

Table 2 shows the limits of breaking strength and modulus of rupture for dry-pressed ceramic tiles according to ISO13006 and ESS3168.
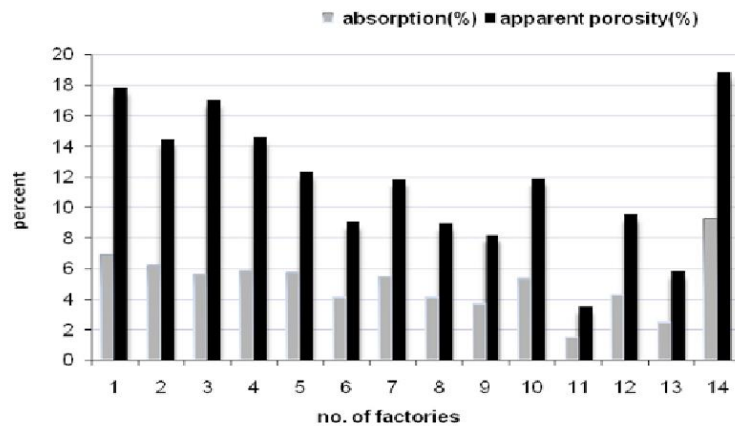
Fig 1: Relationship between absorption , and apparent porposity for the fourteen factories

Table 2: limits of breaking strength and modulus of rupture

Water absorption (%)	Thickness (mm)	Breaking strength (N)	Modulus of rupture (N/mm²)
0.5<E≤3	a) ≥7.5mm	Not less than 1100	Minimum average 30
	b) <7.5mm	Not less than 700	Individual minimum 27
3<E≤6	a) ≥7.5mm	Not less than 1000	Minimum average 22
	b) <7.5mm	Not less than 600	Individual minimum 20
6≤E≤10	a) ≥7.5mm	Not less than 800	Minimum average 18
	b) <7.5mm	Not less than 500	Individual minimum 16

The results of breaking strength and modulus of rupture are shown in table 3. The results were as follows:

Factory 1 did not satisfy the requirement of the breaking strength but met the requirements of the modulus of rupture. Factories numbers 2, 3 and 4 did not meet the requirements of both breaking strength and modulus of rupture. Factories numbers 5 to 14 satisfied the requirements of both breaking strength and modulus of rupture.

Figures 2 and 3 show that the relationship between the breaking strength and modulus of rupture with respect to the factories.

Abrasion resistance

The test results are given in table 3.According to Annex (N) in IS0 13006:1998, class 3 classification is suitable for floor coverings in areas that, with normal footwear, are walked on more often with small amounts of scratching dirt (for example residential kitchens, halls, corridors, balconies, loggias and terraces). This does not apply to abnormal footwear, for example hobnailed boots. It should be noted that it is stated in the Annex this approximate classification is given for guidance only and should not be taken to provide accurate product specification for specific requirements.
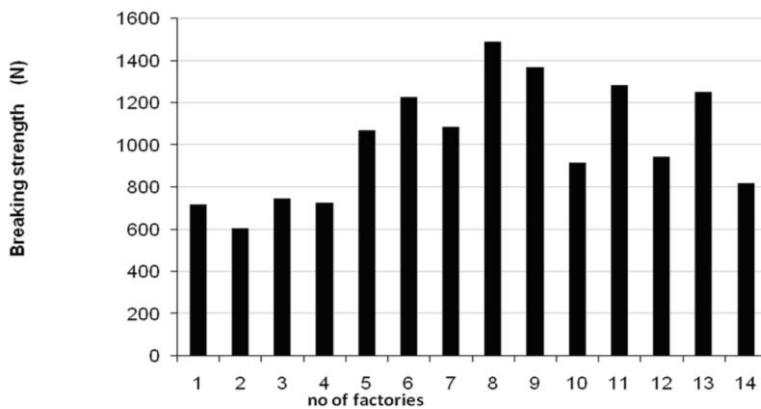
Coefficient of friction

The results of dynamic coefficient of friction are shown in table 3 and figure 4 shows the relationship between the dynamic coefficient of friction with the different factories. The results were in the range of 0.26μ to 0.66μ. ISO 13006 does not state a limit for the dynamic coefficient of friction but requires the manufacturer to state value and test method used.

Table 3: Test results of breaking strength, modulus of rupture, abrasion stage and dynamic coefficient of friction

Factories	Min. thickness (mm)	Breaking strength (N)	Modulus of rupture (N/mm²)	Abrasion stage (Class)	Dynamic coefficient of friction (μ)
1	8.0	719.5	18.21 [1]	Class 3	0.57
			16.20 [2]		
2	8.0	605.64	14.54	Class 3	0.26
			12.98		
3	7.5	747.38	20.81	Class 3	0.66
			18.85		
4	8.0	725.03	17.70	Class 3	0.62
			16.63		
5	8.5	1069.32	23.85	Class 3	0.51
			20.73		
6	>7.5	1227.63	31.41	Class 3	0.35
			29.77		
7	8.0	1084.72	25.71	Class 3	0.39
			24.54		
8	8.0	1488.42	33.55	Class 3	0.29
			29.54		
9	>7.5	1367.32	35.04	Class 3	0.46
			32.70		
10	7.0	916.55	28.55	Class 3	0.37
			26.95		
11	7.5	1283.21	32.34	Class 3	0.45
			28.68		
12	<7.5	944.21	26.64	Class 3	0.31
			24.80		
13	8.0	1250.18	30.95	Class 3	0.30
			28.36		
14	7.5	819.62	21.43	Class 3	0.38
			20.58		

[1] Individual minimum
[2] Minimum average

Fig 2: Relationship between breaking strength and number of factories for ceramic floors
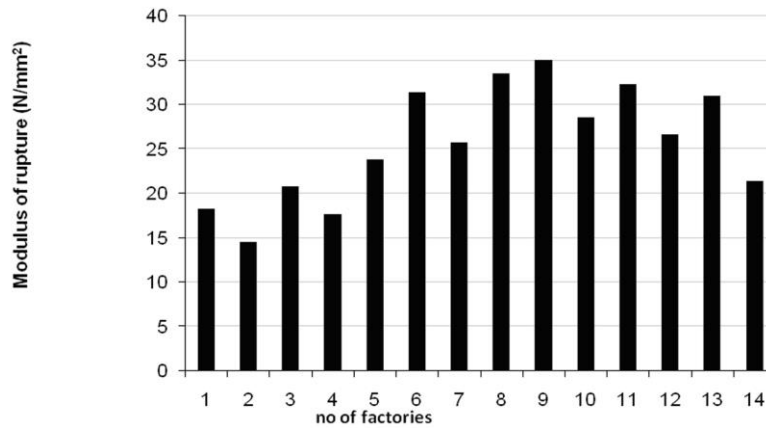
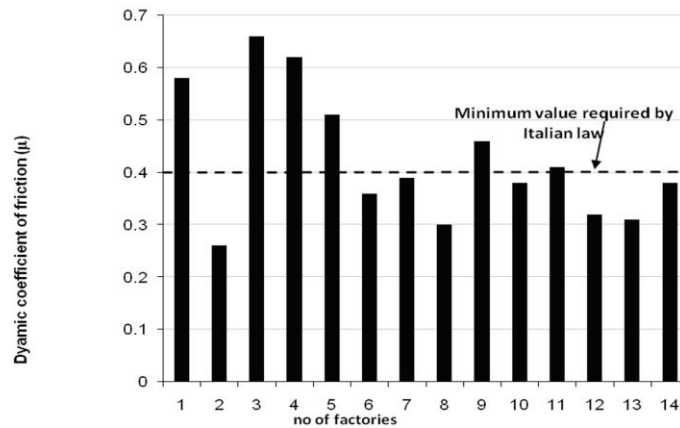**Fig 3: Relationship between modulus of rupture and number of factories for ceramic floors**

Fig 4: Relationship between dynamic coefficient of friction and number of factories for ceramic floors

CONCLUSIONS

Based on the experimental results obtained from this study, the following conclusions can be drawn.
1. Almost 70% of the samples from the different factories satisfied the requirements of both ESS and ISO specifications concerning breaking strength and modulus of rupture (10 factories out of 14 factories).
2. All the samples from the fourteen factories were classified as Class 3 pertaining abrasion resistance.
3. The dynamic coefficient of friction was higher than 0.4 (as stated by the Italian law) for only six factories from the fourteen factories.

REFERENCES

1.   Is it really Porcelain? - columns – Tile Magazine,http://www.magonline.com/Articles/column
2.   "Industrial Minerals Rocks – Google – book search", http://books.google.com/books
3.   http://www.posmci.4fsc.br/teses/oke.pdf
4.   http://www.cmit.csiro.au

5. ISO 10545-3:1995 Determination of water absorption, apparent porosity, apparent relative density and bulk density.
6. ESS 293-1:2002 Determination of water absorption, apparent porosity, apparent relative density and bulk density.
7. ISO 13006:1998 Ceramic tiles-Definitions, classification, characteristics and marking.
8. ESS 3168-2:1997 Ceramic tiles with water absorption≤0.5%.
9. ESS 3168-3:1998 Ceramic tiles with water absorption>0.5% and <3%.
10. ESS 3168-4:2005 Dry pressed ceramic tiles with water absorption>3% and ≤6%.
11. ESS 3168-5:2000 Ceramic tiles with water absorption>6% and ≤10%.
12. ESS 3168-6:2005 Dry pressed ceramic tiles with water absorption E>10%
13. ESS 293-10:2002 Method for determination of modulus of rupture and breaking strength.
14. ISO 10545-4:2004 Determination of modulus of rupture and breaking strength.
15. ESS 293-3:2006 Method for determination of resistance to surface abrasion for glazed tiles.
16. ISO 10545-7:1996 Determination of resistance to surface abrasion for glazed tiles.
17. ISO/DIS 10545-17:1998 Determination of coefficient of friction.

COMPARATIVE STUDY ON USING CFRP WITH BOTH ECC AND CONCRETE SUBSTRATES

*Ahmed M. ANWAR, MANDULA, **Kunio HATTORI, and Hidehiko OGATA**
Doctoral Candidates, Department of Environmental Engineering, United Graduate School of Agricultural Science, Tottori University, Tottori, Japan E-mail: ahmedanwar2000@hotmail.com Professor, and Associate Professor, Faculty of Agriculture, Tottori University, 4-101 Minami Koyama-cho, Tottori, 680-8553, Japan

ABSTRACT

In the framework of strengthening and rehabilitation of concrete structures, the application of carbon fiber reinforced polymers (CFRP) is considered one of the effective techniques. It was noticed that the interfacial debonding of CFRP is the most common mode of failure. The last two decades had witnessed the innovation of extra ductile engineered cementitious composites (ECC). Combinations between both ECC and CFRP are still limited. Yet, this research focuses on the contact performance between ECC and CFRP as well as comparing it with corresponding cases with normal concrete substrate. The induced interfacial stresses were investigated for each case. The effect of CFRP thickness was also examined. The study included the examination of thirteen beams equally made of ECC and plain concrete. The specimens were destructively examined in a four point bending test. The results show that the contact between ECC and CFRP was better than between concrete and CFRP; however, the efficiency of strengthening was higher in case of concrete beams. Moreover, the undesirable interfacial debonding failure mode was not observed in case of ECC. The research ended-up with a recommendation of using ECC to replace the inferior layer in the deteriorated concrete members before strengthening with CFRP.

INTRODUCTION

The application of carbon fiber reinforced polymers (CFRP) is considered one of the effective ways for rehabilitation and strengthening of concrete members. Many researchers have tried some techniques to prevent the occurrence of the undesired debonding mode of failure of the attached CFRP laminate. Xiong et al.[1] have used (U) shape strips from CFRP at the cut-off location of the main CFRP external strengthening. Philip et al.[2] have used fiberglass angles at the end of the attached plates. Tapering of the main CFRP reinforcement was also suggested by Gao et al. [3]. Another group has researched the interfacial shear and normal stresses to avoid reaching the debonding failure load [4-6].

Recently, and since the introduction of the extra ductile engineered cementitious composites (ECC) by Li [7], ECC has shown a promising attitude in enhancing the performance of structures and increase their ductility. The pseudo tensile strain hardening behavior of ECC has drawn the attention of many researchers and contractors to utilize ECC in different research and practical disciplines. ECC can be used in many fields such as strengthening, repair and construction of new structures. ECC has also many advantages such as protecting the the penetration of water to the structure material. ECC was used and developed by many researchers; Kanda et al. [8] used ECC in the form of spray form to strengthen deteriorated

walls. Lim and Li [9] have introduced ECC as a suitable material for trapping cracks in concrete members. Kamada and Li [10] conducted a research showing the adequate bonding between ECC and concrete in repair systems. Kanda et al.[11] extended the use of ECC to practical full scale applications.

The tensile strain-hardening and ultra high tensile strain capacity led ECC to sustain very large deformation without damage localization. This criterion attracted Maalej and Leong [12] to

Table 1: Details of the tested beams

Beam name	Replication	Strengthening condition
C100	2	Concrete beam without strengthening
E100	3	ECC beam without strengthening
C100-1CFRP	2	Concrete beam with one CFRP layer applied at its soffit
E100-1CFRP	2	ECC beam with one CFRP layer applied at its soffit
C100-2CFRP	2	Concrete beam with two CFRP layers applied at its soffit
E100-2CFRP	2	ECC beam with two CFRP layers applied at its soffit

incorporate ECC as a transition material between the original concrete and the attached CFRP for strengthening purpose; however, the study was preliminary and more investigations are still required.

This paper shows different strengthening combinations between ECC and CFRP; the overall member performance together with the bonding behavior were examined. The study started by strengthening two series of beams made of ECC and plain concrete. External CFRP sheets were pasted after polishing the required surfaces. The deformations of the beams were observed and analyzed. The results show that the creation of small size cracks in ECC prevented the concentration of stresses along the attached CFRP sheet; consequently, the interfacial debonding failure mode was prevented. In contrary, all the examined concrete beams strengthened with CFRP ended-up with the undesirable interfacial debonding failure mode. On the other hand, the strengthening efficiency was higher in case of normal concrete beams than that of the ECC beams.

EXPERIMENTAL WORK

Specimen Preparation

In the current experiment, two series of small size beams of dimensions 400 x 100 x 100 mm were examined in a four point loading algorithm with a bending span of 300 mm. The first series was made of ECC and includes seven beams. The second series was made of plain concrete and includes six beams. The beams were divided into three sub-groups; the first was kept as a control beam without attaching CFRP sheets, the second and the third corresponded to beams strengthened with one and two CFRP sheets, respectively. Table 1 shows the details of the tested beams. For CFRP application, the following procedure was adopted; the required surfaces were first polished, left for one day to dry, applying a primary coat, and finally, CFRP was applied using a two compound epoxy resin. Unidirectional CFRP sheet was applied at the beam soffit leaving a 10 mm spacing between the cut-off and the support from both sides. Further details for CFRP application were shown in an early work by the authors [13]. For all the examined beams, the deflections and the strain at the mid-span were measured. Investigation to study the induced interfacial stresses was conducted for beams strengthened with one CFRP sheet

Materials

The mix proportion for both concrete and ECC are shown in Tables 2 and 3, respectively. The concrete mix was designed as per the American Concrete Institute, ACI 211.1 [14]. ECC incorporates high modulus polyethylene fibers. The fiber length is 12.7 mm and diameter 38 microm, tensile strength of 1690 MPa and an elastic modulus of 40,600 MPa. A polycarboxylic-. acid-based superplasticizer was used. A bio-saccharide type viscous agent was also applied to provide compatibility between fluidity and fiber dispersibility. In addition, an expansive agent and an alcohol-type shrinkage reducing agent were added. The commercially ready mixed ECC

mixture was brought from a Technical Research Institute in Japan. More details about the used ECC were reported by Kanda et al. [11]. The measured compressive and flexural strengths of concrete at 28 days were 40 MPa, and 6 MPa, respectively. The corresponding values for ECC were 27 MPa, and 9 MPa, respectively. As supplied by the manufacturer, the used unidirectional CFRP sheets were of 0.111 mm thickness, tensile strength of 3400 MPa and modulus of elasticity of 3400 MPa. The bonding epoxy has flexure strength of 40 MPa, tensile strength of 30 MPa and shear strength of 10 MPa.

Table 2: Mix proportions of concrete

Aggregate size (mm)	Slump (mm)	Air Content (%)	W/C (%)	S/a (%)	Unit content (kg/m^3)			
					Water	Cement	Sand	Gravel
20	100	2	54	38	200	370	650	1056

Table 3: Mix proportions of ECC per unit volume

Ready mixed powder (Kg)	Water (Kg)	W/C (%)	Fiber volume fraction (%)	Supper plasticiz-er (Kg)	Anti-shrinkage agent (Kg)	Surface active agent* (Kg)	Slump Flow (mm)	Air Content
1562	350	46	2	16.9	15.3	3.1	500	10±4

   * **Diluted with 24 times of water mass**

RESULTS AND DISCUSSION

Load capacity
The load-deflection curves of the strengthened ECC and concrete beams are shown in Fig.1 and Fig.2, respectively. Generally, it can be seen that the ultimate loading capacity was significantly enhanced by adding CFRP sheets in case of concrete beams while slight enhancement was achieved in case of ECC beams. The strengthening of ECC and concrete beams with one sheet of CFRP increased the overall loading capacity with 21 and 148%, respectively. For concrete beams, the load-deflection curves started with a linear elastic trend until exceeding the elastic limits. After then, all the tensile stresses were only carried by the CFRP sheets and that was the reason why the more the CFRP thickness continued the loading with higher curve slope and gave higher loading capacity. For the ductile ECC beams with no CFRP, the loading started with a semi-linear trend followed by strain hardening behavior. After applying CFRP, the trend shows enhancement in the overall rigidity of the members, shown in higher initial curves slopes, with a little increase in the total section loading capacity. In general, the external CFRP sheet in case of the strengthened ECC beams minimized the creation of the hair cracks at the mid-span and consequently avoided the high stress concentration at the vicinity of the cracks as in case of concrete substrates. It was observed that the CFRP sheet/s and the ECC beams deformed compatible to each other without the occurrence of the debonding failure for both cases (ECC-1CFRP) and (ECC-2CFRP). The change in the CFRP thickness did not show a significant difference in the section loading capacity in case of ECC beams, it might be attributed to the occurrence of shear failure mode and consequently prevents the beams from reaching their ultimate flexure capacity limits.

The previous illustration can again be seen in Fig. 3, which shows the load-mid span strain for the strengthened beams. It was observed that the strengthened concrete beams with one CFRP layer exhibited a larger strain values than all the other specimens. It was also noted that for both ECC and concrete beams, the increase in CFRP thickness led to minimize the overall deflection and strain value. Fig.4 and Fig.5, show the normalized load carrying capacity and deflection with respect to their control beams, respectively.

Modes of failure
The modes of failure of the examined beams would have a great influence on the final judgment. It was observed that a pure flexure failure mode was governed for both ECC and concrete beams with no strengthening. For ECC with one and two CFRP layers, pure shear failure was observed with no signs of interfacial debonding failure along the CFRP sheet. This

conclusion was found very important, useful and should be utilized for further application. For concrete beams with external strengthening, the conventionally debonding mode of failure was observed started at the crack position, almost under one of the loading points. Fig.6 shows the failure modes for all the examined beams.
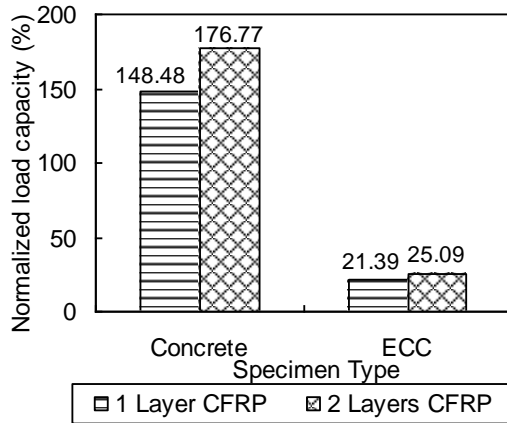

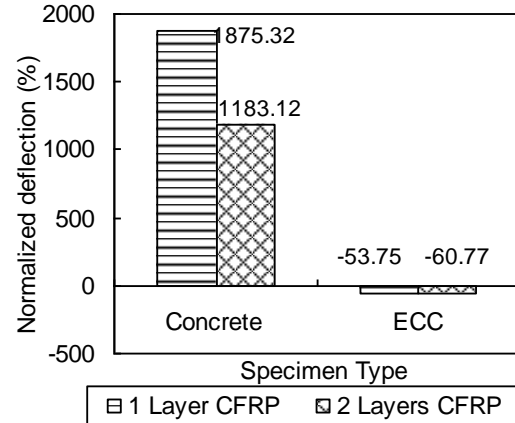**Fig. 4: Normalized Load Carrying Capacity to the Control**

Fig. 5: Normalized Deflection to the Control

The above explanation showed that interfacial debonding failure was common in case of concrete while no debonding was achieved in case of ECC. Moreover, strengthening with CFRP increased significantly the load carrying capacity of the members in case of concrete rather than ECC. This suggested the use of a combination of ECC simultaneously with CFRP sheets to strengthen or repair the deteriorated concrete beams by replacing the inferior layer of concrete with ECC. Thus, ECC could act as a transition material which has a very good contact between both the base concrete and the external CFRP.

To do so, further investigation should be carried out to monitor the induced interfacial stresses between ECC beams and CFRP sheets as well as comparing with normal concrete beams.


C100
Pure flexure

E100
Pure flexure

C100-1CFRP
Interfacial debonding

E100-1CFRP
Shear failure

C100-2CFRP
Interfacial debonding

E100-2CFRP
Shear failure

**Fig. 6: Failure Patterns for the Tested Specimens**

Induced contact stresses

To deeply monitor the difference between the responses of both ECC and concrete beams with the attached CFRP sheet, four strain gauges were mounted along half the length of the CFRP sheet; this was only applied for cases with only one layer of CFRP. The locations of the strain gauges were 5, 25, 55, 140 mm from the sheet cut-off. Fig.7 and Fig.8 show the measured strains for ECC and concrete beams, respectively.

The strain values were first compared at a load value nearly equal to the elastic limits of the concrete beams, it was noted that the developed stains on the ECC beam were more than that in case of concrete. This might be attributed to the high ductility of the ECC which allows compatible deformations with CFRP sheet while the CFRP elongation was resisted in case of concrete substrate. After exceeding the elastic limits of concrete, localized crack was developed nearly at the mid-span, this allowed the strain value to develop significantly in case of concrete substrate. It was noted that at the failure load value of the ECC beam, the value of the strain of the CFRP sheet attached to concrete was almost 40% higher than that attached to ECC beam.
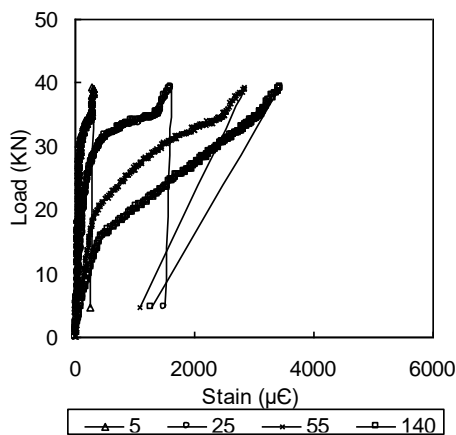
**Fig. 7: Measured Strain along the CFRP Sheet for the ECC Beam**
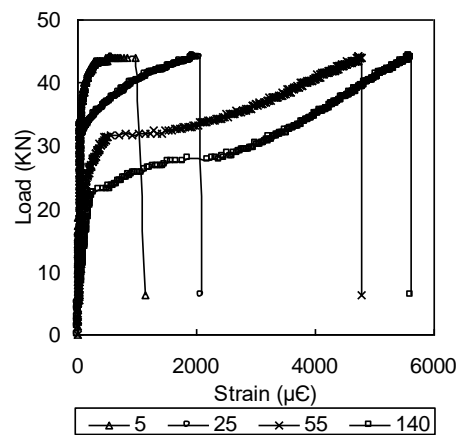
Fig. 8: Measured Strain along the CFRP Sheet for the Concrete Beam
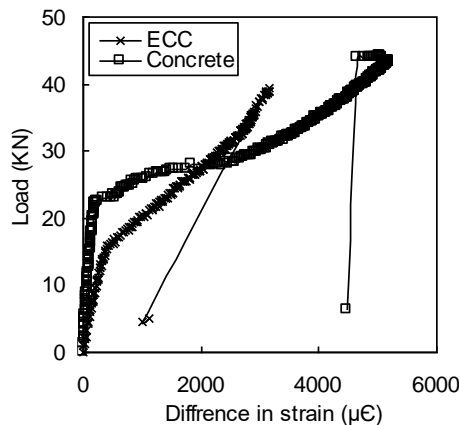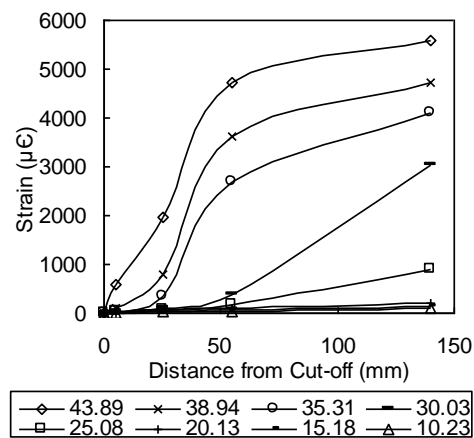

Fig. 9: Difference in the Strain Values at the Cut-off and the Mid-span Position

It was also shown that the strain value at the cut-off was higher in case of ECC substrate than in case of concrete allover the loading time. ECC dissipated the gained energy through excessive deformations among the whole member, while the rigid concrete only dissipated the absorbed energy at locations of very high stresses. It was also noted that the change in the slope of the strain value curves in case of ECC dramatically increased before collapse. This might be attributed to the generation of shear crack which was also a ductile failure, associated with the generation of many fine cracks, and preventing the member from achieving its flexure strength.

In this particular case, ECC released the absorbed energy by means of shear cracks with no interfacial debonding.
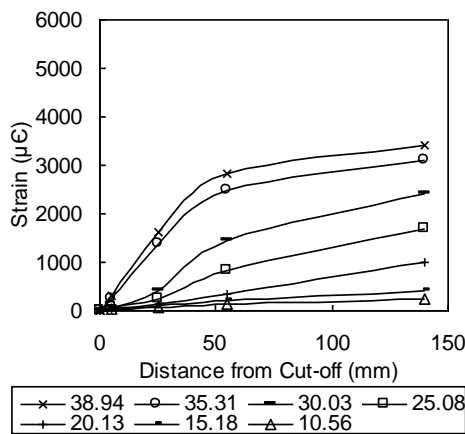
Fig. 10: Strain along the CFRP Sheet Attached to the ECC Beam at Different Loading Values

**Fig. 11: Strain along the CFRP Sheet Attached to the Concrete Beam at Different Loading Values**

For further understanding of this behavior, the difference between the strain values at both the cut-off and the mid-span was calculated for both cases and shown in Fig.9. It was noted that at an early stage of loading the strain difference was slightly larger in case of ECC, after then, the strain difference in case of concrete was extremely increased, which could be attributed to the generation of a local crack. The figure could be used as a double check and confirmation for the reason why the interfacial debonding happened in case of concrete substrate while no debonding occurred in case of ECC beam. Generally, the higher the strain differences along the laminar, the higher the interfacial shear stress, and the ease the occurrence of the interfacial debonding failure.

Fig.10 and Fig.11 show the measured strain at selected loading values for both the ECC and the concrete beam. The figures show the relatively high strain gradient near the cut-off in case of ECC at low level loading which increased slightly without sudden change. In contrary, the concrete beam exhibited low strain gradient near the cut-off and exhibited a sudden variation in the strain values after exceeding the elastic limits. This might also end-up with the same reason for the interfacial debonding that occurred in case of concrete and was avoided in case of ECC.

REASONS BEHIND THE GOOD CONTACT

The reasons for the strong bonding between ECC and CFRP were due to 1) the micromechanical behavior of ECC contaminated with the strain hardening trend, where the ECC can develop a 200 times strain more than that of the concrete [3, 7]. This behavior led the ECC and CFRP not to create large differential strains and consequently decreased the interfacial shear stresses in the adhesive and decelerated the debonding failure mode. 2) ECC creates many but micro-size cracks in the most stressed portions which consequently decreases the shear stress gradient between the CFRP sheet and the ECC substrate near the vicinity of cracks, 3) ECC is relatively of high porosity with high voids ratio (nearly around 12%, while normal concrete is only around 2%). This led a large amount of the adhesive epoxy resin to penetrate through and develop a better contact strength, and 4) the remaining small amount of fiber on the polished surface of ECC along with the high amount of fibers just underneath the prepared surface can create a strong reinforced adhesive compound which helped in decelerating the debonding failure. The previous explanation might not be applicable in case of concrete where one or few localized cracks appeared followed by the concentration of stresses in the vicinity of cracks and subsequently inducing sudden interfacial debonding failure. Fig. 12 shows the concrete and ECC surfaces before pasting the CFRP sheet and after peeling of the

CFRP. It is observed that a very fine layer was spalled out with the CFRP sheet in case of concrete beams, while for ECC beams, relatively thicker layer of ECC was spalled out, traces of the epoxy was observed along with the large amount of fibers.
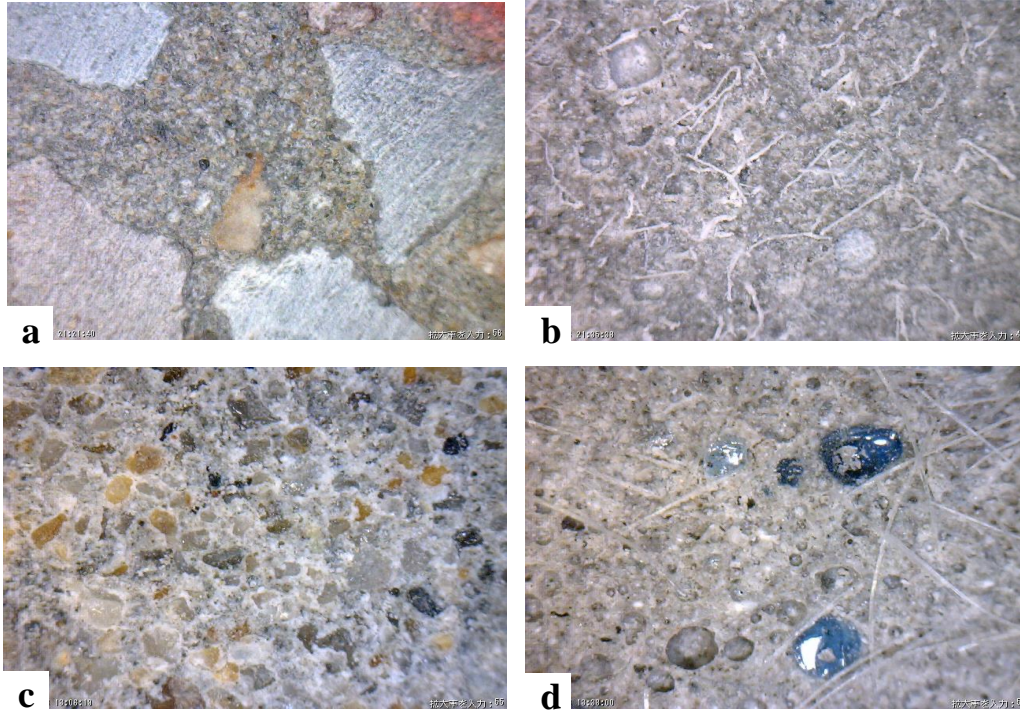
Fig. 12: a)Concrete Surface after Polishing, b) ECC Surface after Polishing, c) Concrete Surface after Peeling the CFRP Sheet, and d) ECC Surface after Peeling the CFRP Sheet

CONCLUSION

In the current research, strengthening of ECC and plain concrete beams was done by means of CFRP. The overall behavior of the beams was examined. The bonding properties were analyzed. The following are among the most important findings:

1. In all the examined ECC beams, the bonding between both CFRP and ECC was found strong enough and even better than that of the concrete due to material ductility.
2. The concrete beams exhibited high strength efficiency when strengthened with CFRP; however, it did not have the same significant in case of ECC beams.
3. The interfacial shear stress gradient at the cut-off was less in case of ECC than in case of concrete beams at high loading values.
4. It is recommended to use ECC with small thickness before pasting CFRP sheets as it has a good contact between both concrete and CFRP. It will act as a transition layer and decelerate the undesired debonding failure.

REFERENCES

1. G.J. Xiong, X. Jiang, J.W. Liu and L. Chen (2007), "A Way for Preventing Tension Delamination of Concrete Cover in Midspan of FRP Strengthened Beams", Construction and Building Materials, 21, pp. 402-408.
2. Philip A. Ritchie, David A. Thomas, Le-Wu Lu and Guy M. Connelly (1991), "External Reinforcement of Concrete Beams Using Fiber Reinforced Plastics", ACI Structural Journal, July-August, pp. 490-500.

3. Bo Gao, Jang-Kyo Kim and Christopher K.Y. Leung (2006), "Strengthening Efficiency of Taper Ended FRP Strips Bonded to RC Beams", Composites Science and Technology, 66, pp. 2257-2264.
4. Amir M. Malek, Hamid Saadatmanesh and Mohammad R. Ehsani (1998), "Prediction of Failure Load of R/C Beams Strengthened with FRP Plate Due to Stress Concentration at the Plate End", ACI Structural Journal, 95(1), pp. 142–152.
5. M. Maalej, Y. Bian (2001), "Interfacial Shear Stress Concentration in FRP-Strengthened Beams", Composites and structures, 54, pp. 417-426.
6. S.T. Smith, J. G. Teng (2001), "Interfacial Stresses in Plated Beams", Eng. Structure, 23, pp. 857–871.
7. Victor C. Li (2002), "Reflections on the Research and Development of Engineered Cementitious Composites (ECC)", JCI International Workshop on Ductile Fiber Reinforced Cementitious Composites (DFRCC) – Application and Evaluation, pp. 1-21.
8. Tetsushi Kanda, Tadashi Saito, Noburu sakata, Masanori Hiraishi (2002), "Fundemental Properties of Direct Sprayed ECC", JCI International Workshop on Ductile Fiber Reinforced Cementitious Composites (DFRCC) – Application and Evaluation, pp. 133-141.
9. Yun Mook Lim, Victor C. Li (1997), "Durable Repair of Aged Infrastuctures Using Trapping Mechanism of Engineered Cementitious composites", Cement and Concrete Composites, 19, pp. 373-385.
10. Toshiro Kamada, Victor C. Li (2000), "The Effects of Surface Preparation on the Fracture Behavior of ECC/concrete Repair System", Cement and Concrete Composites, 22, pp. 423-431.
11. Tetsushi Kanda, Shiro Tomoe, Satoru Nagai, Makoto Maruta, Toshiyuki Kanakubo (2006), "Full Scale Processing Investigation for ECC Pre-cast Structural Element", Journal of Asian Architecture and Building Engineering, JAABE, 5(2), pp. 333–340.
12. M. Maalej, K.S. Leong (2005), "Engineered Cementitious Composites for Effective FRP-Strengthening of RC beams" Composites Science and Technology, 65, pp. 1120–1128.
13. A. M. Anwar, Hattori K., Ogata H. and Goyal A. (2007), "Evaluation of Using CFRP for Strengthening of Arched Hydraulic Structures", JCA, Cement Science and Concrete Technology, 61, pp. 509-516.
14. ACI Committee 211 (1982), Standard practice for selecting proportions for Normal, Heavyweight, Mass concrete (ACI 211.1-32), ACI manual of concrete practice.

EVALUATION OF EXISTING MODEL FOR PREDICTING OF FLEXURAL BEHAVIOUR OF GFRP- REINFORCED CONCRETE MEMBERS

* Dr. Ibrahim M. Metwally

Reinforced Concrete Dept., Housing & Building National Research Center,
P.O.Box 1770 Cairo, Egypt, E-Mail: dr_ibrahimmetwally@yahoo.com, Mobile:002-0102683991

ABSTRACT

Ashour formula [1] for predicting the flexural capacity of glass fiber-reinforced polymer (GFRP) bars reinforced concrete beams is introduced. An implementation of the Ashour model is presented for the purpose of verification and evaluation against the experimental results which were collected from the literature. This paper reported test results of seventy one concrete beams reinforced with GFRP bars subjected to a four point loading system. All beams were governed by two modes of flexural failure; GFRP bars rupture and concrete crushing.
The present study introduces an important modification in Ashour formula to compute the flexural capacity of GFRP bars reinforced concrete beams with high accuracy. The comparisons between the theoretical flexural capacities which were computed by the modified equation and that experimentally measured show a very good agreement. The new proposed equation is not limited to GFRP bars only, but can be used for other FRP bars such as carbon fiber-reinforced polymer and aramid fiber-reinforced polymer. Influences of GFRP reinforcement ratio and the failure type on the beam deformability are also presented.

Keywords: Ashour Model; GFRP; Flexural Capacity; Deformability Factor

INTRODUCTION

Deterioration of reinforced concrete structures has become a serious problem in the last decade. This situation is mainly due to corrosion of steel reinforcing bars embedded in concrete. The inherent incompatibility that exists between concrete and steel reinforcement, which mainly arises from the corrosion of steel, led to the development of new concrete reinforcing materials. With their high strength and corrosion resistance, fiber-reinforced polymer (FRP) bars represent an alternative to steel reinforcement. Low modulus of elasticity, low ductility, and high cost are the main reasons why FRP bars in concrete structures have received limited attention.

The analytical procedure developed for the design of concrete structures reinforced with steel bars is not necessarily applicable to structures reinforced with FRP. The geometrical shape, ductility, modulus of elasticity, and bond characteristics of FRP bars are likely to be different from those of steel bars. Thus, the behavior of FRP reinforced concrete should be independently investigated.

The design of concrete sections in flexure that are reinforced with fiber reinforced polymers (FRP) is different from that of sections reinforced with steel because of the difference in mechanical properties of FRP and steel. Generally, the FRP bars used as reinforcement in concrete have tensile strength varying between 500 and 2200 MPa and modulus of elasticity varying between 40 and 150 GPa. The stress–strain relationship for FRP is linear up to rupture when the ultimate strength is reached. Unlike steel reinforcing bars, FRP bars do not undergo yield deformation or strain hardening before rupture. For this reason, design of sections in flexure has been based upon consideration of ultimate strength, serviceability, and deformability.

The purpose of design for deformability is to ensure that failure of a section in flexure occurs only after development of sufficiently large curvature.

Several experimental studies [2-18] have been performed to understand the behavior of concrete beams reinforced with FRP bars. As a result, few design guidelines [19, 20, 21] have been published to aid the design and construction of concrete structures reinforced with FRP bars. However, these design guidelines emphasized the need for more research to validate the performance of FRP-reinforced concrete beams in flexure and shear.

The principal aims of this paper may be summarized as follows:

1- To present , show, and discuss the test results of 71 concrete beams reinforced with GFRP bars;
2- To validate the accuracy of the proposed equation by Ashour [1] for flexural capacity prediction;
3- To modify the Ashour formula to the new proposed equation which can be used to compute the moment capacity of FRP bars reinforced concrete beams with high accuracy;
4- To study and establish the member deformability with respect to GFRP reinforcement ratio.

TEST SPECIMENS

The test specimens consisted of 71 GFRP reinforced concrete beams collected from the literature. The parameters of this study were beam geometry (width & depth, b×d), amount of GFRP reinforcement (ρ_f , %), and concrete compressive strength (f_{cu}). All beams were tested under two equal concentrated loads.

All beams were deigned to fail under flexure. The flexural failure is mainly occurred due to concrete crushing or tensile rupture of GFRP rebars either within the mid-span region (under pure bending) or under the applied point loads.

THEORETICAL PREDICTION OF FLEXURAL CAPACITY OF GFRP-REINFORCED CONCRETE BEAMS BY ASHOUR MODEL

As FRP bars do not exhibit yielding, flexural failure of FRP-reinforced concrete beams is characterized by either concrete crushing (over-reinforced case) or FRP bar rupture (under-reinforced case). In the following, compatibility of strains and equilibrium of forces are employed for estimating the flexural capacity of FRP concrete sections.
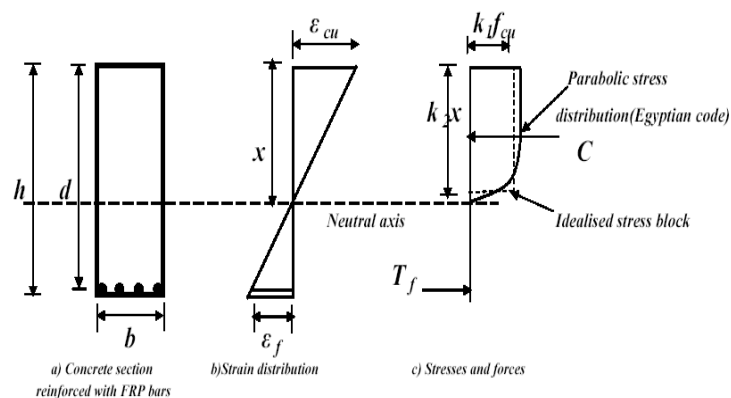

Fig. 1. Strains, stresses and forces on concrete section reinforced with FRP bars at failure.

Fig. 1(a) presents a concrete section reinforced with bottom FRP bars. Those reinforcing bars are not limited to GFRP bars, but the current theoretical analysis can also accommodate other

types of FRP materials such as carbon fiber-reinforced polymer (CFRP) and aramid fiber-reinforced polymer (AFRP) bars.

The parabolic stress distribution and equivalent rectangular stress block of concrete in compression proposed by Egyptian Code [22] are adopted in the present analysis as shown in Fig. 1(c). The concrete compressive force C is then calculated from:

$$C = k_1 k_2 f_{cu} b x$$ ---------------------------- [1]

As concrete is very weak in tension, concrete below the neutral axis is cracked and therefore ignored.

Assuming that the stress-strain relationship of FRP bars is linear up to rupture, the force in the bottom FRP bars is estimated below:

$$T_f = A_f f_f = A_f E_f \varepsilon_f$$ ---------------------------- [2]

The above equation is valid for different types of FRP bars, i.e., GFRP, CFRP, and AFRP.

The moment capacity (M_f) of the section can be obtained by taking moments of forces about any horizontal axis of the section; for instance about the bottom FRP bars

$$M_f = k_1 k_2 f_{cu} b x \left(d - \frac{k_2 x}{2} \right)$$ ---------------------------- [3]

Balanced Reinforcement Ratio

The flexural failure mode (either concrete crushing or FRP rupture) could be identified by comparing the actual FRP reinforcement used with the balanced reinforcement ratio. The balanced ratio of FRP reinforcement is determined when, at the instant of failure, both concrete crushes and FRP bars rupture simultaneously; that is $\varepsilon_c = \varepsilon_{cu} = 0.003$ (concrete crushing) and $\varepsilon_f = \varepsilon_{fu}$ (tensile FRP bar rupture), where ε_{cu} and ε_{fu} are the ultimate strains of concrete and FRP bars, respectively. In such case, the depth of the neutral axis, x_b is

$$x_b = \frac{\varepsilon_{cu}}{\varepsilon_{cu} + \varepsilon_{fu}} d = \frac{0.003}{0.003 + \varepsilon_{fu}} d$$ ---------------------------- [4]

and the balanced ratio ρ_b of FRP reinforcement is

$$\rho_b = \frac{A_{fb}}{bd} = 0.6 \frac{f_{cu}}{f_{fu}} \left(\frac{x_b}{d} \right)$$ ---------------------------- [5]

If the reinforcement ratio is below the balanced ratio ($\rho_f < \rho_b$, where $\rho_f = A_f/bd$), FRP bars rupture. Otherwise, ($\rho_f > \rho_b$), concrete crushing failure mode governs.

MODIFICATION OF THE ASHOUR MODEL

Fig. 2 shows the correlation between M_{exp} and M_f which calculated by Ashour formula (Eq.3). This relationship can be represented by power curve; its equation is $M_{exp} = 1.237 M_f^{0.944}$, this equation gives a good representation with R^2 (correlation factor) = 0.982 and the average and standard deviation of the M_{exp} / M_f for the seventy one studied beams equal 1.027 and 13.7 % respectively as reported in Table1.
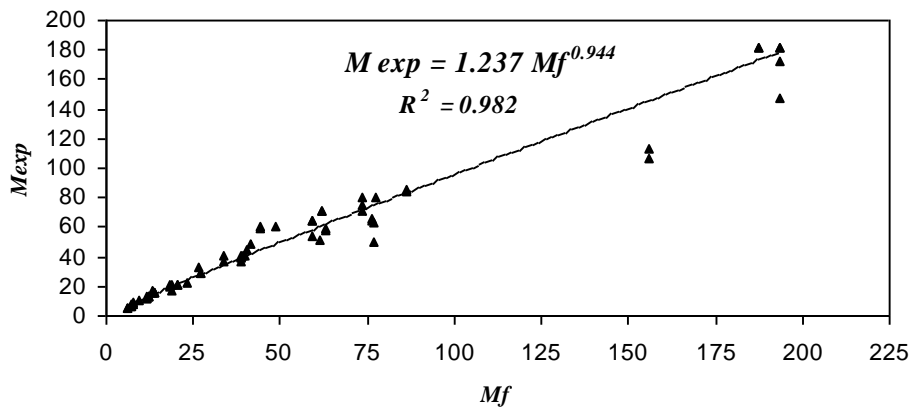
Fig. 2- Correlation between experimental moment capacities for 71 studied beams and the predicted values by Ashour model

To modify the above equation for the best simulation, the power of M_f has changed to 0.94239 instead of 0.944, hence the new modified formula (or the proposed formula) is $M_p = 1.237 M_f^{0.94239}$; this equation gives the best correlation with $R^2 \approx 1$ with the average and standard deviation of M_{exp} / M_p equal 1.013 and 5.9 % respectively as shown in Table 1.

The new proposed modified equation can be re-written as follow:-

$$M_p = 1.237 \left[k_1 k_2 f_{cu} bx \left(d - \frac{k_2 x}{2} \right) \right]^{0.94239}$$ -------------------------- [6]

This equation is valid to predict the moment capacity of RC members with rectangular section reinforced with FRP rebars in tension side.
Fig. 3 shows that M_{exp} / M_p (computed by the proposed equation) is very closed and near to the one line compared to M_{exp} / M_f (computed by Ashour model).


Beams: from 1 to 71
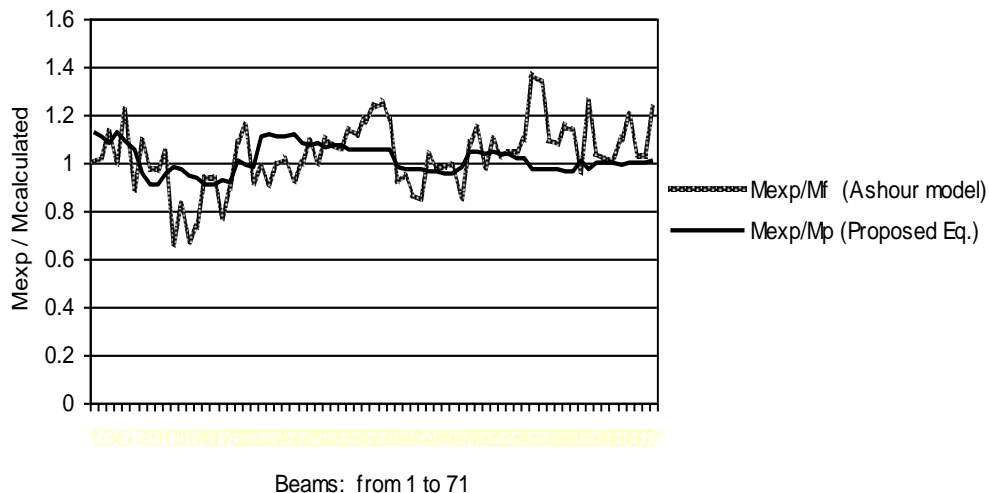
Fig. 3- Comparison between the Ashour model and proposed formula

VERIFICATION OF THE PROPOSED EQUATION

To verify the proposed modification, Equation no.6 was compared to the test results of 71 specimens tested to date. These test data were collected from 13 different investigations. Table1 gives the data of 71 concrete beams reinforced with GFRP bars and failed in flexure; all were simply supported and were tested in four-point bending. The reinforcement ratio of the test specimens ranged between 0.12 and 3.6%. The concrete compressive strength ranged between 32.47 to 67.29 MPa, and the depths ranged between 152 to 550 mm.

Besides the predicted moment capacities according to the proposed equation (Eq. no. 6), the predicted moment capacities according to Ashour model (Eq. no. 3) are also presented in Table1. For 71 beams, the average of M_{exp} / M_p for the proposed equation is 1.013 with a standard deviation equal 5.9 %. One the other hand, the corresponding values were 1.027 and 13.7 % respectively, for the Ashour method.

Fig. 4   shows that the level of accuracy of the moment capacity of GFRP- reinforced beams predicted by the proposed equation is consistent unlike the method of Ashour. The same observation can be made when the results of the proposed equation and those by Ashour were plotted versus the concrete strength, overall depth, and GFRP reinforcement ratio as shown in the following Patterns.
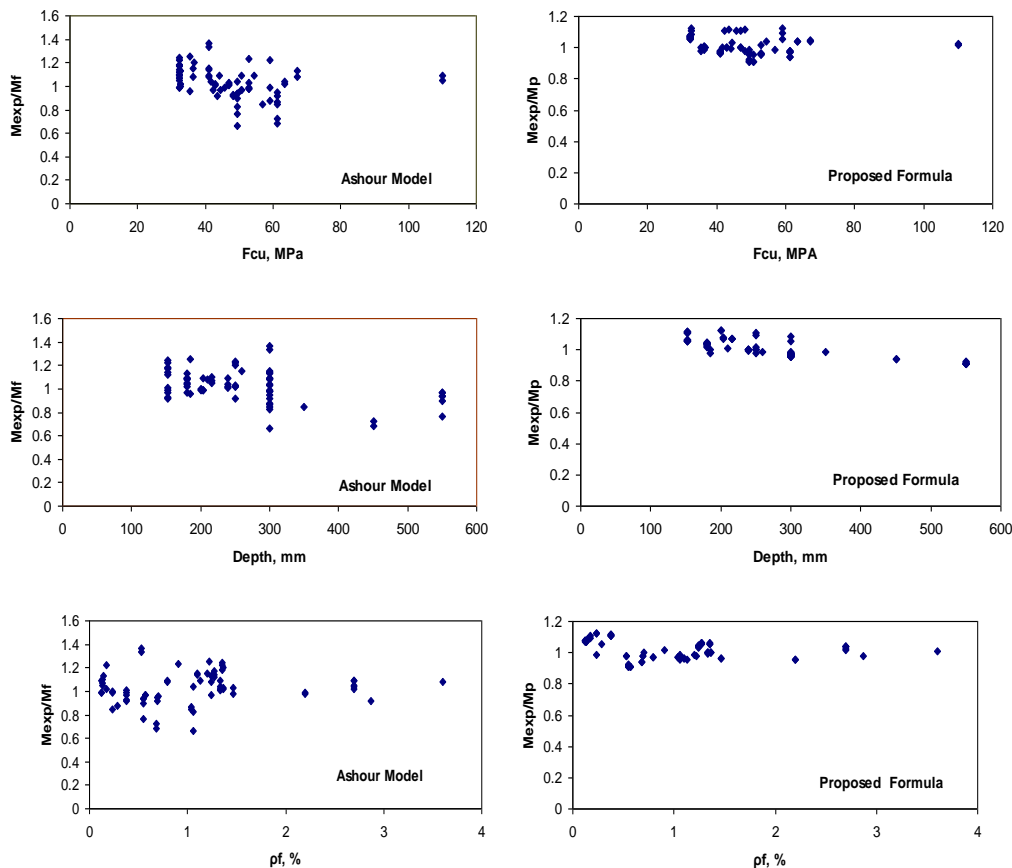
Fig. 4- Influence of different variables as f_{cu}, d, and ρ_f % on $M_{exp} / M_{calculated}$ by Ashour and proposed equations.

Across the range of variables included in the data set, the predictions of the Ashour model appear to have larger band width of the scattered results and higher level of conservatism compared to that of the proposed equation which appears near to the one line.

Thus, proposed equation (no. 6) appears to be more accurate and reliable for predicting the moment capacity of concrete members longitudinally reinforced with FRP rebars.

Table 1- Comparison between the experimental and calculated flexural capacities

No.	Beam notation	Width x overall depth, mm	f_{cu} MPa	ρ_f, %	ρ_b, %	M_{exp}, kN.m	M_f, kN.m (Ashour Eq.1)	M_{exp}/M_f	M_p, kN.m (Proposed Eq.4)	M_{exp}/M_p	Experimental mode of failure
Ashour [1]											
1	Beam 2	150x200	32.56	.23	.49	5.89	5.90	0.998	5.238	1.124	FRP rupture
2	Beam 4	150x250	32.56	.17	.49	7.85	7.72	1.017	7.105	1.105	FRP rupture
3	Beam 6	150x300	32.56	.14	.49	10.79	9.55	1.13	9.958	1.083	FRP rupture
4	Beam 8	150x200	58.93	.23	.84	5.89	5.96	0.988	5.239	1.124	FRP rupture
5	Beam10	150x250	58.93	.17	.84	9.48	7.78	1.218	8.68	1.092	FRP rupture
6	Beam12	150x300	58.93	.28	.84	16.75	19.02	0.881	15.879	1.055	FRP rupture
Benmokrane et al. [6]											
7	ISO 2	200x300	50.59	1.13	0.77	80.4	73.39	1.095	83.89	0.958	Concrete crushing
8	ISO 3	200x550	50.59	0.57	0.83	181.7	187.45	0.969	199.277	0.912	FRP rupture
9	ISO 4	200x550	50.59	0.57	0.83	181.7	187.45	0.969	199.277	0.912	FRP rupture
Benmokrane et al. [5]											
10	ISO30-2	200x300	49.41	1.06	.71	80.4	77.59	1.036	83.89	0.958	Concrete crushing
11	KD30-1	200x300	49.41	1.06	.69	50.6	76.85	0.658	51.323	0.986	Concrete crushing
12	KD30-2	200x300	49.41	1.06	.69	63.8	76.85	0.83	65.635	0.972	Concrete crushing
13	KD45-1	200x450	61.18	.68	.84	106.6	156.09	0.683	113.162	0.942	Concrete crushing[a]
14	KD45-2	200x450	61.18	.68	.84	113	156.09	0.724	120.384	0.939	Concrete crushing[a]
15	ISO55-1	200x550	49.41	.55	.71	181.5	193.27	0.939	199.044	0.912	FRP rupture
16	ISO55-2	200x550	49.41	.55	.71	181.5	193.27	0.939	199.044	0.912	FRP rupture
17	KD55-1	200x550	49.41	.55	.69	146.9	193.29	0.76	159.03	0.924	FRP rupture
18	KD55-2	200x550	49.41	.55	.69	172.5	193.29	0.892	188.587	0.914	FRP rupture

Table 1- (Continued)

No.	Beam notation	Width x overall depth, mm	f_{cu}, MPa	ρ_f, %	ρ_b, %	M_{exp}, kN.m	M_f, kN.m (Ashour Eq.1)	M_{exp}/M_f	M_p, kN.m (Proposed Eq.4)	M_{exp}/M_p	Experimental mode of failure
Al-Sayed [3]											
19	B	200x210	36.47	3.6	.17	36.5	33.84	1.079	36.29	1.006	Concrete crushing
20	C	200x260	36.47	1.2	.27	48.1	41.68	1.154	48.636	0.989	Concrete crushing
21	D	200x250	48.24	2.87	.57	53.98	59.07	0.914	54.968	0.982	Concrete crushing
Brown and Bartholomew [7]											
22	1	152x152	42.24	.38	.40	7.04	7.26	0.97	6.329	1.112	FRP rupture
23	2	152x152	43.41	.38	.41	6.64	7.27	0.913	5.948	1.116	FRP rupture
24	4	152x152	45.76	.38	.43	7.23	7.29	0.992	6.511	1.11	FRP rupture
25	5	152x152	46.94	.38	.44	7.35	7.30	1.01	6.625	1.109	FRP rupture
26	6	152x152	48.12	.38	.45	6.75	7.31	0.923	6.053	1.115	FRP rupture
Yost et al. [17]											
27	1FRP1	381x203	32.47	.12	.34	11.49	11.59	0.991	10.644	1.079	FRP rupture
28	1FRP2	381x203	32.47	.12	.34	12.67	11.59	1.093	11.808	1.073	FRP rupture
29	1FRP3	381x203	32.47	.12	.34	11.49	11.59	0.991	10.644	1.079	FRP rupture
30	2FRP1	318x216	32.47	.13	.34	13.62	12.4	1.098	12.75	1.068	FRP rupture
31	2FRP2	318x216	32.47	.13	.34	13.26	12.4	1.069	12.392	1.07	FRP rupture
32	2FRP3	318x216	32.47	.13	.34	13.06	12.4	1.053	12.194	1.071	FRP rupture
33	4FRP1	203x152	32.47	1.27	.34	15.78	13.88	1.137	14.905	1.059	Concrete crushing
34	4FRP2	203x152	32.47	1.27	.34	15.58	13.88	1.122	14.705	1.059	Concrete crushing
35	4FRP3	203x152	32.47	1.27	.34	16.29	13.88	1.174	15.417	1.057	Concrete crushing
36	5FRP1	191x152	32.47	1.35	.34	16.37	13.35	1.226	15.497	1.056	Concrete crushing
37	5FRP2	191x152	32.47	1.35	.34	16.65	13.35	1.247	15.778	1.055	Concrete crushing
38	5FRP3	191x152	32.47	1.35	.34	15.78	13.35	1.182	14.905	1.059	Concrete crushing

Table 1- (Continued)

No.	Beam notation	Width x overall depth, mm	f_{cu}, MPa	ρ_f, %	ρ_b, %	M_{exp}, kN.m	M_f, kN.m (Ashour Eq.1)	M_{exp}/M_f	M_p, kN.m (Proposed Eq.4)	M_{exp}/M_p	Experimental mode of failure
Masmoudi et al. [11]											
39	CB2B-1	200x300	61.18	.69	.65	57.9	63.22	0.916	59.213	0.978	Concrete crushing
40	CB2B-2	200x300	61.18	.69	.65	59.8	63.22	0.946	61.277	0.976	Concrete crushing
41	CB3B-1	200x300	61.18	1.04	.66	66	76.41	0.864	68.039	0.97	Concrete crushing
42	CB3B-2	200x300	61.18	1.04	.66	64.8	76.41	0.848	66.727	0.971	Concrete crushing
43	CB4B-1	200x300	52.94	1.47	.59	75.4	73.31	1.028	78.365	0.962	Concrete crushing
44	CB4B-2	200x300	52.94	1.47	.59	71.7	73.31	0.978	74.291	0.965	Concrete crushing
45	CB6B-1	200x300	52.94	2.20	.60	84.8	86.23	0.983	88.77	0.955	Concrete crushing
46	CB6B-2	200x300	52.94	2.20	.60	85.4	86.23	0.99	89.436	0.955	Concrete crushing
Grace et al. [10]											
47	cb-st	152x350	56.78	.23	.26	51.91	61.48	0.844	52.734	0.984	FRP rupture
Thériault and Benmokrane [14]											
48	BC2HA	130x180	67.29	1.24	.62	19.7	18.15	1.085	18.862	1.044	Concrete crushing
49	BC2HB	130x180	67.29	1.24	.62	20.6	18.15	1.135	19.777	1.042	Concrete crushing
50	BC2VA	130x180	114.59	1.24	1.02	22.7	23.33	0.973	21.923	1.035	Concrete crushing
51	BC4NB	130x180	54.35	2.7	.36	20.6	18.91	1.089	19.777	1.042	Concrete crushing
52	BC4HA	130x180	63.41	2.7	.44	21	20.51	1.024	20.185	1.04	Concrete crushing
53	BC4HB	130x180	63.41	2.7	.44	21.4	20.51	1.043	20.593	1.039	Concrete crushing
54	BC4VA	130x180	110	2.7	.85	28.4	27.14	1.046	27.806	1.021	Concrete crushing
55	BC4VB	130x180	110	2.7	.85	29.5	27.14	1.087	28.951	1.019	Concrete crushing

Table 1- (Continued)

No.	Beam notation	Width x overall depth, mm	f_{cu}, MPa	ρ_f, %	ρ_b, %	M_{exp}, kN.m	M_f, kN.m (Ashour Eq.1)	M_{exp}/M_f	M_p, kN.m (Proposed Eq.4)	M_{exp}/M_p	Experimental mode of failure
Toutanji and Saafi [15]											
56	GB1-1	180x300	41.18	0.53	0.60	60	44.07	1.361	61.494	0.976	Concrete crushing[a]
57	GB1-2	180x300	41.18	0.53	0.60	59	44.07	1.339	60.407	0.977	Concrete crushing[a]
58	GB2-1	180x300	41.18	0.79	0.62	65	59.35	1.095	66.946	0.971	Concrete crushing
59	GB2-2	180x300	41.18	0.79	0.62	64.3	59.35	1.083	66.181	0.971	Concrete crushing
60	GB3-1	180x300	41.18	1.10	0.63	71	61.91	1.147	73.521	0.966	Concrete crushing
61	GB3-2	180x300	41.18	1.10	0.63	70.5	61.91	1.139	72.972	0.966	Concrete crushing
Pecce et al. [13]											
62	F2	500x185	35.29	.70	.33	36.8	38.51	0.955	36.606	1.005	Concrete crushing
63	F3	500x185	35.29	1.22	.26	60.7	48.51	1.251	62.256	0.975	Concrete crushing
Al-Musallam et al. [2]											
64	comp-00	200x240	41.65	1.33	.41	40.25	38.86	1.036	40.258	1	Concrete crushing
65	comp-25	200x240	42.82	1.33	.30	40.25	39.52	1.018	40.258	1	Concrete crushing
66	comp-50	200x240	42.94	1.33	.30	40.25	39.83	1.01	40.258	1	Concrete crushing
67	comp-75	200x240	44.12	1.33	.31	44.28	40.63	1.09	44.548	0.994	Concrete crushing
Duranovic et al. [9]											
68	GB5	150x250	36.71	1.36	.29	40.3	33.46	1.204	40.311	1	Concrete crushing
69	GB9	150x250	46.82	1.36	.36	39.73	38.56	1.03	39.706	1	Concrete crushing
70	GB10	150x250	46.82	1.36	.36	39.5	38.56	1.024	39.462	1	Concrete crushing
71	GB13	150x250	52.81	.91	.39	32.68	26.57	1.23	32.273	1.013	Concrete crushing
Mean								**1.027**		**1.013**	
St. dev.								**13.7 %**		**5.9 %**	

Note: [a] indicates disagreement between the predicted and experimentally observed flexural failure modes

DUCTILITY

The ductility of a beam can be defined as its ability to sustain inelastic deformation without loss in its load carrying capacity prior to failure. Following this definition, ductility can be expressed in terms of deformation or energy absorption. In the case of steel reinforced beams, where there is clear plastic deformation of steel at yield, ductility can be calculated as the ratio of ultimate deformation to deformation at yield. With FRP reinforced beams, there is no yield point; consequently, this simple definition can not be applied. ACI Committee 440-2001 [19] reported that the ductility of the FRP reinforced beams can be evaluated by means of the deformability factor (DF), defined as the ratio of the energy absorption at ultimate (area under load-deflection curve up to ultimate load) to the energy absorption at service load (at the serviceability deflection limit of span / 180).

Table 2 shows the values of DF for 35 GFRP reinforced concrete beams covered the big range of ρ_f from 0.14 % to 3.6%.

Examining the graph in Fig. 5, it can be seen that the GFRP reinforced concrete beams which failed under compression failure (concrete crushing) achieved higher DF values compared with those failed due to GFRP rupture (tension failure), and the value of DF increases with the increase of ρ_f till a certain value equal nearly 1.5% after this limit the DF decreases.

Table 2 and Fig. 5 also show that, DF for compression failures were observed to be in the range of 4 to 15, whereas for tension failure, the ratios where observed to be in the range of 2 to 7.
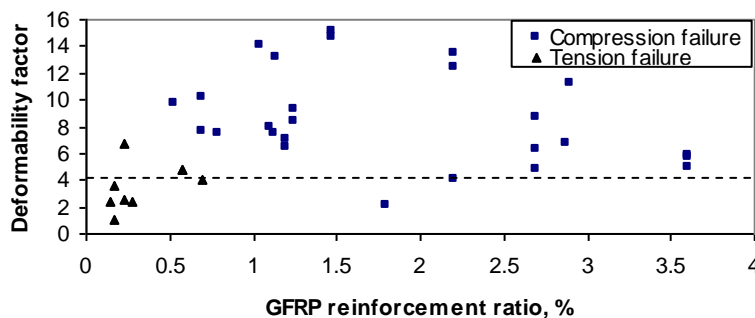
Fig. 5- Influence of GFRP reinforcement ratio and failure type on deformability factor

The graph in Fig. 5 indicates that the all sections reinforced with GFRP rebars and failed under compression (over reinforced sections) have DF exceeding a minimum value of 4 to ensure a ductile failure as specified by CSA-S6-00 [26]. Whereas, 55% of the sections failed due to GFRP rupture have DF under this limit. Consequently, it is very needed to check the deformability in design of FRP-under reinforced sections.

CONCLUSIONS

Based on this study, the following conclusions can be made:

1. In this study, the Ashour model has been modified to give a more accurate and simple mathematical model for predicting the moment capacity of RC members with rectangular section reinforced with FRP rebars. It has been developed and validated against the experimental results of 71 GFRP-reinforced concrete beams from different recent researches. The new proposed equation provided an excellent correlation with test results. It is not limited to GFRP bars only, but can be used for other types of FRP bars.
2. Compression failure is a better mode of failure than tension failure in GFRP- reinforced concrete beams. This observation is based on the following factors; compression failure attained higher moment capacity, relatively gradual failure, and higher deformability factor i.e. better member deformability.
3. This study indicates that the values of deformability factor increase with increase of GFRP-reinforcement ratio up to 1.5 %; after this limit the deformability factors decrease.

4. Deformability factor in the range of 4 to 15 were observed for the beams failing in compression, where a higher percent of tension reinforcement provided a higher deformability factors. Whereas, for tension failure, the ratios where observed to be in the range of 2 to 7.

5. From this study, 55% of GFRP-reinforced concrete beams failed under tension have deformability factors less than a minimum value of 4. Therefore, it is strongly recommended to check the deformability in design of FRP-under reinforced sections.

Table 2- Deformability factors of various GFRP- reinforced concrete beams

No.	Beam notation	f_{cu}, MPa	ρ_f, %	DF	Experimental mode of failure
Ashour [1]					
1	Beam 2	32.56	0.23	6.75	FRP rupture
2	Beam 4	32.56	0.17	1.08	FRP rupture
3	Beam 6	32.56	0.14	2.33	FRP rupture
4	Beam 8	58.93	0.23	2.59	FRP rupture
5	Beam10	58.93	0.17	3.65	FRP rupture
6	Beam12	58.93	0.28	2.4	FRP rupture
Benmokrane et al. [6]					
7	ISO 2	50.59	1.13	7.5	Concrete crushing
8	ISO 3	50.59	0.57	4.72	FRP rupture
9	ISO 4	50.59	0.57	4.72	FRP rupture
Masmoudi et al. [11]					
10	CB2B-1	61.18	.69	7.6	Concrete crushing
11	CB2B-2	61.18	.69	10.15	Concrete crushing
12	CB3B-2	61.18	1.04	14	Concrete crushing
13	CB4B-1	52.94	1.47	15.13	Concrete crushing
14	CB4B-2	52.94	1.47	14.7	Concrete crushing
15	CB6B-1	52.94	2.20	13.4	Concrete crushing
16	CB6B-2	52.94	2.20	12.4	Concrete crushing
Toutanji and Saafi [15]					
17	GB1-1	41.18	0.53	9.7	Concrete crushing
18	GB2-1	41.18	0.79	7.5	Concrete crushing
19	GB3-1	41.18	1.10	8	Concrete crushing
Thériault and Benmokrane [14]					
20	BC2HA	67.29	1.24	8.3	Concrete crushing
21	BC2VA	114.59	1.24	9.2	Concrete crushing
22	BC4HA	63.41	2.70	8.6	Concrete crushing
23	BC4VA	110	2.70	6.3	Concrete crushing
Al-Sayed et al. [23]					
24	II	36.8	3.6	4.9	Concrete crushing
25	III	36.8	1.2	6.5	Concrete crushing
26	IV	47.9	1.14	13.2	Concrete crushing
27	V	47.9	2.87	6.7	Concrete crushing
Diaa [24]					
28	1FIC	44	1.8	2.14	Concrete crushing
29	2FIC	66.7	2.7	4.8	Concrete crushing
30	3FIC	66.7	3.6	5.8	Concrete crushing
Habeeb and Ashour [25]					
31	GsO	33	2.2	4.11	Concrete crushing
32	GsU	36	0.7	4	FRP rupture
Al-Sayed [3]					
33	B	36.5	3.6	5.7	Concrete crushing
34	C	36.5	1.2	7	Concrete crushing
35	D	48.2	2.9	11.2	Concrete crushing

LIST OF SYMBOLS

A_f	area of bottom FRP bars
A_{fb}	area of FRP bars at balanced conditions
b	width of concrete beam
C	concrete compressive force
d	effective depth of section
DF	deformability factor
E_f	elastic modulus of FRP bars
f_{cu}	concrete cube compressive strength
f'_c	cylinder compressive strength
f_f	stress in bottom FRP bars
f_{fu}	tensile rupture of FRP bars
h	overall depth of test specimens
k_1	ratio of the average compressive stress to the concrete cube strength
k_2	ratio of the depth of the idealized rectangular stress block to the neutral axis depth
M_{exp}	experimental moment capacity
M_f	theoretical moment capacity of GFRP sections calculated by Ashour formula
M_p	theoretical moment capacity of GFRP sections calculated by the proposed equation.
P	total failure load
P_{cr}	total load at first visual crack
T_f	force in bottom FRP bars
x	depth of the neutral axis
x_b	depth of the neutral axis for balanced section
ε_c	strain at the top compression level of the concrete section
ε_{cu}	ultimate strain of concrete (=0.003)
ε_f	strain in bottom FRP bars
ε_{fu}	ultimate strain of FRP bars
ρ_b	balanced reinforcement ratio of FRP bars
ρ_f	FRP reinforcement ratio (A_f/bd)

REFERENCES

1. Ashour, A. F. (2006)," Flexural and Shear Capacities of Concrete Beams Reinforced with GFRP bars", Construction & Building Materials Journal ,(20), pp.1005–1015.
2. Al-Musallam, T. H.; Al-Salloum, Y. A.; Al-Sayed, S. H; and Amjad, M. A. (1997),"Behavior of Concrete Beams Doubly Reinforced by FRP Bars", Third International Symposium on Non-Metallic(FRP) Reinforcement for Concrete Structures (FRPRCS-3), Japan, Vol. 2, pp. 471–478.
3. Al-Sayed, S. H.(1998)," Flexural Behaviour of Concrete Beams Reinforced with GFRP Bars" , Cement & Concrete Composites Journal, 20(1),pp.1–11.
4. Al-Sayed, S. H.; Al-Salloum, Y. A.; and Al-Musallam, T. H. (1997)," Shear Design for Beams Reinforced by GFRP Bars", Third International Symposium on Non-Metallic (FRP) Reinforcement for Concrete Structures (FRPRCS-3), Japan, vol. 2,pp. 285–292.
5. Benmokrane, B.; Chaallal, O.; and Masmoudi, R.(1995),"Glass Fiber Reinforced Plastic (GFRP) Rebars for Concrete Structures", Construction & Building Materials Journal, 9(6),pp.353–364.
6. Benmokrane, B.; Chaallal, O.; and Masmoudi, R.(1996)," Flexural Response of Concrete Beams Reinforced with FRP Reinforcing Bars", ACI Structural Journal ,91(2),pp.46–55.
7. Brown, V. L.; and Bartholomew, C. L.(1993)," FRP Reinforcing Bars in Reinforced Concrete Members", ACI Materials Journal, 90(1),pp.34–39.
8. Deitz, D. H.; Harik, I. E.;and Gesund, H.(1999)," One-Way Slabs Reinforced with Glass Fiber Reinforced Polymer Reinforcing Bars", In ACI Proceedings, the Fourth International Symposium, Detroit, pp. 279–286.

9. Duranovic, N.; Pilakoutas, K.; and Waldron, P.(1997),"Tests on Concrete Beams Reinforced with Glass Fiber Reinforced Plastic Bars", Third International Symposium on Non-Metallic (FRP) Reinforcement for Concrete Structures (FRPRCS-3), Japan, vol. 2,pp. 479–486.

10. Grace, N. F.; Soliman, A.K.; Abdel-Sayed, G.; and Saleh, K.R.(1998)," Behavior and Ductility of Simple and Continuous FRP Reinforced Beams", Journal of Composites for Construction, 2(4),pp.186–194.

11. Masmoudi, R.; Theriault, M.; and Benmokrane B. (1998)," Flexural Behavior of Concrete Beams Reinforced with Deformed fiber reinforced plastic reinforcing rods", ACI Structural Journal,95(6),pp.665–676.

12. Michaluk, C.R.; Rizkalla, S., H.; Tadros, G.; and Benmokrane, B.(1998)," Flexural Behavior of One-Way Concrete Slabs Reinforced by Fiber Reinforced Plastic Reinforcements", ACI Structural Journal ,95(3),pp.353–365.

13. Pecce, M.; Manfredi, G.; and Cosenza, E.(2000)," Experimental Response and Code Models of GFRP RC Beams in Bending", Journal of Composites for Construction, 4(4),pp.182–190.

14. Theriault, M.; and Benmokrane, B. (1998)," Effects of FRP Reinforcement Ratio and Concrete Strength on Flexural Behavior of Concrete Beams", Journal of Composites for Construction ,2(1),pp.7–16.

15. Toutanji, H. A.; and Saafi, M. (2000)," Flexural Behavior of Concrete Beams Reinforced with Glass fiber-Reinforced Polymer (GFRP) Bars", ACI Structural Journal, 97(5), pp712–719.

16. Tureyen, A. K.; and Frosch, R. J. (2002),"Shear Tests of FRP-Reinforced Concrete Beams without Stirrups", ACI Structural Journal, 99(4), pp. 427–434.

17. Yost, J. R.; Goodspeed, C. H.; and Schmeckpeper, E.R. (2001)," Flexural Performance of Concrete Beams Reinforced with FRP Grids", Journal of Composites for Construction, 5(1), pp.18–25.

18. Yost, J. R.; Gross, S. P.; and Dinehart, D.W. (2001)," Shear Strength of Normal Strength Concrete Beams Reinforced with Deformed GFRP Bars", Journal of Composites for Construction, 5(4), pp. 268–275.

19. ACI Committee 440 (2001)," Guide for the Design and Construction of Concrete Reinforced with FRP Bars", Farmington Hills (MI): American Concrete Institute, 41pp.

20. Canadian Standards Association,(1996), Canadian Highways Bridge Design Code, Section 16, Fiber Reinforced Structures; 28 pp.

21. Sonobe, Y. et al. (1997),"Design Guidelines of FRP Reinforced Concrete Building Structures", Journal of Composites for Construction,1(3), pp. 90–115.

22. Egyptian Code for Design and Construction of Fiber Reinforced Polymers in Construction Fields, (2005), EC-208, Housing & Building Research Center, Cairo, Egypt, Chapter 5, pp.1.5-22.5.

23. Al-Sayed, S. H.; Al-Sallum, Y. A.; and Al-Musallam, T. H. (2000),"Performance of Glass Fiber Reinforced Plastic Bars as a Reinforcing Material for Concrete Structures", Composites Journal: Part B (31), pp. 555-567.

24. Diaa, G., (2004),"Short-Term and Long-Term Behavior of Concrete Beams Reinforced with GFRP Bars", M. Sc. Thesis, Cairo University, 133pp.

25. Habeeb, M. N., and Ashour, A. F. (2008), "Flexural Behavior of Continuous GFRP Reinforced Concrete Beams", Journal of Composites for Construction, 12(2), pp.115-124.

26. CSA-S6-00 (2000),"Canadian Highway Bridge Design Code (CHBDC), Section 16, Fiber Reinforced Structures, Canadian Standards Association, Rexdale, Canada.

NATURAL VENTILATION INSIDE TRAIN TUNNEL

*Nabil M. Guirguis , Mofrh M. Nassief , Mahmoud A. Hassan

Housing and Building National Research Center- Cairo – Egypt nabilmilad@yahoo.com
Faculty of Engineering- Shoubra- Banha University- Egypt mofrehmelad@yahoo.com
Housing and Building National Research Center- Cairo – Egypt waghassan@yahoo.com

ABSTRACT

The need for rapid and comfortable urban mass transportation has been increasing parallel to the increasing duration of traffic in the twentieth century. Underground transportation is one of the most effective and rapid means of urban mass transportation. Today, more rapid transport systems involving subway facilities are so popular that every year a transportation line is planned, design and built. In Egypt, the underground train (Tunnel Train) suffers from lots of passengers, exceeding one hundred passengers in each carriage at rush hours. The mechanical ventilation in the system of the carriage is unable to remove the excess heat and humidity, especially in summer seasons. Therefore, the need for an additional natural ventilation system is necessary to create comfortable environment inside. This paper discusses the natural ventilation of the underground train experimentally and theoretically. In the experimental work, a train model was fabricated (using Plexiglas to scale 1 : 30) and an electric heating plate was fixed in the floor of the train. Different cases of window vanes location were studied by measuring the temperature of the heated plate (33 points) and calculating the average temperature for each case, which gave a guide for ventilation. In the theoretical work, the software ANSYS Flotran [1], was used to solve the problem using the finite element and with 50,000 nodal points. The air flow distribution inside the train was presented in the form of contours and vectors. The results showed the optimum vanes location to give the most efficient air movement inside the train resulting in a sensible temperature reduction of the heated plate inside the model.

NOMENCLATURE

A: Projected area of the model normal to the air flow, m^2.
T_i : Inlet temperature, $C°$.
U_{ref} : Free stream velocity, m/s.
u, v, w : Velocity-components in x, y and z directions, m/s.
T_{norm} : normalized temperature, $°C$.
T_{sav} : average surface temperature, $°C$.
T_f : air flow temperature, $°C$.

INTRODUCTION

The purposes of ventilation system are to provide acceptable microclimate in the space being ventilated; microclimate refers to thermal environment as well as air quality.
There are two factors must be considered in the design of the ventilation system which are

fundamental to the comfort and well-being of the human occupants performance.

Brown (1966) [2], carried out an analysis for the basic mechanism of rapid-transit tunnel ventilation due to train piston action and for the temperatures resulting in the system. The effect of train scheduling on ventilation rate is discussed, as is the possibility of using models to obtain more precise design data.

Gouse, et al [3], studied on the aerodynamic drag on vehicles moving in guide ways of varying degrees of enclosure. The reason for the study was that several potential high speed ground transport system concepts involve high speed motion of vehicles in enclosed guide ways for significant portions of their travel time. Analytical and experimental investigations have been carried out.

Also, some experiments were conducted using spheres as vehicle models. Miklos and Sajben [4], studied the dynamic characteristics of bodies moving in long, finite channels using a one-dimensional, incompressible fluid description. The findings were compared with numerically integrated solutions yielding body and fluid speeds, as well as drag coefficients. The effects of various body speeds were studied. Compressibility effects were estimated and found slight for present systems.

Fox and Vardy [5] investigated the design of a rail tunnel with minimized air pressure transients generated during the entry of a high speed train, introducing the equations of motion for compressible flow in a one-dimensional duct.

Henson and Fox (1974) [6], described a practical method of calculating the aerodynamic effects of trains passing through interconnected tunnel systems so that these can be designed for acceptable pressure pulse levels, air velocities and train drag. Results obtained were compared with measurements taken on models and real tunnels and some of the comparisons are shown and discussed.

Woods and Pope [7] predicted a generalized one-dimensional flow method for calculating the flow generated by a train in a single-track tunnel. The method is capable of modeling the effects of friction, gradual area change, heat transfer, locomotive heat release, vehicle leakage and gravity body forces.

Fuji and Ogawa [8] studied aerodynamics of high speed trains passing by each other. A three dimensional flow field induced by two trains passing by each other inside a tunnel is studied based on the numerical simulation of the three dimensional compressible Euler/Navier-Stokes equations formulated in the finite difference approximation. The results show that the phenomenon is complicated due to the interaction of the flow induced by two trains.

Gerhardt and Krüger [9] presents data of investigations into the wind and train driven air movements into three new stations in Germany. Means to control the air movement and in particular to prevent excessive air infiltration into the train stations are proposed and discussed in the paper.

Howe [10]. Studied the validity of various approximations by comparison with the exact solution available for potential flow from a two-dimensional, flanged duct.

Holmes et al [11], performed a solution to the problem of predicting the airflow over a train entering a tunnel is presented using parallel processing and moving boundary condition scheme. The method is demonstrated using both incompressible and compressible flow solvers based on finite element formulation.

Tayfun [12], provided an overview of some of the CFD methods for three-dimensional computation of complex flow problems. The methods and tools include the formulations of flow with moving boundaries and interfaces. Flow around two high-speed trains in a tunnel is given as an example of flow simulation.

Auvity et al [13] studied experimentally the unsteady aerodynamic field outside a tunnel during a train entry. Unsteady velocity measurements were taken to attempt to clarify the influence of the train speed on the jet induced at the tunnel portal when the train enters.

Howe et al [14] studied theoretical and experimental investigation of the compression wave generated by a train entering a tunnel with a flared portal.

Howe [15] made an analysis on the pressure transients generated when two high speed trains meet in a tunnel. His solution is used to devise a general procedure for calculating pressure transients generated by trains of arbitrary nose profiles in tunnels of arbitrary cross-sectional shape in terms of a knowledge of the local incompressible potential flow produced by each train travelling separately in the tunnel.

Arturo et al [16] pointed out that the design of new high-speed railway lines requires longer and more numerous tunnel sections, where aerodynamic effects limit the maximum allowed train velocity for a given tunnel cross-section area. A numerical code named "Tunnel Nets and Trains (TNT)" has been developed based on the physical model and numerical method.

Mok and Yoo [17] showed a numerical study on high speed train and tunnel hood interaction. A numerical computation of the train-tunnel interaction at a tunnel entrance with real dimensions is discussed.

This work is divided into two parts, the first is experimental on a scale train model tested in a wind tunnel for different window-vanes locations to achieve maximum air flow inside the model (low average temperature). The Second part is theoretical using CFD program (ANSYS software) to investigate the air flow velocity inside the train in the form of velocity contours and vectors. The average air velocity inside the train was also calculated for comparison.

EXPERIMENTAL WORK

The first carriage of the train is taken as a model to simulate the air flow and thermal performance inside it. The model was fabricated with a scale 1:30 and tested experimentally in wind tunnel as shown in Figs. 1-a,b. Figure 2 shows a photo of the tunnel train. The model was made of plexiglass with three openings at left and right sides of the model, as shown in Fig. 3. This model was provided with an electric heating plate fixed at the floor of the metro and was isolated from the bottom. The heating plate was made of ceramic plate of dim 0.1 x 0.6 m and an electric hating wire (nickel –chrome, resistance 87 Ω) was wounded around the plate with increment 0.005 m to have a uniform heat flux along the plate. This heating source inside the metro simulates the heat generation from passengers due to metabolic processes. The heater was connected to a power supply 25 volt, 33 thermocouples were fixed along the heating plate and connected to a data logger to measure the surface temperature at different locations as shown in Fig. 4. Different experimental tests were conducted for different opening and fins arrangements to deduce the best one which attains a reduction in plate temperature which in accordance gives the best air movement inside the train.
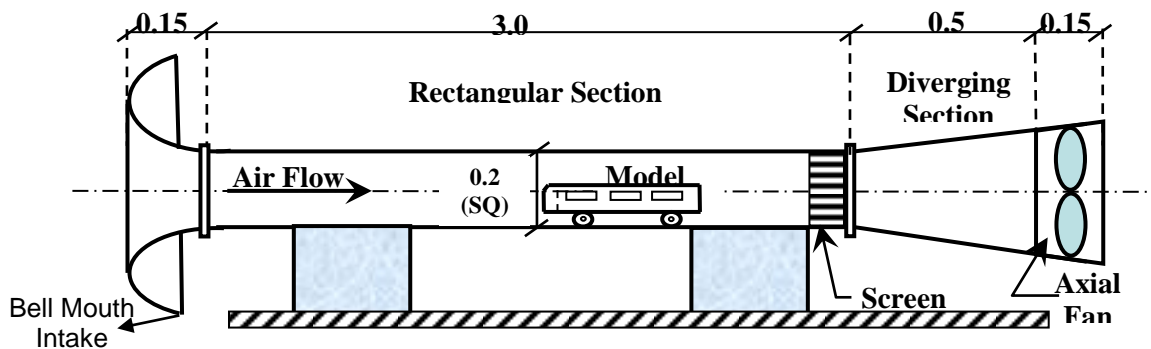
Fig 1 - a: Schematic diagram of wind tunnel, (Dim. in m).

Fig. 1-b: A Photo of wind tunnel

Fig. 2 : A photo of the metro   Fig. 3 : A photo of the Metro Car model.
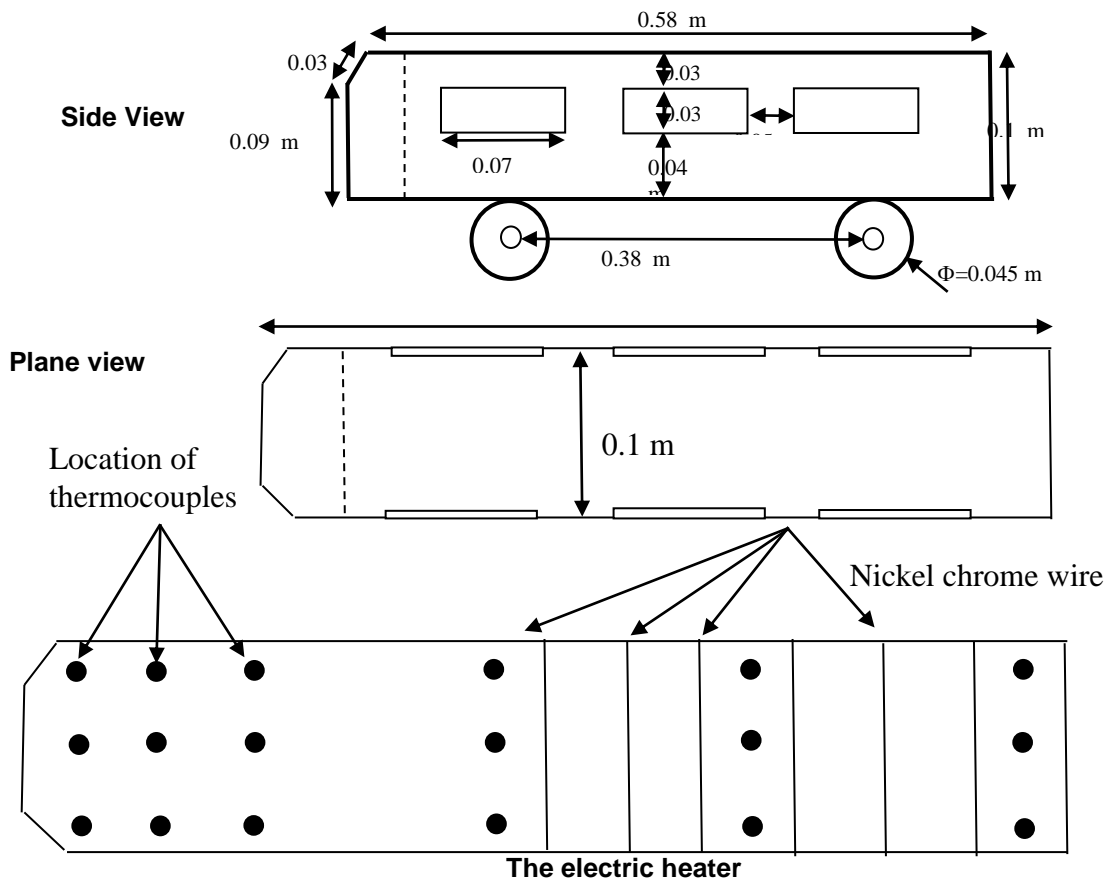

Fig. 4 : Schematic diagram of the metro Car model (side view & top view) and the layout of thermocouples

THEORETICAL WORK

The prediction of air flow patterns (velocity and pressure distribution) inside the train model in the wind tunnel requires the application of a computational fluid dynamics (CFD) program. ANSYS CFD FLOTRAN is a computer package used for predicting the air flow patterns, pressure and velocity contours. The program is a three dimensional one, that utilizes the finite element approach which uses the k-ε turbulence model and solves the Reynolds equations, the energy equation and the equations for turbulence energy and its dissipation. In the present work, the boundary conditions stipulated that the flow velocity at all the solids surfaces is zero (satisfying the real viscous fluid configuration). As shown in Fig. 5. Also the approaching velocity profiles were described by a logarithmic law. Three general assumptions are considered , the

first that the fluid is Newtonian, the flow is a single-phase one and the solution domain is of constant geometry, in addition, the flow is steady incompressible and the body forces are neglected.
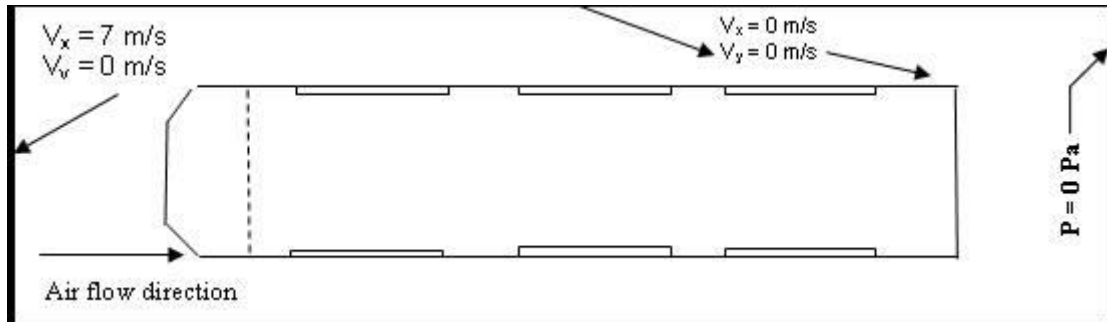
Fig. 5 : The boundary condition at the wind tunnel and model surfaces (Plane view).

To obtain a solution of the above governing equations, boundary conditions related to the physical model under consideration must be specified as no slip condition is assumed at all solid boundaries (model surfaces & ground). Thus the flow velocity is set to zero at these boundaries and the velocity profile of the undisturbed flow (upstream of the model) is assumed uniform.

Details of the solution of the above governing equations based on the k-ε turbulence modeling and the eddy viscosity approach are given in ANSYS [1]. Table 1 illustrates the different cases studies experimentally and theoretically for different window locations and fines construction.

RESULTS

Experimental Results

This paper presents the analysis and discussion of the experimental data obtained for temperature measurements inside the train model for different window and fins geometry. The test models as described were constructed for wind tunnel tests in which the average temperature inside the metro was calculated,

Fig. 6 shows the normalized average temperature ($T_{norm} = T_{av}/ T_f$) inside the train for different window construction. It is noticed that the cases when window are closed and or no air flow (cases 2,3 &4) give the higher average temperature than other cases (windows open) while the actual case gives the higher average temperature in comparison with the cases of different window locations (open cases) since the air flow inside the metro in actual case is very small than other cases. The figure shows also the best reduction in average temperature for the cases all window were opened and with fines at the external sides of the windows. These results were agreed with the theoretical one as will discuss below. The figure shows also the effect of the distance between the side wall of the tunnel and the metro side case No. 9 , since as the distance (x) increases the average temperature increase this is due to the pressure difference between the front and rear opening decrease with increasing x (lower air flow).

Theoretical Results

The prediction of air flow patterns (velocity distribution) inside the train model in the wind tunnel requires the application of a computational fluid dynamics (CFD) program. The results were obtained in the forms of velocity contours and vectors, the velocity contours and vectors give a good picture for the air flow inside the model , stagnation zones reverse flow and zero flow zones inside the train model which help in develop of the opening construction and layout which

give more air flow inside the train, the average velocity inside the train model was also predicted for different window-fins construction.

Table 1 : Experimental (wind tunnel) and Theoretical (ANSYS) Program for Metro Car Model with Different Window Locations and Construction.

Tests / Cases	Wind tunnel	ANSYS	Description	Model sketch
Case 1	√	√	Actual case One third of windows are open to the inside with tilt angle 30º , air flow=7 m/s	Front view air flow Top view
Case 2	√	X	All window are closed and no air flow	Top view
Case 3	√	X	All window are closed (air flow = 7m/s	Top view
Case 4	√	√	Window open – no air	Top view
Case 5	√	√	Window open with air flow	Top view
Case 6	√	√	Vanes are end to end of the window	Top view
Case 7	√	√	Vanes are at the centre of the window	Top view
Case 8	√	√	Vanes at 1 cm from the end of the window	Top view
Case 9	√	X	Window open & the distance between the side of the metro and the tunnel (x) was varied (1,2,3,4,5 cm)	Top view x
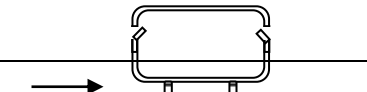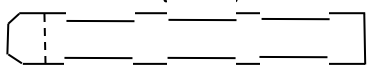
Figures from 7 to 11 give the velocity contours and vectors different w fins combination, case 1 , Fig. 6 gives the lower air flow inside the train this represents the actual
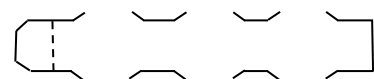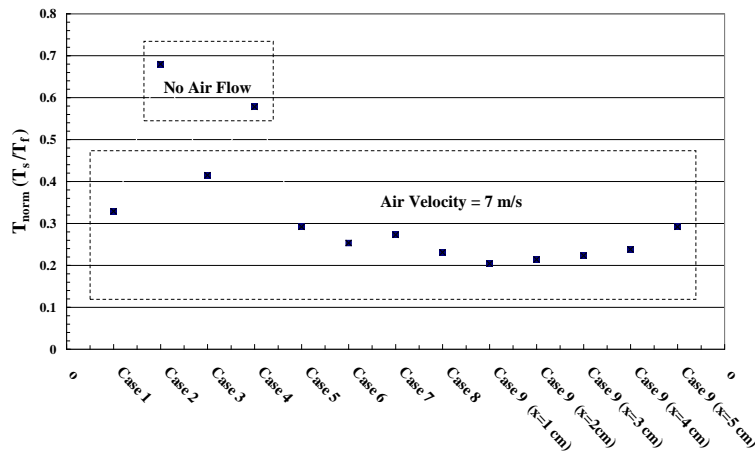
Fig. 6 :Normalized average temperature. for different window shapes with and without Vanes.

case in which the one third of the window was open to the inside with tilt angle 30° the other cases with fines supported at the external sides of the window give a reasonable air flow inside the train. Generally the air flow passes from the first and second windows and exhausted from the rear windows that may concluded that any opening at the rear side of any carriage of the train will give more air movement inside it this is due to the pressure difference between the front and rear openings.
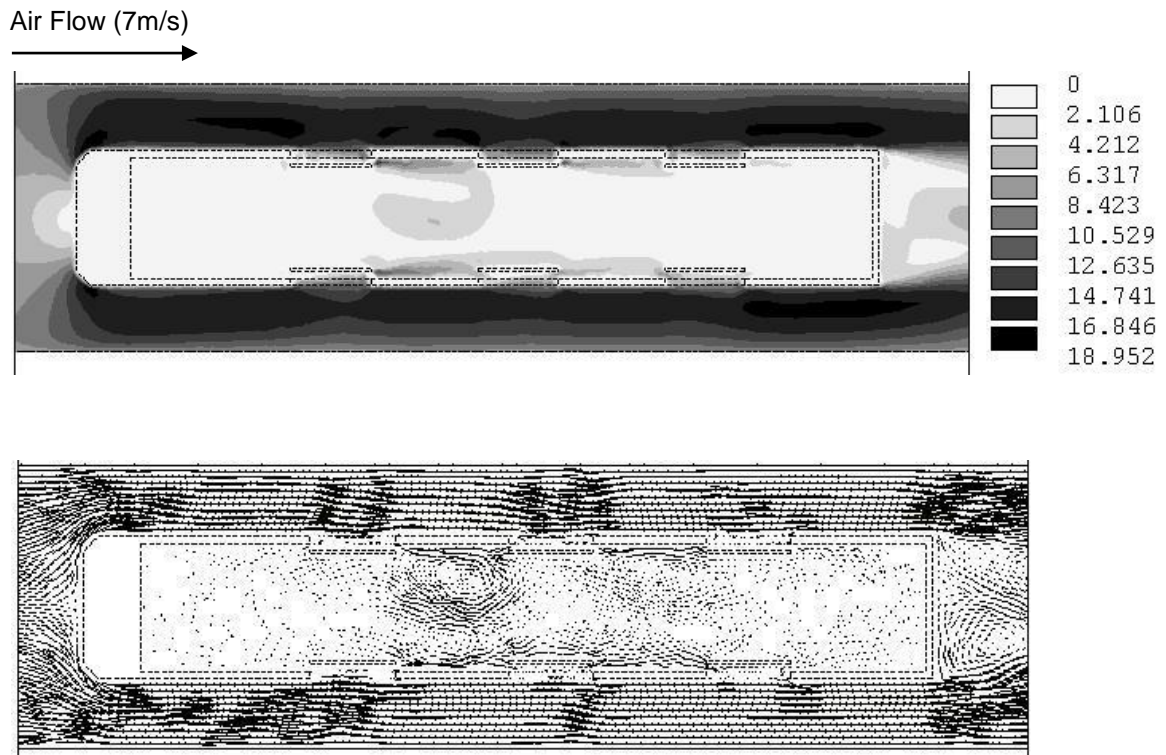
Air Flow (7m/s)

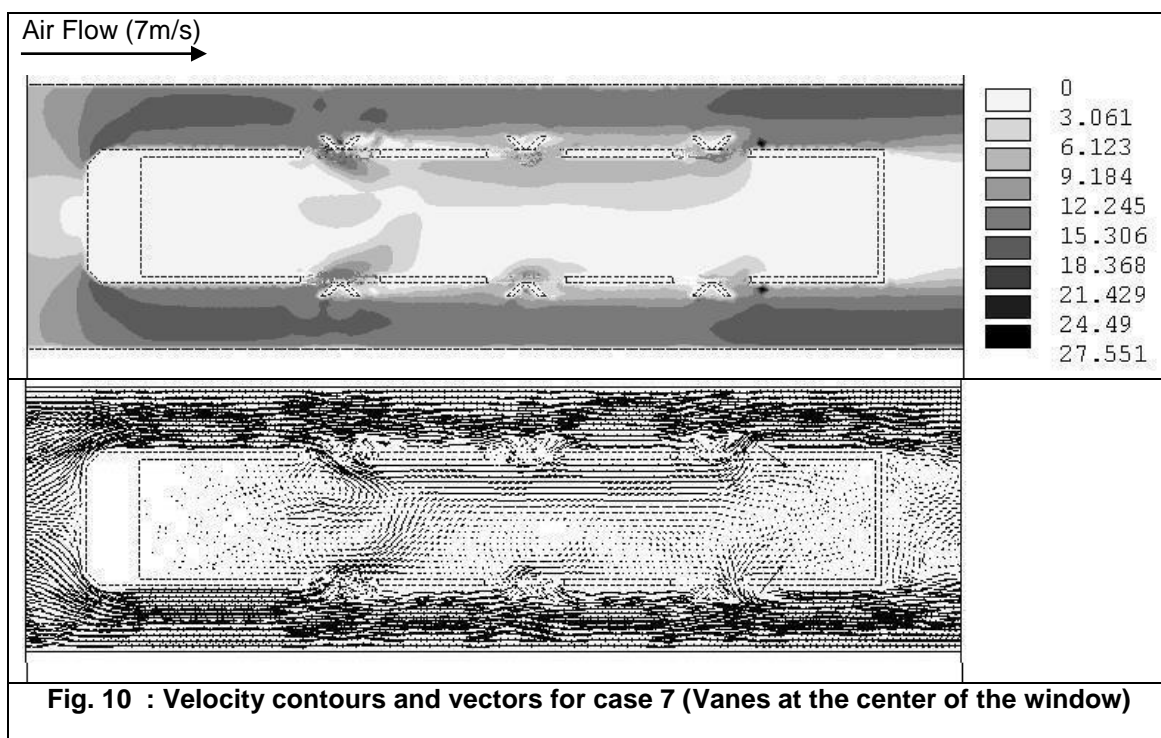**Fig. 7 : Velocity contours and vectors for case 1 (Actual case, one third of windows are open to the inside with tilt angle 30° , air flow=7 m/s (Top view)**

Air Flow (7m/s)

Fig. 8 : Velocity contours and vectors for case 5 (all windows are closed) (Top view)

**Fig. 9 : Velocity contours and vectors for case 6 (Vanes at the end to end of the window)**
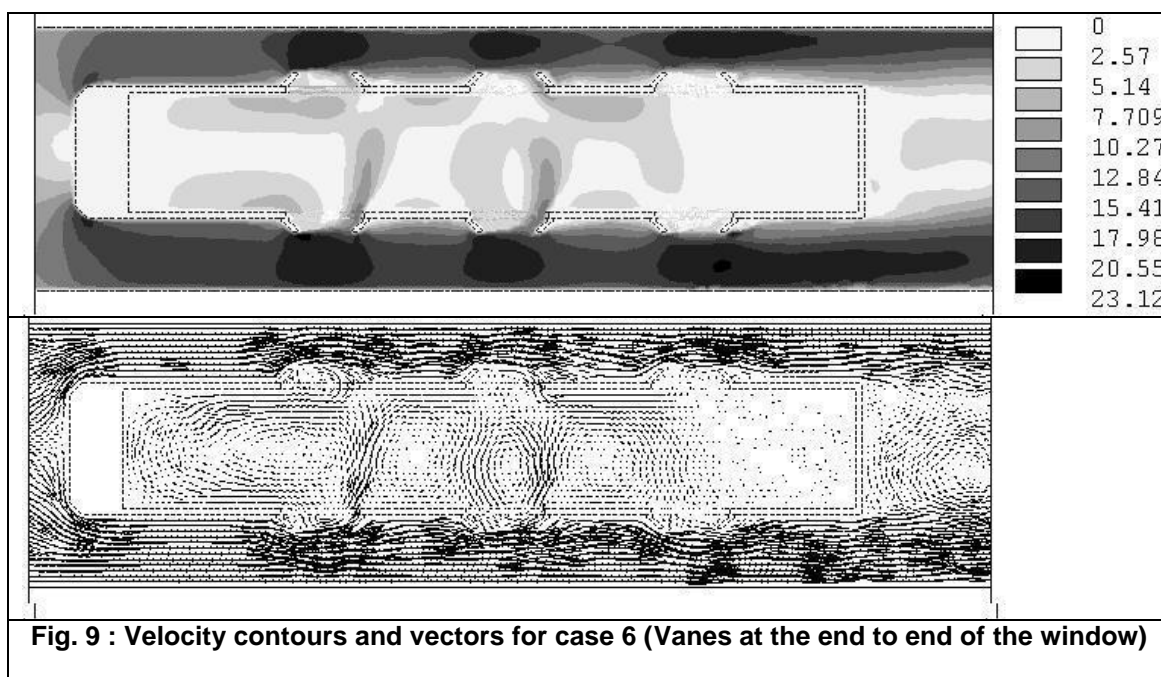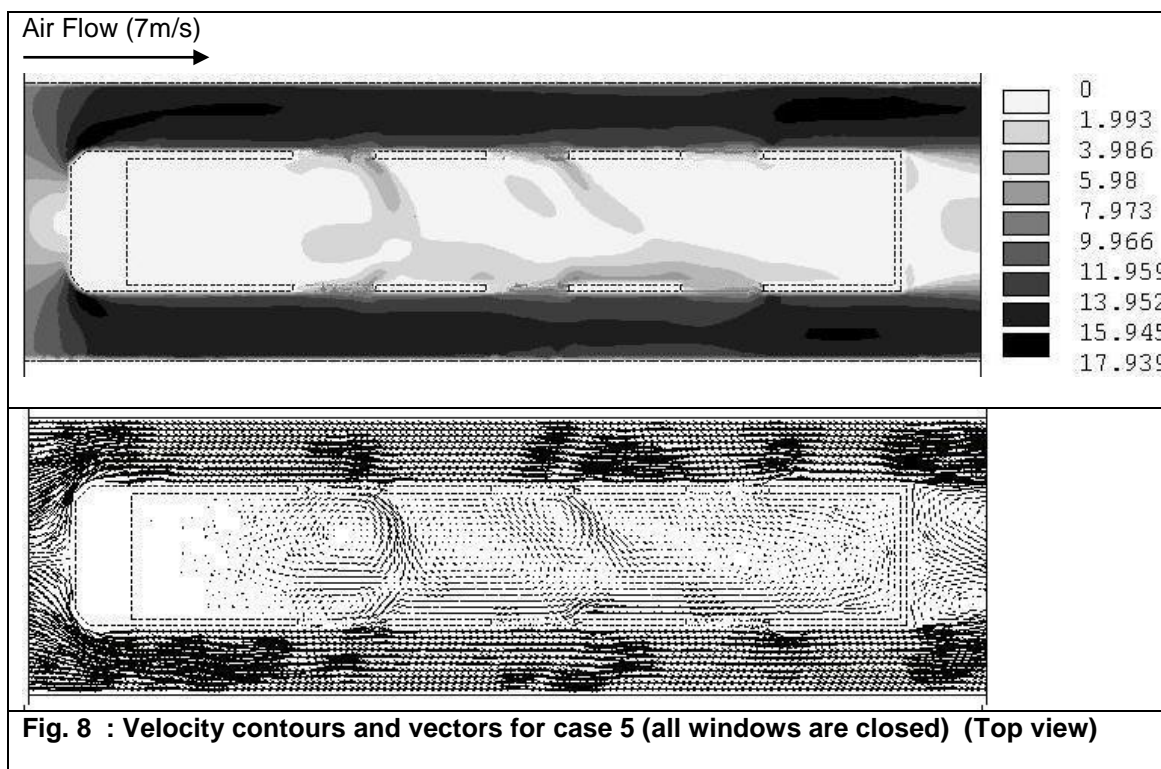
Figure 12 shows a relation between experimental results (T_{norm}) and theoretical results (average velocity) of the tunnel train model for different cases of the window-vanes combination, the two trend show that as the average air velocity inside the carriage model increases the mean average temperature decreases this means that good ventilation can relieve the temperature stress inside the train.

Air Flow (7m/s)

Fig. 10 : Velocity contours and vectors for case 7 (Vanes at the center of the window)

Fig. 11 : Velocity contours and vectors for case 8 (Vanes at 1 cm from the window edges)
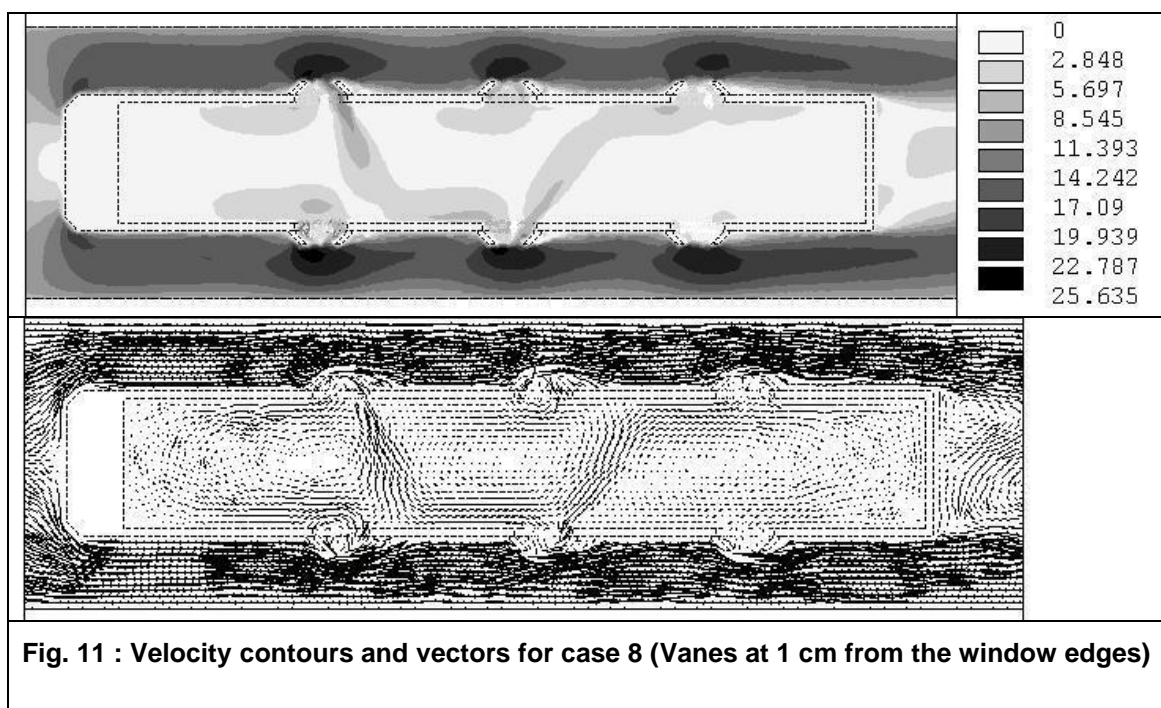
CONCLUSION

1. Natural ventilation is important for removing the excess heat inside the train in addition to mechanical ventilation.
2. Wind tunnel testing gives a reasonable idea for the effect of window-vanes combination on the air motion inside the train.

3. Cases in which the vanes mounted in the outside of the window give better ventilation than the actual case (vanes are inside).
4. As the distance between the side tunnel wall and train side (case 9) decreases while the train motion, is in the differences in pressure between train front and rear increases, and the speed of the air flow inside the train increases and more excess heat is removed
5. Rear openings are important in removing the excess heat inside the train.
6. Theoretical results give a good picture of the air flow distribution inside the train and can be applied to the whole train carriages where it is difficult to study experimentally.
7. Results can be applied for any ground transportation vehicles.
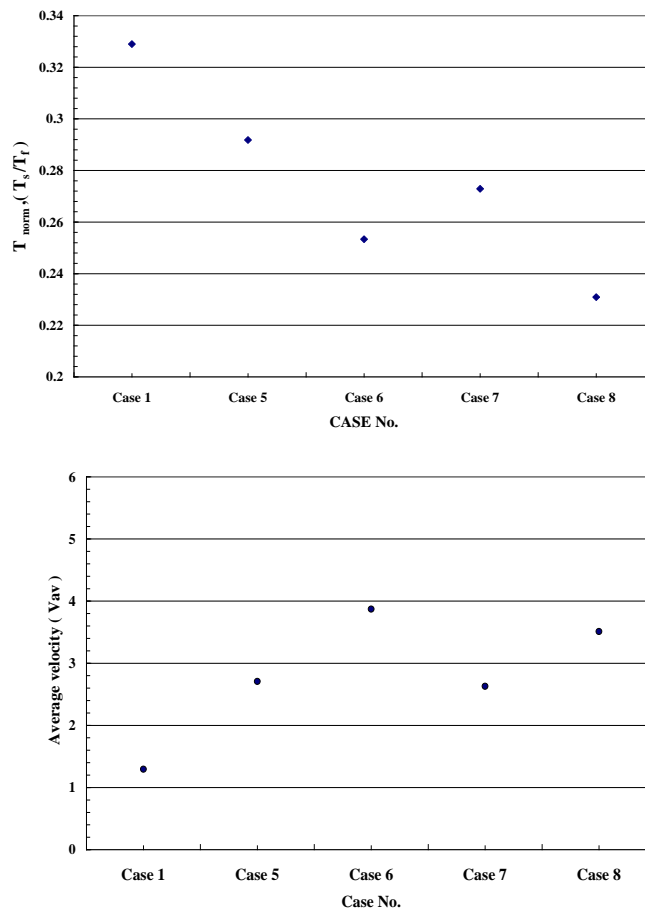
Fig. 12: Relation between experimental results (T_{norm}) and theoretical results (average velocity) of the tunnel train model.

REFERENCES

1.   ANSYS, "FLOTRAN Analysis Guide", ANSYS, Inc. 1997 .
2.   W.G. Brown (1966), "Basic Theory of Rapid Transit Tunnel Ventilation", Journal of Engineering for Industry, (65).
3.   S.W. Gouse, B.S. Noyes, J.K. Nwude, M.C. Swarden (1969), "Aerodynamic Drag on Vehicles in Tunnel", Transaction of ASME.
4.   Miklos and Sajben. (1971), "Fluid Mechanics of Train-Tunnel Systems in Unsteady Motion", AIAA Journal, 9(8).
5.   J.A. Fox and A.E. Vardy (1973), "The Generation and Alleviation of Air Pressure Transient in Tunnel", Tunnels and Tunneling.

6. Henson and Fox (1974), " Transient Flows in Tunnel Complexes of the Type Proposed for the Channel Tunnel", Journal of Proc Instn Mech Engrs, Vol. 188, pp,15-74.
7. W. A. Woods, C. W. Pope (1981), "A Generalized Flow Prediction Method for the Unsteady Flow Generated by a Train in a Sigle Tract Tunnel" Journal of Wind Engineering and Industrial Aerodynamics, 7, pp,331-360..
8. Fuji and Ogawa (1995), "Aerodynamics of High Speed Trains Passing by Each Other", Vol.24   No. 8, pp,897-908.
9. H.J. Gerhardt and O. Krüger (1998), "Wind and Train Driven Air Movements in Rain Stations", Journal of Wind Engineering and Industrial Aerodynamics, 74-76, pp,589-597.
10. B.S. Holmes, J.Dias, S.M. Rifai, J.C.Buell, Z. Johan, T. Sassa and T. Sato (1999), "Solution of Train Tunnel Entry Flow using Parallel Computing", Journal of Computational Mechanics,(23), pp,124-129.
11. M.S. Howe (1999), "On Rayleigh's Computation of the End Correction with Application to the Compression wave Generated by a Train Entering a Tunnel", Journal of Fluid Mechanics, Vol.385, pp, 63-78.
12. Tayfun E. Tezduyar (1999), "CFD Methods for Three-Dimensional Computation of Complex Flow Problems", Journal of Wind Engineering and Industrial Aerodynamics, (81), pp, 97- 116.
13. B.Auvity,M.Bellenoue,T.Kageyama,(2001), "Experimental Study of the UnsteadyAerodynamic field outside a Tunnel During a Train Entry", Experiments in Fluids, 30, pp.   221-228.
14. M.S. Howe, M. Iida, T. Fukuda and T.Maeda (2000), "Theoretical and Experimental Investigation of the Compression wave Generated by a Train Entering a Tunnel with a Flared Portal", Journal of Fluid Mechanics, (425), pp, 111-132.
15. Arturo Baron, Michele Mossi, and Stefano Sibilla (2001), "The Alleviation of the Aerodynamics Drag and Wave Effects of High-Speed Trians in Very Long Tunnels", Journal of Wind Engineering and Industrial Aerodynamics, (89), pp, 365-401.
16. B. Auvity, M. Bellenoue and T. Kagayema (2001), "Experimantal Study of the Unsteady Aerodynamic Filed Outside a Tunnel During a Train Entry", Journal of Experiments in fluids (30), pp, 221-228.
17. J.K. Mok and J. Yoo (2001), "Numerical Study on High Speed Train Tunnel Hood Interaction", Journal of Wind Engineering and Industrial Aerodynamics, (89), pp, 17-29.

PHYSICOCHEMICAL AND BACTERIOLOGICAL CHARACTERISTICS OF BIOFILM IN DRINKING WATER DISTRIBUTION SYSTEM AT POPULAR HOUSES WITH PLASTIC PIPES AND JOINTS

Dr. Mohamed Hassan Mohamed
Associate Professor in Sanitary & Environmental
Institute, Housing & Building National Research Center (HBRC)

ABSTRACT

The objective of this study is to evaluate bacteriological and physicochemical characteristic of biofilm with plastic pipes and joints in popular houses in Helwan area.

The results of this study showed that, the maximum values of turbidity (NTU), EC (Mmho/cm), total dissolved solids (mg/l) and total organic carbon (mg/l) were 33,1746,1046.5,12.1 for pipe biofilm and 25,1362,814.3,7.8 for joint biofilm respectively. On the other hand the minimum values were 19, 1231, 734, 8.1 for pipe biofilm and 13, 577, 346, 4.7 for joint biofilm in the suspensions respectively. According to bacteriological results, the total bacterial counts of either pipes or joints biofilm were more than 50 cfu/ml at 37 ºC or at 22 ºC.

 The counts of pipe biofilm were higher than the counts of joints biofilm. The highest bacterial counts were (1.98×10^2), (1.99×10^2) but the lowest counts were (1.43×10^2), (1.44×10^2) both at 37 ºC and at 22 ºC cfu/ml with pipes biofilm respectively. Eleven samples were positive for coliform detection. (1-2 MPN-index/100ml) out of 15 samples with pipes biofilm.Total bacterial counts of joint biofilm ranged from (53-96) cfu/ml both at 37 ºC and at 22 ºC. Six samples were positive for coliforms (1.MPN-index/100ml) out of 15 samples with joints biofilms.

This biofilm of drinking water distribution system is considered as an important part of the operation of drinking water plants and distribution systems.

Keywords : (Biofilm, Califorms, Total organic carbon [TOC]).

INTRODUCTION

Within drinking water distribution system biofilms grow readily on the inner walls of pipes, even in the presence of a disinfectant residual. Biofilms in distribution system pipes may affect drinking water taste and odour (Astier et al 1995).During the distribution of drinking water, bacterial regrowth may lead to a deterioration of water quality, generation of bad taste and odors proliferation of micro in vertebrates (Volk and lechevallier 1999).It is known that microbial growth in drinking water and biofilms cause aesthetic and health problems.The majority of this microbial growth accuses in biofilms of the pipes and joints. These biofilms can deteriorate the microbial quality of water (Percival and Walker, 1999, Schwartz et al 1998).

There are several studies showing that plastic materials can support the growth of biofilm in the surface inner of plastic and joints (Niquette et al 2000, Zecheus et al 2001). Also there are several factors which can influence the information of biofilms e.g microbial intrient, pipe material, disinfectants, bacteria from water and the hydraulic regine (Niquette et al 2000, Zacheus et al 2000). Pipes and joints located inside of popular building houses which have more than five years old are usually mode of plastic.

There are several studies showed that biofilms can form on that material (Schwartz et al 1998, Zacheus et al 2001).

Thus, the objective of this study was to evaluate microbiogcal and chemistry characteristics of biofilm with plastic pipes and joints of popular houses in Helwan area.

Material and Methods:
Fifteen sampling points from the popular houses in Helwan area were chosen in this study. These houses use plastic pipes and joints in house connections of drinking water distribution system. The plastic pipes and joints have more than two years old. These pipes and joints sampling were collected from fifteen popular building houses (First floor) at Helwan area which are supplied by treated water.

The pipes were cut to segments of approximately (5 cm) in length. Biofilm was sampled from an inner surface of both 5 cm from pipe and also 5 cm from joint. The biofilm of pipe and joint was aseptically removed by scraping using sterile cell scraper in 200 ml tap water from the sampling site. Thirty suspension water biofilms samples were obtained from both pipe (15 samples) and joints (15 samples).

All samples were vortexed for 5 minutes with using a vortex mixer. Some physicochemical such as conductivity, pH, TDS and Toc and bacteriological parameters such as total bacterial count and total coliform (MPN) were carried out according to APHA (2005).

RESULTS

Physicochemical and Bacteriological quality of water suspension of plastic pipes biofilms are represented in tables 1, 2.

Table 1 : Physicochemical characteristics of pipes biofilm

No of Sample	P_H	Turbidity (NTU)	EC (MMohs/cm)	TDS (mg/L)	TOC (mg/L)
1	7.2	25	1420	849	9.0
2	6.9	28	1509	892	10
3	7.1	31	1611	963	10.1
4	7.3	22	1261	754.1	8.2
5	6.8	26	1451	858.4	8.4
6	7.3	25	1422	849	9.1
7	6.8	31	1611	964	10.2
8	7.1	19	1231	734	8.1
9	7.2	19	1241	739	8.1
10	7.5	33	1746	1046.5	12.1
11	6.9	21	1256	744	8.3
12	7.0	30	1568	940.5	9.4
13	7.3	31	1572	942.5	9.3
14	7.0	22	1418	844	8.1
15	7.8	25	1421	847	8.3

The results showed that pH, turbidity and EC values ranged from (6.8-7.8), (19-33) NTU and (1231-1746) Mmho/cm respectively

Also, total dissolved solid concentrations (TDS) and total organic values ranged from (734-

1046.5 mg/l) and (8.1-12.1 mg/l) respectively.

According to the results in table 2, total bacterial count at 37 ºC ranged from (1.43x10^2 - 1.99x10^2) cfu/ml. Coliform detection was positive in 11 samples (1-2 MPN/100ml) out of 15 samples.

Also, physicochemical and bacteriological characteristics of joints biofilm are represented in tables 3, 4 .

Table 2 : Bacterial load in the suspension of biofilm

No of Sample	Total bacterial (cfu / ml)		MPN-index/100 Total coliform
	count at 37 º (C)	at 22 º (C)	
1	1.9×10^2	1.93×10^2	2
2	1.83×10^2	1.99×10^2	2
3	1.56×10^2	1.58×10^2	ND
4	1.54×10^2	1.54×10^2	ND
5	1.91×10^2	1.94×10^2	2
6	1.98×10^2	1.12×10^2	1
7	1.82×10^2	1.88×10^2	2
8	1.78×10^2	1.76×10^2	2
9	1.61×10^2	1.58×10^2	1
10	1.77×10^2	1.74×10^2	1
11	1.68×10^2	1.66×10^2	1
12	1.43×10^2	1.45×10^2	ND
13	1.46×10^2	1.44×10^2	ND
14	1.76×10^2	1.75×10^2	1
15	1.55×10^2	1.57×10^2	1

The values of pH, turbidity and EC for joints biofilm ranged from (6.8-7.5), (13-25) NTU and (577-1362) Mmho/cm respectively.

In addition to that, total dissolved solid and total organic carbon of joints biofilm ranged from (346 – 814.3) and (4.7 – 7.8) respectively.

Table 3 : PHysicochemical characteristics of joints biofilm

No. of Sample	PH	Turbidity (NTU)	EC (MMohs/cm)	TDS (mg/l)	TOC (mg/l)
1	7.2	16	866	516.5	5.7
2	7.0	17	1026	614.3	6.8
3	7.1	14	577	346	4.7
4	7.2	16	791.6	475	4.9
5	6.8	18	1036	618	6.9
6	7.3	16	732	436	5.1
7	6.9	17	860	515.1	6.0
8	7.2	18	1021	612	7.1
9	7.2	18	1023	612.1	7.1
10	7.4	19	1196	714	6.7
11	7.0	13	821	464.2	5.7
12	7.1	24	1354	812	7.2
13	7.2	22	1206	713.5	6.6
14	7.1	24	1254	749	7.1
15	7.5	25	1362	814.3	7.8

Table 4 : Bacterial load in the suspension joints biofilm

No of Sample	Total bacterial count /ml		MPN-index/100 Total coliform
	at 37 º (C)	at 22 º (C)	
1	81	83	ND
2	57	56	1
3	73	72	ND
4	69	89	1
5	81	68	ND
6	94	96	1
7	89	82	1
8	78	76	ND
9	74	76	ND
10	61	64	ND
11	63	66	ND
12	77	78	1
13	68	58	ND
14	76	74	1
15	58	53	ND

Total bacterial count of joint biofilm ranged from (57-94) cfu/ml at 37 ºC and (53 -96) cfu/ml at 22 ºC in table 4.

Coliform detection was positive (1-MPN/100ml) in sex sample out of 15 samples.

As general results, total bacterial count was more than 50 cfu/ml either with pipe biofilm or joints biofilm in tables 3, 4.

The phisicochemical and bacteriological water quality in Helwan area table 5 were (7.2-7.3), 0.4, (190-243) for P_H, turbidity and TDS.

Total bacterial count at 37ºC and 22ºC were 1-5 cfu/ml with drinking water from Tabbin, Kafer El-Elow and Shamal Helwan drinking water treatment plant.

The result of drinking water in distribution system in Helwan area, (7.3 – 7.4) pH, (0.2 – 0.4) Turbidity (NTU), (193 – 212) TDS (mg/l).

Total bacteriological counts with drinking water in distribution system of Helwan area (1 – 4) cfu/ml.

Table 5 : PHysicochemical and Bacteriological characteristic of Water in Helwan Area

Sample	PH	Turbidity (NTU)	T.DISTRIBUTIONS (mg/l)	Total bacterial count/ml		MPN/100 ml Total coliform
				at 37 º (C)	at 22 º (C)	
1-Tebbin Treatment Plant						
• Intake Row Water	8.3	5.5	173	200	100	230
• Effluent Treatment	7.3	0.4	190	1	2	ND
• Distribution System	7.3	0.4	193	1	1	ND
2-Kafer El-Elow Treatment Plant						
• Intake Row Water	8.3	5.0	210	220	800	150
• Effluent Treatment	7.2	0.4	243	3	6	ND
• Distribution System	7.4	0.4	212	4	3	ND
3-Shamal (South Helwan) Treatment Plant						
• Intake Row Water	8.0	4.5	187	230	110	230
• Effluent Treatment	7.2	0.4	195	5	5	ND
• Distribution System	7.3	0.2	193	1	1	ND

On the other hand, total coliform was absence with all drinking water table 5.
From the physicochemical and bacteriological results, it can be observed that the content of biofilm of pipes or joints release in to drinking water could lead to a risk of pathogenic or opportunistic bacterial infection and have a negative effect on consumer health.

DISCUSSION

Maintaining drinking water quality in distribution system is a main challenge for drinking water producers. Biofilm formation in water distribution system depends on a variety of factors e.g.

water composition, amount and types of nutrient, disinfectant, residuals, thermal and hydraulic condition but also on the type and composition of pipe and joint motional as a substratum. Composition of pipe and joint material affects the attachment rate of bacteria (Lechevallier at al 1990) but certainly also e.g. by release of compounds which may be excellent substrates for bacterial growth. In this study the pipes biofilm results, it can be observed that turbidity, total dissolved solid and total organic carbon values ranged from(19-33,734-1046.5) and (8.1-12.1) table(1) with pipe biofilm.

The bacterial result with suspension of the pipe biofilm, total bacterial count ranged from $(1.43x10^2 – 1.99x10^2)$ cfu/ml and coliform density was (1 – 2) MPN/100 ml.

Coliform density was 1-2 MPN-index/100 ml in 11 samples out of 15 samples in pipe biofilms.

On the other hand the joint biofilm, turbidity, total dissolved solid and total organic carbon values ranged from (13-25), (346-814.3 mg/l) and (4.7-7.8 mg/l) table[2].

The bacteriological result with joint biofilm suspension in table [4], total bacterial count ranged from (53-96) cfu/ml and coliform density was 1 MPN-index/100ml in 6samples out of 15 samples. Drinking water quality either from Tebbin, Kafer El-Elow and Shamal Helwan.

Drinking water treatment plant and its distribution system comply with Egyption standard 2007.

The link between organic content and bacterial growth resulting in biological slines that may attach to the surface of distribution pipes has been reported by (Fewtrell and Bartram 200l, lenton at al 2005).

Within drinking water distribution system biofilm grows readily on the inner walls of pipes or joints even in the presence of a disinfectant residual.

During the distribution of drinking water, bacterial regrowth may lead to a deterioration of water quality, generation bad taste and odors and proliferation of microinvertebrat (Volk and lechevalles 1999)

It is known that microbial regrowth in biofilm cause aesthetic and health problems (Sihan et al 2006, Hallam et al 2001)

There are several studies showing that plastic materials can support the growth of biofilm (Silhan et al 2006, Schwartz, et al 1998, Zacheus et al 2001).

Generally biofilm control is becoming recognized as an important part of the operation of drinking water plant and distribution system (Jagals2006).

From these results it can be concluded that biofilm should be controlled by choosing the type of pipes and joints material and survival time of these material in using the connection of housing according to the water quality of drinking water from drinking water treatment plant.

REFERENCES

1. Hallam, N.B, West, J.R, Forster, C.F. and Simms, J. (2001) "The potential for biofilm growth in water distribution systems" water Res.35:4063-4071.
2. Schwartz, T, Hoffman, S. and Obst, U (1998) Formation and bacterial composition of young natural biofilms Obtained from public bank-fettered drinking water system. Water Res. 32(9): 2787-2797.
3. Niquette,p., Servais, p. and Savoir, R. (2000) Impacts of pipe materials on densities of fixed bacterial biomass in a drinking water distribution system. Water Res. 34 (6): 1952-1956.
4. Volk, C.J. and Lechvallier, M.W (1999) Impacts of the reduction of nutrient levels on bacterial water quality in distribution systems "J. Applied environ. Microbal. 65: 4957-4966.
5. Parcival, S.L and Walker.J.T. 1999 "potable water and biofilms a review of the public health implications" Biofouling 42(2): 99-115.
6. Fowtrell, L. and Bartram, J. (2001) Water quality: Guidelines standards and health-assessment of risk and risk management of water-related in fectious Disease. World Health organization IWA London UK.
7. Silahan, S., Carfitzen, C.B and Abrechtsen, H.J. (2006) Effect of temperature and pipe material on bifilm formation and survival of Eschevchia in used drinking water pipes: a laboratory- based study water science & technology 54 (5):49-56.
8. Astier, F., Paquin J.L, Mathieu L..Morlot M. and Hartman P. (1995) Study of the development of musty taste in water according to its ageing process in pilot plant. Environ. Technology 16:955-965.

9. Zacheus, O.M, Livanainen, E.K. Nissinen T.K, Lehtola, M.J. and Martikainen P.J. (2000) Bactrial biofilm formation on polyvinyl chloride polyethylene and stinless steel exposed to ozonated water .Water Res. 34(1):63-70.

10. Zacheus,O.M.Lehtola M.J.,Korhonen.L.K. Martikainen P.J. (2001) "Soft deposits the key site for microbial growth in drinking water distribution net works. Water Res. 35(7) :1757-1765 .

11. Echevallier M.W., Lowry C.EDISTRIBUTION and lee R.G (1995). Disinficting biofilms in a medal distribution system .J. American water works Assoc., 82 (7) 87-99.

12. Lenton, R. Wright, A.M and Lewis,K, (2005).Health dignity and development : what will it take ? UN .Millennium project task force on water sanitation Earth scan London 15BN-1 84407-219-3.

13. Jagals,P.(2006) Does improved Access to water supply by rural houses holds, enhance the concept of safe water the point of use? A case study from deep rural South Africa wate science & technology 54 (3):6-16.

14. APHA,2005 Standard methods for the Examination of water and wastewater 21th Edn.,public Health Association Washington,

HALF INDUSTRIAL MODEL STUDY FOR HEAVY METAL REMOVAL USING UNTREATED AND ACTIVATED RICE STRAW

* M. M. El Shafei [1] , A.A. K. Karakish [1], A. Abd El Maguid [2]
[1]*Associate Professor, Housing & Building National Research Center*, *Cairo, Egypt*
[2]*Researcher, Housing & Building National Research Center*, *Cairo, Egypt*
m.elshafi@hbrc.edu eg.

ABSTRACT

This paper reports the results of the study on the performance of low-cost adsorbent such as raw rice straw (RRS) and activated straw with sodium hydroxide in removing the heavy metals such as iron and manganese from a ground water plant in Manial Sheiha village –Abou El Nomros district –Giza governorate; where the concentrations of iron & manganese are above the permissible level, which are 0.3 Mg/lit. for iron and 0.1 Mg/lit. for manganese ; this derived the people of the village to bring water from outside the plant for drinking & cooking. The adsorbent materials adopted were found to be an efficient media for the removal of heavy metals in continuous mode using Half industrial model. The column studies were conducted with steady flow plus studying the effects of changing parameters like flow and straw activation on removal process.
It is found that the adsorption capacity and adsorption rate constant were increased when the rice straw is treated with sodium hydroxide, when compared with that of RRS. Also the process of iron and manganese removal from ground water depended on the inlet flow to the unit where the efficiency increases with decrease of the flow and vice versa.
This research is considered a preliminary experiment for a deep study to determine a design & operation characteristics for water treatment plant using rice straw for removal of iron & manganese. Limited numbers of parameters were used in the research in order to put the main lines for a detailed research plan in a longer study period to reach the best operating methods for best percentages of iron & manganese.

Keywords: Heavy metal removal, Adsorption study, Continuous experiments, iron, Manganese and straw.

INTRODUCTION

Ground water is considered one of the purest water sources from the bacteriological side as long as it has not been contaminated from soil surface. The concentration of solutes especially iron and manganese salts limits the use of ground water sources in water treatment plants plus the possibility of its content of bacteria and parasites in certain areas. Ground water is treated and converted into drinking water through removal of manganese by traditional methods and its chlorination before being pumped into water networks. The decade of Egyptian ministry of health number 108 for year 1995 determines manganese concentration in ground water as follows:

> 0.1   Mg/ml for filtered water.
> 0.5   Mg/ml for mixed & ground water.

Rice planted areas in Arab Republic of Egypt are 1232 thousands hectares according to the reports of ministry of agriculture and land reclamation - sector of economic affairs. The amount of agricultural wastes from these planted areas are 2168 thousands tons yearly. The main compound of husk is cellulose which is 43% of the total weight and the inorganic materials are about 16%, 83% of it is silica.

One of the easiest ways to get rid of rice straw is by burning it in the field which doesn't cost the farmer any transportation costs, husk reuse or providing large storage areas plus its low nutrional value as animal food.

Burning rice straw in open fields leads to extreme air pollution, and it affects the residential areas on its movement by wind, plus it produces large amount of harmful gases.

Heavy elements have toxic effects on human & animal due to their presence as ions in water and they are ready for absorption by the body, even a very small amount can cause severe physiological or neurological damage to the human body [1-9] , e.g. lead & copper are present in industrial sewage water; therefore there must be a method for their removal [10]

In recent years, attention has been focused on the utilization of unmodified or modified rice husk as a sorbent for the removal of pollutants. Unmodified rice husk [11-13] has been evaluated for their ability to bind metal ions. Various modifications on rice husk have been reported in order to enhance sorption capacities for metal ions and other pollutants [14-21]. There is a need to carryout the columns studies to assess the required contact time for the adsorbate to achieve equilibrium as the results obtained from the batch studies for the heavy metal adsorption studies may not be directly applied for field applications in the treatment of wastewater [22-25].

In this reported study, an effort has been made to study the removal of heavy metals in fixed bed column with rice straw and arrive at the adsorption column design parameters.

This research is considered an application on half industrial level based on a research done by the same authors published in the same issue of the journal. It was about the possibility of using rice straw to remove manganese from water and it studied the quality of rice straw in removing manganese from water in different rice straw sizes, different activating methods and degrees, plus different temperature and pH .

In this research an experiment was done using rice straw for removal of iron & manganese from a ground water plant in Manial Sheiha village –Abou El Nomros district –Giza governorate; where the concentrations of iron & manganese are above the permissible level, which are 0.3 Mg/lit. for iron and 0.1 Mg/lit. for manganese ; this derived the people of the village to bring water from outside the plant for drinking & cooking.

This research is considered a preliminary experiment for a deep study to determine a design & operation characteristics for water treatment plant using rice straw for removal of iron & manganese. Limited numbers of parameters were used in the research in order to put the main lines for a detailed research plan in a longer study period to reach the best operating methods for best percentages of iron & manganese.

Through the first part of the research concerning the detailed study using rice straw for manganese adsorption under several research parameters as: temperature, mixing speed, Ph, manganese concentration, husk size, types & degrees of activation, the following was found:

Best manganese adsorption efficiency using washed straw also, activated straw with sodium hydroxide happened at 1 liter solution with 0.1mol,.So,we have been used the previous two types of straw in this research.

The aim of the research is to study the possibility of using rice straw for removing iron & manganese from the natural ground water with steady flow plus studying the effects of changing parameters like flow and straw activation on removal process.

Materials & methods

Half industrial model was carried out in the research using natural ground water containing iron and manganese through up vertical flow filters. The model was operated in the same way as ground water plant where the model existed.

Rice straw

Characterization of raw rice straw (RRS) were characterized by using X-ray diffraction (XRD) (Figure 1) and scanning electron microscope (SEM). (Figure 2) The X-ray diffraction spectra were obtained by using a Shimadzu XRD 6000 X-ray diffractometer. XRD analysis was carried out to identify the mineral composition and morphological features of adsorbents. The prepared rice straw samples were exposed to X-ray (k = 1.54060 A°) with the 2θ angle varying between 10 and 40 with Cu K_ radiation. The applied voltage and current were 40 kV and 30 mA, respectively. Scanning electron microscopy (SEM) investigations of the rice straw samples were

conducted in a JEOL JMT-300 operated at 30 kV and linked with an energy dispersive X-ray spectrometry (EDXS) attachment. The SEM analysis was done at 500× magnification to examine the morphological characteristics of both the adsorbents.

Two types of rice straw were used:
Type (A): washed straw
Type (B): sodium hydroxide activated straw

Washed straw type (A): raw rice straw was horizontally cut into lengths about 2-4 cm using grinder with out grinding or vertical cutting of the rice straw (Figure 3).

Straw was washed by submerged method for several times, 60 minutes for each time with changing of water and its replacement with another amount each time. The process was repeated until the yellow color resulting from the washing process disappeared. This was followed by drying the straw over metal surface for 24 hours at temperature 105°C as the first part of the research.

Activated straw type (B): rice straw was chemically activated with sodium hydroxide with the help of previous researches (13). Activation method was done by soaking 50 gm of straw in 1 liter of 0.1 mol concentrated sodium hydroxide solution. straw was left for 24 hours then washed by water using soaking method for several times with measuring the pH of washing water until reaching pH value 7, then it was dried in temperature 50 °C for enough period.
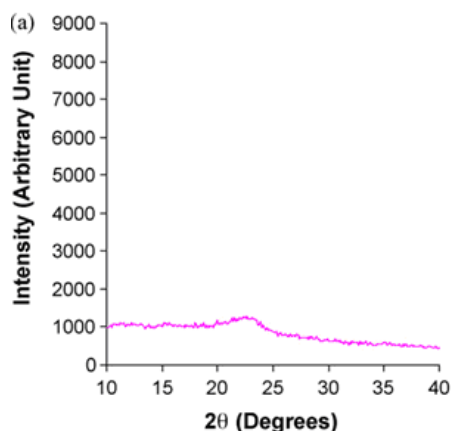
Fig.1: X-ray Diffraction of RRS

Half industrial model
Model components
The model is composed of a group of units connected to each other with plastic tubes as follows:

***Columns**: 4 P.V.C columns 100mm in diameter and 1.5m height supplied with an inlet opening from below and outlet opening from above 10mm in diameter, an iron tarnish resistant mesh with openings 30mm in size was placed above the level of straw and below the outlet opening, the mesh prevents the exit of straw from the outlet opening. Lower and higher openings allow vertical movement of water through straw from below to above. The columns were filled straw with light pressure from below to 1.0 m height.

***Water tanks**: Plastic water tank 60 liter in capacity supplied with floating valve at the outlet at the height of water level in the tank. The outlet opening was directly connected to the water line coming from the starting pumps.

The tank contains an outlet opening at 5cm height from the bottom, attached to it water distributor gate valve with four outlets openings on each there is a gate valve.

The tank maintains constant level inside it leading to constant static pressure on the model for constant flow.

***Flow meter**: Four flow meters model (Cole Parmer) with sensitive flow control valve were used. The inlets of the four flow meters were connected to the outlets of water distributor present after the tank with connecting their outlets to the inlets of the four columns. The flow meter was adjusted to allow a flow of 10-200 ml/min. (Figure 4 shows half industrial model).

(a)

(b)
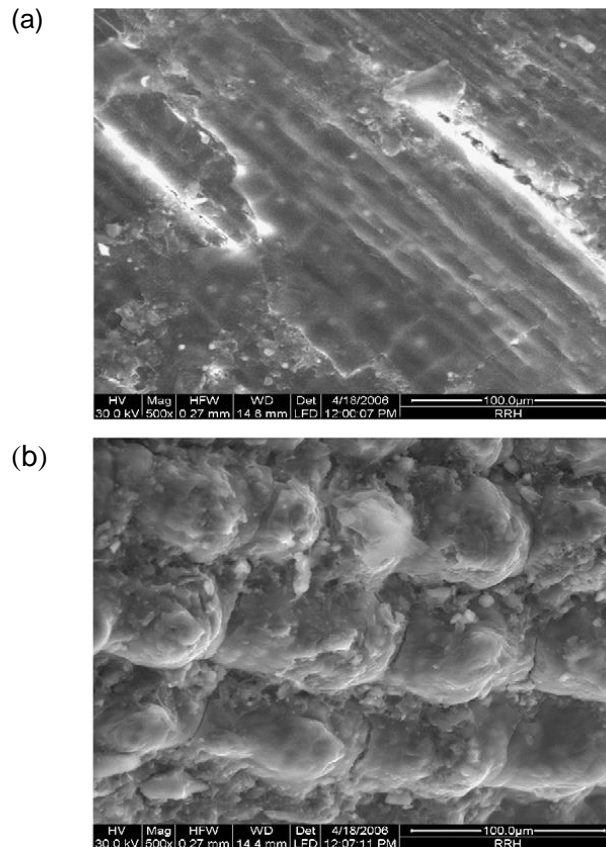
Fig.2: Scanning electron micrographs of RRS: (a) for inner side of RRS, (b) for outer side of RRS

Fig.3: Rice straw size

Fig.4: Half industrial model

Model location
The model was placed in ground water plant in Manial Sheiha village at Giza governorate which is located about 15 km south of Cairo city. The plant supplies the village with water with the help of compact water unit present on the Nile bank.
People of the village bring drinking water from outside because water coming from the plant contains about 0.9mg/lit. Iron and 1.0mg/lit. Manganese which leads to problems and there are no water treatment process for iron and manganese removal in Manial Sheiha water plant.
An experimental model was built in the plant in year 1991 for iron and manganese removal using limestone filters and was operated for one year.

Analysis:
An analysis to iron and manganese concentration in experimental water was carried out following the laboratorial plan using colorimetric method by using spectrometer model Cecillce 3021 using ready made chemicals from Hanna HI 93709.

Water well:
Regarding the water well supplying the model, it was found that concentration of iron and manganese were slightly changing through the day.
At the time of taking the samples from the water entering the model, the concentrations were shown in Table no. (1):

Table 1

Concentration	Time	Parameter
from 0.808 to 1.034 mg/lit	6.00 pm	Iron
from 0.63 to 0.75 mg/lit	12.00 pm	Iron
from 101 to 1.236 mg/lit	6.00 pm	Manganese
from 0.82 to 1.01 mg/l	12.00 pm	Manganese

Model operations:
Manial Sheiha plant works continuously for 12 hrs daily from 12.00 am to 12.00 pm. The model was operated in the same way with taking samples from in and out water twice daily. The first sample was taken 6 hours after the beginning of the operation and the second sample was taken after 12 hours i.e. at 6.00 pm and 12.00 pm.
The first sample was given code (A) and the second sample was given code (B). The columns were operated for continuous 10 days according to Table no. (2)

Table 2

Flow rate (ml/min)	Type of straw	Column no.
30	washed type (A)	1
60	washed type (A)	2
30	activated type (B)	3
60	activated type (B)	4

Parameters:

As mentioned before the research plan was based on two main parameters which are:
1   Column inlet flow: two flows were used one was 30 ml/min. and the other was 60 ml/min. which permitted 4.4 and 2.2 hours detention time for the empty column.
2   Straw type: constant straw size was used (2-4 cm) and they were prepared as follows:
 Washed straw type (A)
Sodium hydroxide activated straw type (B)

RESULTS

Results of column no. (1):
Column no. (1) contained washed rice straw (type A) with flow of 30 ml/min. the concentration of iron in out water ranged between 0.29 mg/lit to 0.43 mg/lit for sample A during the operation period with an average iron removal efficiency about 61% while for sample B iron concentration in the out water ranged from 0.23 mg/lit to 0.53 mg/lit with an average iron removal efficiency about 40% (Figure no. 5 demonstrates iron concentration for column no.1)
Regarding concentration of manganese in out water for sample (A) ranged between 0.46 mg/lit and 0.66 mg/lit with an average manganese removal efficiency about 50% while for sample B it ranged in out water between 0.55 mg/lit to 0.45 mg/lit with an average manganese efficiency of 45%. (Figure no. 5 shows manganese concentration for column no.1)

Results of column no. (2)
Column no.2 contained washed rice straw type (A) with a flow of 60ml/min and iron concentration in water coming out from the column ranged between 0.34mg/lit to 0.51 mg/lit for sample (A) with an average iron removal efficiency about 48% while for sample (B) iron concentration in out water ranged between 0.45mg/lit and 0.58mg/lit with an average iron removal efficiency about 25%.
Regarding manganese concentration for out water in sample (A) it ranged between 0.6 mg/lit and 0.73mg/lit with an average removal efficiency of 41% while for sample B manganese concentration ranged between 0.5mg/lit and 0.68mg/lit with an average manganese removal efficiency about 38%. (Figure 7&8 show iron & manganese concentration for column no.2)

Results of column no. (3)
Column no.3 contained type B activated rice straw with a flow of 30ml/min with iron concentration in out water ranged between 0.24mg/lit to 0.31mg/lit for sample (A) with an average iron removal efficiency about 69%, while for sample (B) iron concentration ranged between 0.18mg/lit and 0.27mg/lit with an average iron removal efficiency about 67%.
Manganese concentration in out water for sample (A) ranged between 0.25mg/lit and 0.44mg/lit with an average manganese removal efficiency of 69%, while for sample(B) manganese concentration ranged between 0.32mg/lit and o.4mg/lit with an average manganese removal efficiency about 63%. (Figure 9&10 show iron and manganese concentration for column no.3)

Results Column no. (4)
Column no.4 contained type (B) activated rice straw with a flow of 60ml/min, iron concentration in out water ranged from 0.22mg/lit and 0.34mg/lit for sample (A) with average iron removal efficiency about 67%, while for sample (B) iron concentration in out water ranged between 0.26mg/lit & 0.43 mg/lit with an average iron removal efficiency about 48%.
Manganese concentration in out water for sample (A) ranged between 0.25mg/lit and 0.55mg/lit

with an average manganese removal efficiency about 61% while for sample (B) manganese concentration ranged between 0.3mg/lit and 0.53mg/lit with an average manganese removal efficiency about 55%. (Figures 11&12 show iron and manganese concentration for column 4).

DISCUSSION

Results showed that change in iron and manganese removal efficiency during the period of the experiment was not clearly declined which meant that columns didn't reach the level of losing their ability of removal that requires the change of straw in the columns. Since the well operation system depends on stopping the well for 12 hours daily, it always found that iron and manganese concentration at the time of sample (A) more than on the time of taking sample (B).
Average removal efficiency for the four columns at sample (A) was higher than at sample (B) which explained the decrease of the efficiency with the decrease of the concentration and vice versa. (Figures 13&14 show comparison between the average removal efficiency of iron and manganese for the four columns)
Iron and manganese removal efficiency was affected by the inflow of the column and that was for type A washed straw and type B activated straw, where average removal efficiency decreased more in column 2 than in column 1 also decreased in column 4 more than in column 3. Type (B) sodium hydroxide activated straw showed more efficiency in iron and manganese removal than in type (A) washed straw at the same flow while it was found that average removal efficiency for column 3 was more than in column 1and for column 4 more than in column 2.
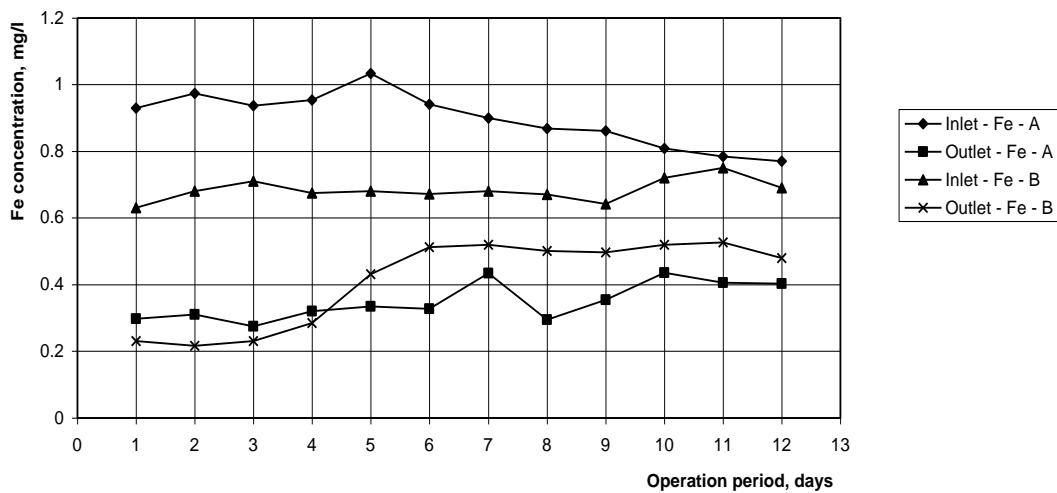
Fig.5: Iron Concentration Column no. (1)
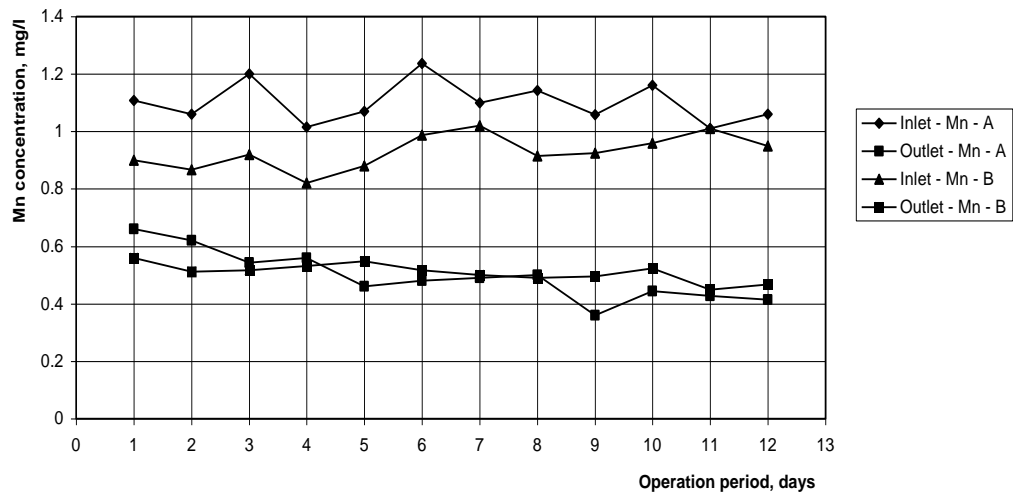
Fig.6: Manganese Concentration Column no. (1)
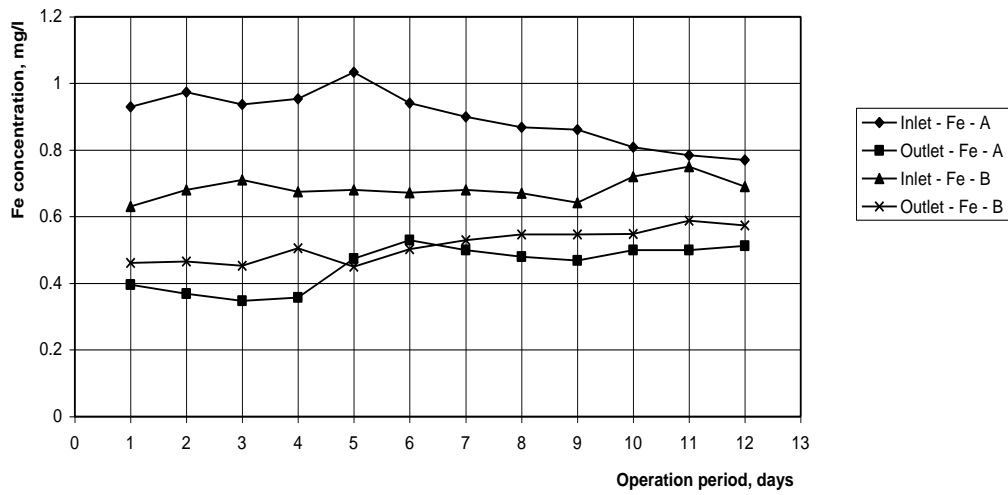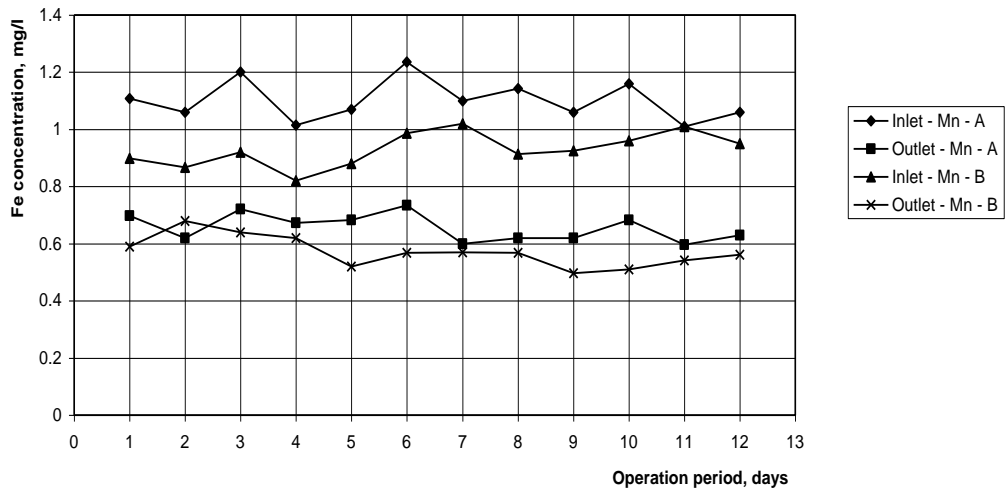
Fig.7: Iron Concentration Column no. (2)

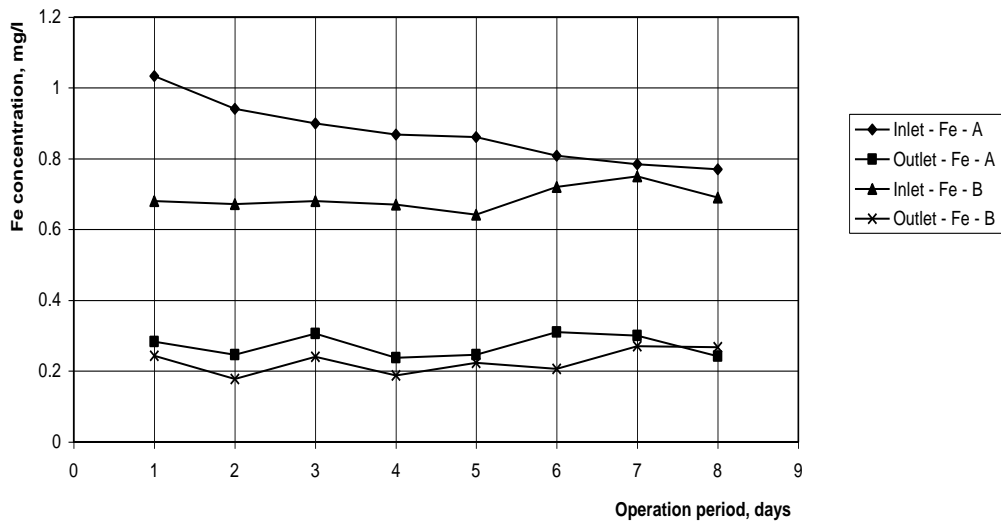**Fig.8: Manganese Concentration Column no. (2)**

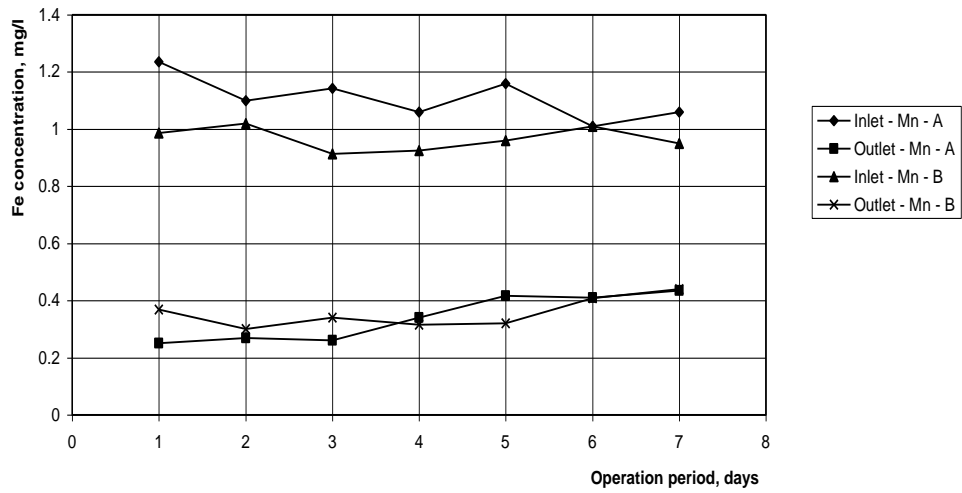**Fig.9: Iron Concentration Column no. (3)**

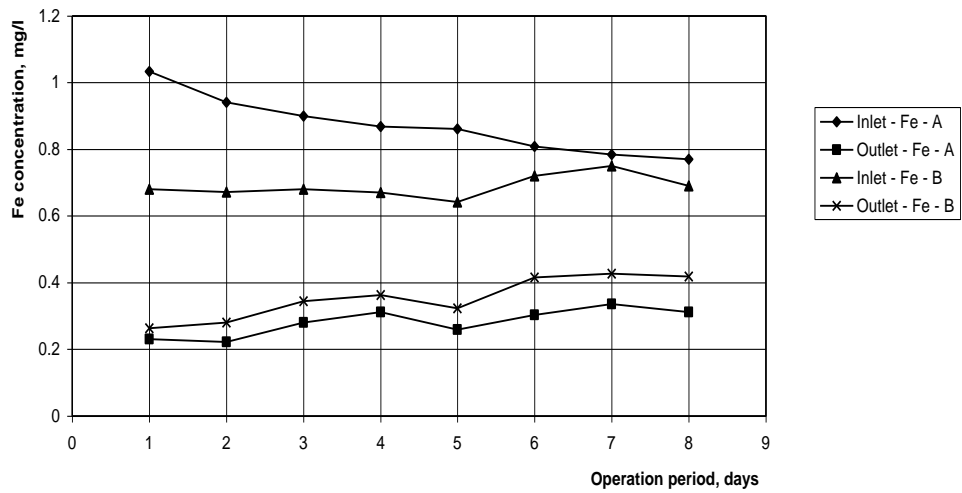**Fig.10: Manganese Concentration Column no. (3)**

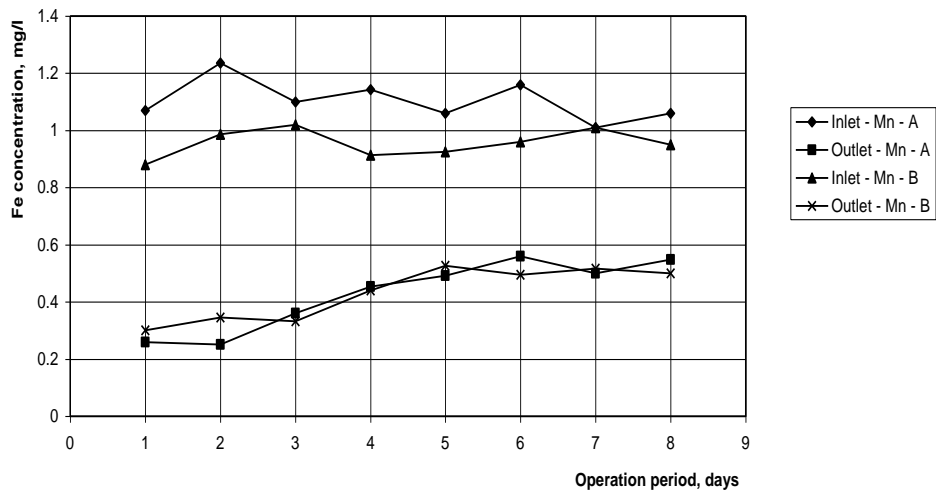**Fig.11: Iron Concentration Column no. (5)**
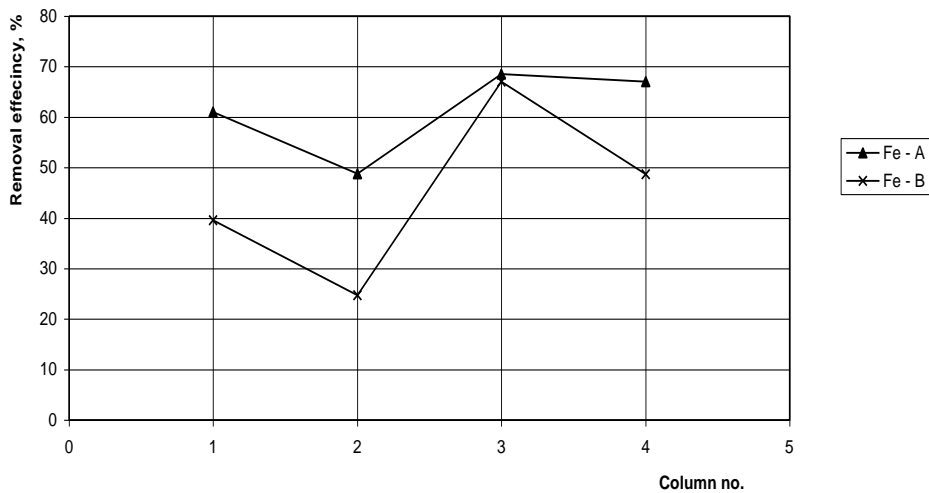

Fig.12: Manganese Concentration Column no. (4)

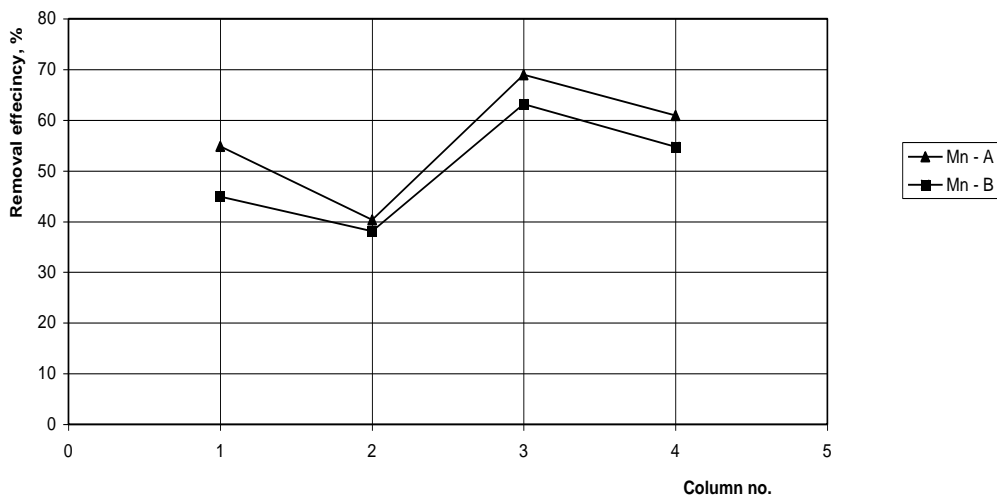**Fig.13: the average removal efficiency of iron for the four columns**

Fig.14: the average removal efficiency of manganese for the four columns

CONCLUSION

Half industrial model used in the research removed iron and manganese from natural ground water in different efficiency percentages.
The process of iron and manganese removal from ground water depended on the inlet flow to the unit where the efficiency increases with decrease of the flow and vice versa.
Ativated straw showed higher efficiency in iron and manganese removal than washed straw only.
The results showed that the period of using straw in the model can be more than 12 days for a period of 12 hours daily.
The results aroused from the study of the model furnishes a bed for doing further detailed research to put the basics for a design and better operating system for iron and manganese removal plant using rice straw.

REFRANCE

1. Kumar, P., Dara, S., "Removal of toxic Heavy metal ions from wastewaters using modified agricultural waste materials", (1980), Prog. Wat. Tech. Vol. 13 Brighton (353 – 361)
2. Suemitsu, R. Uenishi, R., Akashi, I., Nakanom, M., "The Use of dyestuff – treated rice hulls

for removal of heavy metal from wastewater", (1986), J. Appl. Polym. Sci. 31 (1) 75 – 83.

3. Srinivasan, "Evaluation of rice husk carbon for the removal of trace inorganic from water", (1986), Ph.D. Dissertation, Indian Inst. Technol. Madras.

4. Marshall,W.E., Champagne, E.T., Evans, J.E., 1993 "Use of rice milling by-product(hulls and bran)to remove metal ions from aqueous solution", (1993), J. Environ. Sci. Health A 28 (9), 1977 – 1992.

5. Roy, D., Greenlav, P.N Shane. B.S., "Adsorption of heavy metals by green algae and ground rice husks", (1993) J. Environ. Sci. Health A 28 (1) 37 (1) , 37 – 50.

6. Mohammad Ajmal, Rifaqat Ali Khan Rao, Shahana Anwar, Jameel Ahmad, Rais Ahmad, "Adsorption Studies on Rice Husk: Removal and Recovery of Cd (II) from Wastewater" (2002)

7. P.B Nagarnaik, A. G. Bhole and G. S. Natarajan "Arsenic (III) Removal by Adsorption on Rice Husk Carbon" (2002).

8. M. Ajmal, R.A. Rao, S. Anwar, J. Ahmad, R. Ahmad, Adsorption studies on rice husk: removal and recovery of Cd(II) from wastewater, Bioresour Technol. 86 (2003) 147–149.

9. A.S. Dadhlich, S.K. Beebi, G.V. Kavitha, Adsorption of Ni(II) using agrowaste, rice husk, J. Environ. Sci. Eng. 46 (2004) 179–185.

10. K.K.Wong, C.K. Lee, K.S. Low, M.J. Haron, Removal of Cu(II) and Pb(II) by tartaric acid modified rice husk from aqueoussolutions,Chemosphere 50 (2003) 23–28.

11. Low, K.S, Lee, C.K., "Quaternized rice husk as sorbent for reactive dyes", (1997), Biores. Technol. 61 (2) 121 – 125.

12. Lee, C.K., Low, K.S., Mah, S.J., "Removal of a gold (III) complex quaternized rice husk", (1998), Adv. Environ. Res. 2 (3) 351- 359.

13. Daifullah, A.A., Girgis, B.S., Gad, H.M., "Utilization of agro-residues (Rice Husk) in small wastewater treatment plant Materials ", (2003) letters 57 (1723 – 1731).

14. V.P. Della, I. Kuhn, D. Hotza, Rice husk ash as an alternate source for active silica production, Mater. Lett. 57 (2002) 818–821.

15. U. Kumar, M. Bandyopadhyay, Sorption of cadmium from aqueous solution using pretreated rice husk, Bioresource Technol. 97 (2006) 104–107

16. Vimal Chandra Srivastava, Indra Deo Mall, Indra Mani Mishra , Removal of cadmium(II) and zinc(II) metal ions from binary aqueous solution by rice husk ash, Colloids and Surfaces A: Physicochem. Eng. Aspects 312 (2008) 172–184

17. Gupta, V.K., Mittal, A., Jain, R., Mathur, M., Sarwar, S., 2006b. Adsorption of Safranin-T from wastewater using waste materials activated carbon and activated rice husks. J. Colloid Interf. Sci. 303, 80–86.

18. Guo, Y. Qi, J, Yang, S., Yu, K., wong, Z., Xu. H., "Adsorption of Cr (VI) on micro – and meso porous rice husk – based active carbon", (2002),   Materials and Physics 87 (132 – 137)

19. N.R. Bishnoi, M. Bajaj, N. Sharma, A. Gupta, Adsorption of   Cr(VI) on activated rice husk carbon and activated alumina, Bioresour. Technol. 91(2004) 305–307.

20. C.R.T.Tarley, S.L.C. Ferreira, M.A.Z. Arruda, Use of modified rice husks as a natural solid adsorbent of trace metals: characterization and development of an online preconcentration system for cadmium and lead determination by FAAS, J. Microchem. 77 (2004) 163–175

21. U. Kumar, M. Bandyopadhyay, Sorption of cadmium from aqueous solution using pretreated rice husk, Bioresource Technol. 97 (2006) 104–107.

22. Goel, J., Kadirvelu, K., Rajagopal, C., Garg, V.K., 2005. Removal of lead(II) by adsorption using treated granular activated carbon: batch and column studies. J. Hazard. Mater. 125, 211–220.

23. U. Kumar, M. Bandyopadhyay, Fixed bed column study for Cd(II) removal from wastewater using treated rice husk, J. Hazard. Mater. B129 (2006) 253–259.

24. S. Mohan, G. Sreelakshmi , Fixed bed column study for heavy metal removal using phosphate treated rice husk, Journal of Hazardous Materials 153 (2008) 75–82

25. Runping Han, Dandan Ding, Yanfang Xu, Weihua Zou, Yuanfeng Wang, Yufei Li, Lina Zou, Use of rice husk for the adsorption of congo red from aqueous solution in column mode, Bioresource Technology 99 (2008) 2938–2946

THERMAL ASPECTS OF BUILDING DESIGN IN ALGERIAN SAHARA

*Brahim BELGAID
Department of architecture – University of Batna (ALGERIA)
Personal address: 6 Rue des freres Bouchemal – 05000 BATNA (ALGERIA*)*
Email: bel_bra@yahoo.fr

ABSTRACT

In regions with warm and dry climates, case of Algerian Sahara, the external morphology of buildings has to answer the possibilities of passive heating, cooling, requirements of natural ventilation and be correctly configured to get natural light effectively distributed in internal spaces.
Some arrangements of passive architecture (such as shape or orientation), allow to obtain a minimal comfort level.
In this study, the concept of Δt_m was applied, which is allowing a fast estimation of the level of internal temperature for summer warm period for the city of Biskra (Southern Algeria), situated in Sahara which characterized by a warm and dry climate.

Keywords: climate of Sahara, thermal comfort, building shape, building orientation, solar radiation.

INTRODUCTION

The main characteristics of the well designed buildings are to catch the sun, the light or the wind.
In the regions of the Southern Algeria, traditional buildings often eased the outside rigours' climate, even though comfort was not obtained at all hours of day or in any seasons.
Solar radiation intensity on a large part of the Algerian territory during the year, requires most of the time the use of air conditioning installations, to provide the internal conditions of comfort.
This easy access to active solutions had the effect of forgetting all the knowledge accumulated during centuries concerning traditional solutions.
It would be very likely, that in the first third of the next century, the broadcasts emissions of gas with greenhouse effect of the Southern countries will be as important as those of Northern industrialized countries [1].
Objective is to promote new concepts and considerations during the buildings design in these regions.
The building design optimization from thermal point of view is a very ambitious question because of the problem complexity. This procedure brings in so many concepts linked to the aesthetics of the building (shape, facades) as the considerations linked to environmental aspects (orientation).
Pioneers of the passive buildings design [2] had said that there were three important factors for passive buildings: 1) orientation, 2) orientation and 3) orientation, to take advantage of daylighting and easier sun control.

THE CASE OF ALGERIAN SAHARA

Since Algeria was a producing country of oil and gas, applying certain strategies that are related

---

to the use and consumption of energy in buildings was marginalized. This fact not only created the high amount of energy consumed through the heating and cooling systems, but also the creation of uncomfortable spaces and buildings, which are hot in summer and cold in winter.

It would be necessary to know that in Algeria case, the buildings sector represents more than 40 % of the final demand in energy for national level, what represents an important potential of intervention for a rationalization of the energy consumption [3].

The climatic architecture benefits from a free energy in the form of heat and light. Every region in the world uses its own techniques and conceptions in its buildings construction, which are the most adapted to the appropriate climate for that region.

In the case of Algeria, Sahara represents about 87 % of the global surface that represents the major part of the Algerian territory, located globally between latitudes 20 ° N and 34 ° N.

The climatic environment of the Saharan regions is characterized by daily high temperatures during the warm season, diurnal temperature change, intense solar radiation as well as dryness of the atmosphere.

In the arid and semi-arid regions (corresponding to the Algerian climatic summer zones E3, E4 and E5 as shown in figure 1) which constitute the major part of the Algerian territory, the harsh desert climate during the summery period makes the living conditions in buildings extremely difficult.
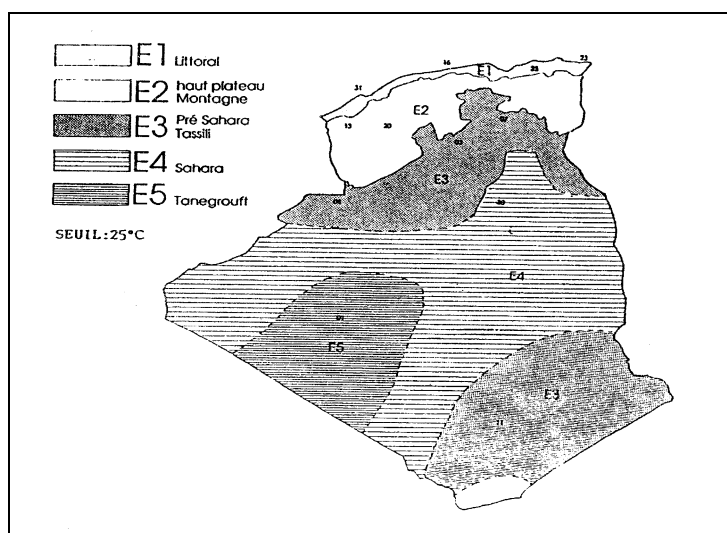

Fig. 1: Algerian climatic summer zones.

Several solutions can be envisaged to remedy this problem, among which, the exploitation of the building's shape and orientation effects.

This solution will allow to avoid (or at least limiting) appeal to the solutions of mechanical ventilation and air conditioning, in addition to this, involves reduction of running costs and problems of conversation and maintenance.

In the cities of Sahara, heat is the dominant problem and the warm and dry climate imposes mostly to have closed façades and courtyards, which are opened inward houses, with openings of small dimensions. According to A'Zami [4], a courtyard is a social space with an environmental function.

In North Africa, it is possible to see the common use of courtyards in the living houses of the Saharan cities. Figures 2 and 3 allow to see the use of inner courtyards of houses in warm and dry region, for Ghardaïa in M'Zab, Algeria [5] and Marrakech, Morocco [6].

Fig. 2: Example of design in M' Zab (Algeria).

**Fig. 3: View of houses with inner courtyards
at Marrakech (Morocco).**

The courtyard choice is a strategy of simple conception, allowing increasing of daylight availability for every room.

Buildings with courtyards were conceived and developed in a period when artificial air conditioning was not even possible.

It is well known that for a given climate, the rate of renewal of air, the thermal capacity of the building and the heat exchanged between the air and the thermal mass, define the functioning of the night-natural ventilation.

The warm and dry summer air, characteristic of dry zones, imposes a reduction of the amount of ventilation at its minimum (to keep internal coolness), and increase the renewal of air at the maximum during the night because of the cool air of evenings (at least 4 volumes / hour).

It is appropriate to focus on a specific aspect with the aim of the solar radiations reduction.

Generally, for the case of the private builders, the use of roof insulation is very rare. It remains limited specially to public buildings subjected to control on behalf of specialized research departments.

Thermal long wave radiations between the sky and the external surface can have an important influence on the hygrometric and thermal performance of the building's envelope, because the radiative heat transfer causes a significant decrease of the superficial temperature of the external surfaces.

Generally, the importance of the above phenomena becomes more important by increasing of the thermal insulation level of the buildings envelopes.

BUILDING'S ENVELOPPE CHARACTERISTICS

One of the general characteristics of the Saharan dry regions is that buildings are constructed with flat roofs, windows have small dimensions and heavy materials are used.

The roof and the thick external walls help to absorb the outdoor temperature fluctuations, and contribute to maintain acceptable conditions inside the buildings.

The colour of the roof is considered as an important feature in the building, since a roof with white or clear colour generally has similar temperature as the outside air during the day. While a roof with dark colour has a temperature greater than the outside air temperature [7].

The traditional materials that used in these regions are mainly stone, clay bricks and gypsum. Walls constructed with these materials are thick (of 0.40 m in 0.50 m), and roofs are flat or vaulted.

For example, table (I) shows an external wall from clay bricks of 0.20 m of thickness achieve a thermal delay of about 9 hours and a decrement factor of 0.0052, which is satisfactory [8].

Thermal inertia improves the use of solar gains as well as the thermal comfort by reducing the indoor temperature fluctuation.

The colour and reflective properties of the external surface of walls and roofs influence the building thermal behaviour.

Table I: Types of external walls.

Type of external wall	Coefficient U $[W/m^2.°C]$	Time lag φ $[h]$	Decrement factor μ
Concrete blocks (0.20 m)	3.94	4	0.044
Stone (0.20 m)	4	4	0.095
Stone (0.30 m)	3.40	6	0.056
Clay bricks (0.20 m)	1.35	9	0.0052

Dark colours absorb more solar radiations and increase thermal load, whereas light colours reflect solar radiations and decrease cooling load.

Now days, the mode of realization of constructions in the South of Algeria is not very different from that practised in the North where more moderate climatic conditions exist. This fact takes place despite of the existence of several specific recommendations for these regions, South and North.

The same building materials are mostly used (brick, parpen, concrete), besides the traditional materials (stone, mud, gypsum...) which are less used now days.

In the aim to reintroduce these traditional materials to the present construction market, as construction materials to be used once again in buildings in the south region, many detailed studies and critical analysis of their mechanical and thermal qualities, as well as where exactly they could be used, are required.

Roofs and walls of light colour have the big advantage to reflect much more heat than darker materials.

Knowing that a white colour roof absorbs on average 25 % only of solar heat, much less than 90 % absorbed by that of the dark colour or black, which reduces significantly the heat flow penetrating into the building and simplifies the cooling task.

For the most part of cases, the thermal resistance of the external walls and the roofs used in Southern Algeria is weak (for our study the thermal resistance of external walls and the roof is respectively 0.65 $m^2.K/W$ and 0.41 $m^2.K/W$).

OVERHEATING ANALYSIS

If we consider the internal atmosphere of the building is at an average uniform temperature t_{im} , and that external environment is at an average temperature t_{em} , there will be a difference of temperature Δt_m expressed by equation (1).

$$\Delta t_m = t_{im} - t_{em} \qquad\qquad \textbf{(1)}$$

This difference of temperature results from a thermal balance between various thermal quantities given by equation (2), expressing gains (solar contributions by opaque and glazed surfaces of the building envelope, plus internal contributions), as well as losses (through the envelope and by renewal of air).

$$\Delta t_m = \frac{P_i + P_{cv} + P_{co}}{k_T + A.q} \qquad (2)$$

Where:

P_i = heat generated inside the building by users (cooking, lighting …). $[W]$

P_{cv} = gains through glazed areas of the building, following various orientations. $[W]$

P_{co} = gains through the opaque surfaces of the building (external walls and roof). $[W]$

k_T = total conductance of the building. $[W/{}^{\circ}C]$

$A.q$ = heat exchanged by renewable air. $[W/{}^{\circ}C]$

The method of the overheating Δt_m developed by Lavigne et al. [9], calculated according to the equation (2), is a way of estimating the comfort level of an internal atmosphere with regard to internal and external average temperatures t_{im} and t_{em}, and allows to understand the overheating effect during the warm summer months.
Hence, for a building located at Biskra (southern Algeria, latitude = 34.48 °N), with floor area equal to 144 m^2, with glazing on the north and south facades of surface S = 6 m^2, we will study three different cases following the building dimensions ratio L/l, as well as the building orientation axis (fig. 4):

   a) square shape ($L/l=1$),
   b) rectangular shape ($L/l=1.5$), building axis oriented N/S.
   c) rectangular shape ($L/l=1.5$), building axis oriented E/W,
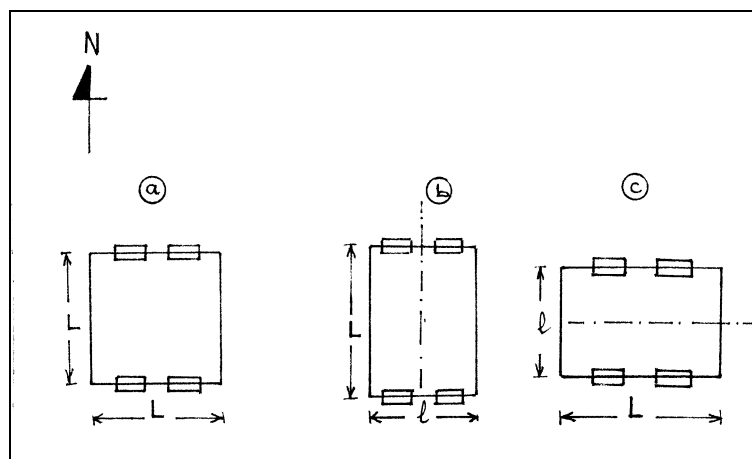

Fig. 4: Various building's dimensions ratios.

The change of building shape that consists of a reduction of dimensions (ratio length / width $L/l=1$ for the square shape and $L/l=1.5$ for the rectangular shape), as well as a variation in surfaces exposed to the solar radiation.

A change of the building axis orientation following E/W or N/S direction allows to find out the effect of the rectangular shape along the axis E/W or N/S on the Δt_m values.

For the square shape, the four façades exposed to the solar radiations have each a surface equal to $36\,m^2$.

For the case of the rectangular shape, the exposed surface to the North and to the South is equal to $44.10\,m^2$, and the one exposed to the East and to the West equal to $29.40\,m^2$ for an E/W axis. Whereas for the N/S axis the surface exposed to the North and to the South is equal to $29.40\,m^2$ and the one exposed to the East and to the West equal to $44.10\,m^2$. This means a variation of the surface closely of 18 % in both cases with regard to the square shape.

RESULTS

Figures 5 to 7 show the calculated values of Δt_m for warm period, following three forms studied with the building, for the various values of the air change rate.

It would also be necessary to know that ventilation is of modulated type, varying from a minimal rate during the day (minimal hygienic rate for $t_{em}\rangle t_{im}$) to a maximal rate during the evening ($t_{em}\langle t_{im}$).
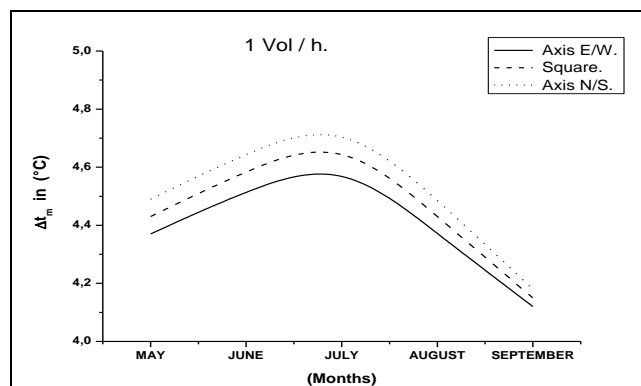
Fig. 5: Variation of Δt_m for warm period (1 volume / hour).
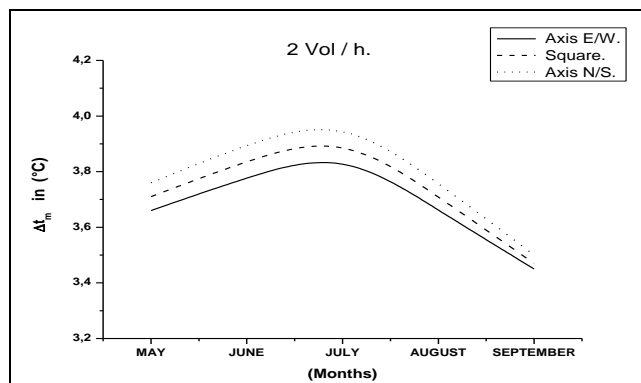
Fig. 6: Variation of Δt_m for warm period (2 volumes / hour).
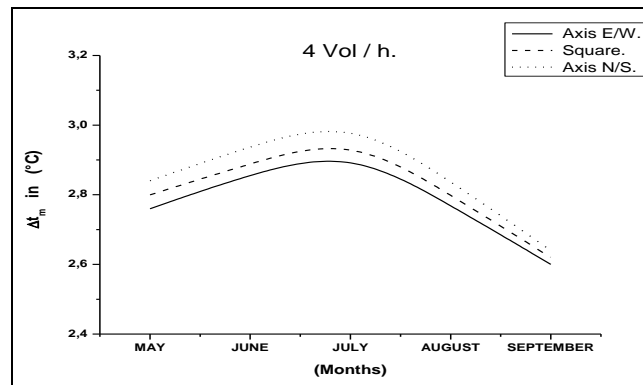
Fig. 7: Variation of Δt_m for warm period (4 volumes / hour).

It could be noticed according to the calculated values of the overheating for various studied cases, that the values of Δt_m are reduced for the rectangular shape compare to the square shape of the building, and that Δt_m could be also reduced by the ventilation effect.

The ventilation effect is very considerable with air change rate of 4 volumes / hour, this air amount being possible during the evening, because the outside air has a lower temperature than the internal air, which would give a possibility to realize an effective night-cooling of the building thermal mass.

CONCLUSIONS

Both geometry and orientation play an important role in determining of the building thermal efficiency.

The method used in this study allows designers to understand the influence of changing the shape of the building on Δt_m .

Studying the shape of the building as a thermal aspect, shows that the reduction in the building surfaces exposed to the outside, lead to the decrease in heat losses in winter-time and in the decrease of external gains, mainly solar heat in summer-time.

Natural ventilation is an effective measurement for the improvement of the thermal comfort in summer. However a reduction of the exposed surface to the external climate would limit possibilities or potential of night-cooling by long wave radiative heat exchange between the envelope surface and the sky.

Neglecting these problems implies a poor appreciation of energy savings and economic profits that are considered one of aims of the users. Consequently, the building energy consumption is greater than necessary, a waste in energy use during building life-cycle.

NOMENCLATURE

U heat transfer coefficient,

φ time lag,

μ decrement factor,

P_i heat generated inside the building by users (cooking, lighting …),

P_{cv} gains through glazed areas of the building, following various orientations,

P_{co} gains through the opaque surfaces of the building (external walls and roof),

k_T total conductance of the building,

$A.q$ heat exchanged by renewable air,

Δt_m overheating.

REFERENCES

1. Mousel, M. & Weill, C. (1999), ''Maîtrise de l'Energie et Effet de Serre - De la Maîtrise de l'Energie aux Politiques et Mesures'', Liaison Energie-Francophonie, 42, pp. 4-7.
2. Docherty, M., & Szokolay, S.V.(1999), ''Climate Analysis'', Plea Notes, No 5, Passive Low Energy Association Intl, p. 39.
3. Harrar, M. (2006), ''Confort Thermique et Economie d'Energie'', La lettre de l'Aprue, 9 (April), p.3.
4. A'Zami, A. et al.(2005), ''Climatic Responsive Architecture in Hot and Dry Regions of Iran'', International Conference Passive and Low Energy Cooling for the Built Environment, Santorini, Greece, May, pp. 613-617.
5. Ravereau, A. (1981), ''Le M'Zab une Leçon d'Architecture'', Sindbad.
6. Fathy, H. (1986), ''Natural Energy and Vernacular Architecture: Principles and Examples with Reference to Hot Arid Climates'', University of Chicago Press.
7. Givoni, B. (1978), '' L'Homme l'Architecture et le Climat'', Paris : Le Moniteur.
8. Belgaid, B., Benmoussa, H., & Boumaza, M. (2007), ''Bioclimatic Approach of Building Design in Hot Climate – An Example of Biskra'', Asian Journal of Civil Engineering (Building and Housing), Vol. 8, 4, pp. 461-468.
9. Lavigne, P., Brejon, P., & Fernandez, P. (1994), ''Architecture climatique'', Edisud Editions.